Mira Geoscience
...modelling the earth

409 Granville Street, Suite 512 B
Vancouver, BC
Canada V6C 1T2

Tel: (778) 329-0430
info@mirageoscience.com
www.mirageoscience.com

Yukon Geological Survey Miscellaneous Report MR-18

Ross River geothermal exploration project: Review of the 2014 work program

Prepared for Dena Nezziddi Development Corp.
Project #4300
February 25, 2015

Yukon Geological Survey

Yukon
Energy, Mines and Resources

Canadian Northern Economic Development Agency
Agence canadienne de développement économique du Nord

PREFACE

This report presents the results of an integrated geothermal exploration program of part of the Tintina Trench near Ross River, Yukon. This study was commissioned by the Dena Nezziddi Development Corp. of the Kaska First Nation, and benefited from funding by CanNor (the Canadian Northern Economic Development agency) and the Yukon government. The Ross River geothermal project represents the most comprehensive geothermal exploration program to date in Yukon. It integrates field-based structural analysis and mapping with acquisition and interpretation of aeromagnetic and magnetotelluric geophysical data. The Yukon Geological Survey contributed by providing geological advice to the exploration team. Together these data provide an improved and more detailed understanding of the geology of the Tintina Trench near Ross River, and represent a solid foundation to guide future geothermal exploration in the area.

The Yukon Geological Survey is making this report available, with consent of the Dena Nezziddi Development Corp. and project partners, as part of its ongoing efforts to advance knowledge regarding the geothermal potential of Yukon.

Maurice Colpron
Head, Bedrock Geology

Mira Geoscience
...modelling the earth

Table of Contents

Mira Geoscience
...modelling the earth

List of Figures

Mira Geoscience
...modelling the earth

List of Tables

Mira Geoscience
...modelling the earth

1. Introduction

In September 2014, the Dena Nezziddi Development Corp. engaged a geoscience team with diverse skillsets to assist in year two of their ongoing effort to explore for geothermal energy resources on Kaska First Nation traditional lands. This report documents the parties involved, the work performed, and the results obtained from the 2014 exploration program. The area that forms the focus of this project lies within the Tintina Fault Zone between the townships of Ross River and Faro in the south central Yukon (Figure 1). New geological and geophysical data were collected, analyzed and interpreted from the project area shedding new light on our understanding of the subsurface. The new data were critical to help the project team select target areas for exploratory temperature-gradient drilling. A shallow drilling program is the recommended next step in this geothermal exploration effort to test for elevated thermal signatures in the subsurface. If a shallow drilling program is successful in demonstrating high sub-surface temperature potential then additional geoscience data collection followed by a deeper exploratory drilling program may be warranted.

What follows is a general summary of the 2014 geothermal exploration effort; detailed technical reports written by various team members that provide specifics on data collection, analysis, and interpretation can be found in the appendices.

1.1. Background

Exploring for geothermal energy resources is challenging whether you are searching for high temperature electricity-grade resources or lower temperature resources for direct-use applications (e.g. home heating or greenhouses). In either case, the two requirements for a geothermal resource include heat and fluid flow in the subsurface. One possible source of heat is subterranean magma bodies in volcanic areas. Alternatively, heat can come from groundwater that circulates deep into the earth along faults. In these areas, the Earth's natural geothermal gradient warms the water before it

buoyantly rises back to shallow levels. A third potential source of heat is from rocks that contain unusually high concentrations of radioactive elements. Radioactive decay can provide limited amounts of heat to geothermal waters.

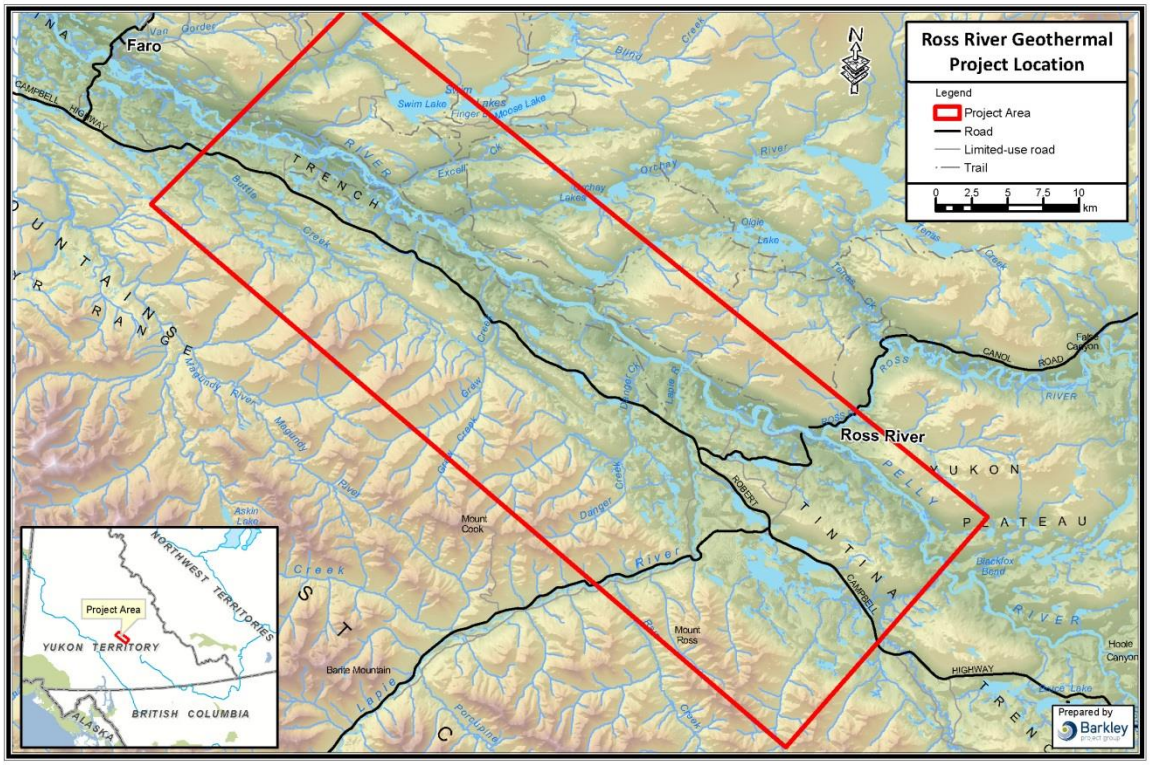

Figure 1. Location map for the Ross River geothermal project in the south central Yukon. The project area is outlined in red.

Recent studies suggest that the Earth's crust in the southern Yukon is unusually hot (like much of the Northern Canadian Cordillera). Although data points are sparse, the rate at which heat is coming out of the Earth in the region around Ross River is estimated to be ~105 milliWatt per square metre (mW/m^2) (Lewis et al., 2003). This is much higher than heat flow estimates of ~42 mW/m^2 further east in Canada near Yellowknife. The higher heat flow estimates for the southern Yukon are comparable with

heat flow values measured in known geothermal regions such as Nevada in the United States.

In contrast to these high heat flow estimates for the southern Yukon, there is no evidence in the Ross River project area for modern-day hot springs, other surface thermal manifestations, or even warm water wells. Nor is there evidence for recent volcanism within the project area. Instead, old volcanic rocks and an epithermal gold deposit at Grew Creek indicate that an active geothermal system did exist in the past at the project area. However, this geothermal activity occurred about 50 million years ago (Christie, et al., 1992). Any residual heat associated with the volcanism and mineralization at Grew Creek has long since dissipated. Thus, based upon the evidence it is improbable that subterranean bodies of hot magma serve as a source of geothermal heat in the project area. Deep circulation and heating of groundwater and/or heat from radioactive decay are the more likely options.

The project area straddles the Tintina Fault Zone, a major, crustal-scale, northwest-trending system of faults. Such a significant geologic structure could provide the vertical pathways within the Earth's crust that would allow for deep circulation and heating of groundwater. Active movement of the Earth's crust along a fault zone (i.e. earthquakes) is helpful for creating the cracks and permeability that can facilitate deep fluid circulation. Although data are sparse, the estimated deformation rate along the Tintina Fault Zone is only ~0.5 mm/year (Leonard et al, 2008). This compares with ~3 cm/year relative plate motion along the San Andreas Fault in California. The Tintina Fault Zone, therefore, is relatively inactive. Lower levels of fault movement in the Tintina Fault Zone likely causes geothermal fluid flow in the area to be less robust compared to more active fault zones.

For geothermal fluids to flow in the subsurface, faults and fractures need to be open, not shut. Studies from the southern Yukon show that the tectonic regime in the area is under compression in a direction oriented approximately NNE-SSW (Hyndman et al., 2005). Compressional conditions in the crust tend to close fractures and inhibit

subsurface fluid flow. In contrast, extensional tectonic conditions are commonly more conducive for the formation of geothermal reservoirs. For example, as the crust pulls apart and extends, faults pull open to allow for geothermal fluid flow. Crustal extension that runs parallel to the Tintina Fault Zone has occurred in the past in the Ross River project area, developing into narrow pull-apart basins that have filled with Tertiary age volcanic and sedimentary rocks. Such pull-apart basins are good indicators of the tectonic conditions that would help facilitate subsurface geothermal fluid flow. These areas are important to focus on for geothermal exploration. The low deformation rate for the Tintina Fault Zone mentioned above, however, suggests that such fault-parallel extension does not appear to be highly active in the present day.

Unfortunately, we have not yet analysed any data on the level of radioactivity for the rocks in the project area. Granitic rocks, which could potentially have high concentrations of radioactive elements do exist within the project area, however, no effort has been made to test this hypothesis. Thus, the heat generation potential of radioactive rocks in the project area is currently unknown.

Overall, in the Ross River project area, there are some indicators which would favor geothermal resources (e.g. high regional heat flow and crustal-scale fault zone). However, more direct indicators of the specific locations of geothermal resources (e.g. hot springs or volcanoes) are lacking. Thus, the approach taken in this geothermal exploration program is to utilize modern geological and geophysical tools in an attempt to identify specific geologic structures along the Tintina Fault Zone which may be favorable environments for the upwelling of deeply circulated geothermal fluids. If such geologic structures can be identified, a shallow exploratory drilling program can be used to test the identified structures. The key test is to measure the subsurface temperature gradient to see if elevated subsurface temperatures are encountered to warrant even deeper exploratory drilling.

1.2. Summary of Exploration Strategy

The primary goal of the 2014 geothermal exploration program at Ross River is to select locations for shallow, exploratory drill holes. As such, new geoscience evidence is required to justify each proposed drilling location. Geologic maps from the Yukon Geological Survey contain valuable information for the project area on bedrock type, bedrock age, and mapped faults. However, more detailed information is needed.

An important part of any geothermal exploration program is to characterize the distribution of different rock types and faults in the subsurface. Different faults and strata may serve as geothermal fluid pathways and certain rock types may be better as geothermal reservoirs. Surface geological studies as well as geophysical surveys provide the raw data needed for such an effort. Rigorous 3D modelling and interpretation of multiple lines of geological and geophysical evidence is one way to increase confidence in the selection of subsurface drilling targets. With this in mind, the 2014 Ross River geothermal exploration program contained five elements:

1) Reconnaissance geologic mapping and structural data collection in the project area to build upon the information already found in Yukon Geological Survey maps
2) Analysis and interpretation of a high resolution airborne magnetic survey data to help identify faults and structure
3) Analysis and interpretation of ground-based magnetotelluric (MT) survey data to help understand the geometry of major rock units and faults
4) 3D modelling of the compiled geoscience data to help facilitate effective visualization, interpretation, and drill target selection
5) A team-based interpretation approach to retain the value of each group's expertise while at the same time obtain a consensus interpretation

Thus, through an integrated understanding of the collected geoscience data, the project team aimed to identify specific locations within the Ross River project area which

showed evidence for geologic structural environments potentially conducive to geothermal fluid upflow.

1.3. **Project Participants**

Several groups were involved in the 2014 Ross River geothermal exploration program. Table 1 provides an overview of the groups involved and their roles in the project.

Organization	**Role**
Barkley Project Group	• Overall project management and oversight • Client liaison • Funding agency liaison • GIS mapping support
Sadlier-Brown Consulting Ltd.	• Geothermal exploration oversight • Field team technical coordination • Geoscience data analysis & interpretation • Yukon Geological Survey liaison
Mira Geoscience Ltd.	• Field collection of rock property data • Field team technical coordination • Airborne magnetic data analysis • 3D magnetic modelling • Geoscience data analysis & interpretation
University of Nevada at Reno	• Reconnaissance geologic mapping • Structural geology interpretation • Geoscience data analysis & interpretation
University of Alberta	• 3D modelling of MT data • Geoscience data analysis & interpretation
Phoenix Geophysics Ltd.	• Collection of MT data in the field
Precision GeoSurveys Inc.	• Collection of airborne magnetic survey data (occurred in 2011)
Snider Geophysics	• Field supervision and logistics support for geophysical data collection

Table 1. List of groups involved in the project and their respective roles.

2. Fieldwork and Data Collection

Originally, we proposed a new airborne survey to collect magnetic data for this project. However, during the planning stages, we discovered that a significant portion of the project area had already been covered by a high-resolution airborne magnetic survey flown in 2011 (Figure 2). Purchasing this existing magnetic dataset was the more cost-effective and timely option and these data were bought from Golden Predator Corp. in October 2014. Details of the airborne magnetic survey are provided in the Precision GeoSurveys data acquisition report which can be found in Appendix 1.

In October 2014, all the project field teams deployed to the Ross River area to collect the new geoscience data. Over the course of the month, reconnaissance geologic mapping was completed by foot, road, and helicopter covering as much ground as possible. In addition, magnetic rock property data were collected on exposures of bedrock and glacial sediments at 45 different locations covering most of the major rock types within the project area. Lastly, an MT survey was performed that consisted of 25 new MT stations to supplement the 24 existing MT sites collected along the Canol Road in 2013 (Figure 2).

The footprint of the MT survey overlaps with the southern third of the footprint of the airborne magnetic survey. Attempting to cover the entire magnetic survey area with MT stations would have been challenging due to the high cost and access difficulties. We chose the southern portion to expand outwards from the existing 2013 MT dataset and to take advantage of co-located magnetic survey data.

Details of the 2014 MT survey are provided in the Phoenix Geophysics logistics report (Appendix 2). Details of the magnetic rock property data collection are in Appendix 3. Details of the geologic mapping effort can be found in Appendix 4.

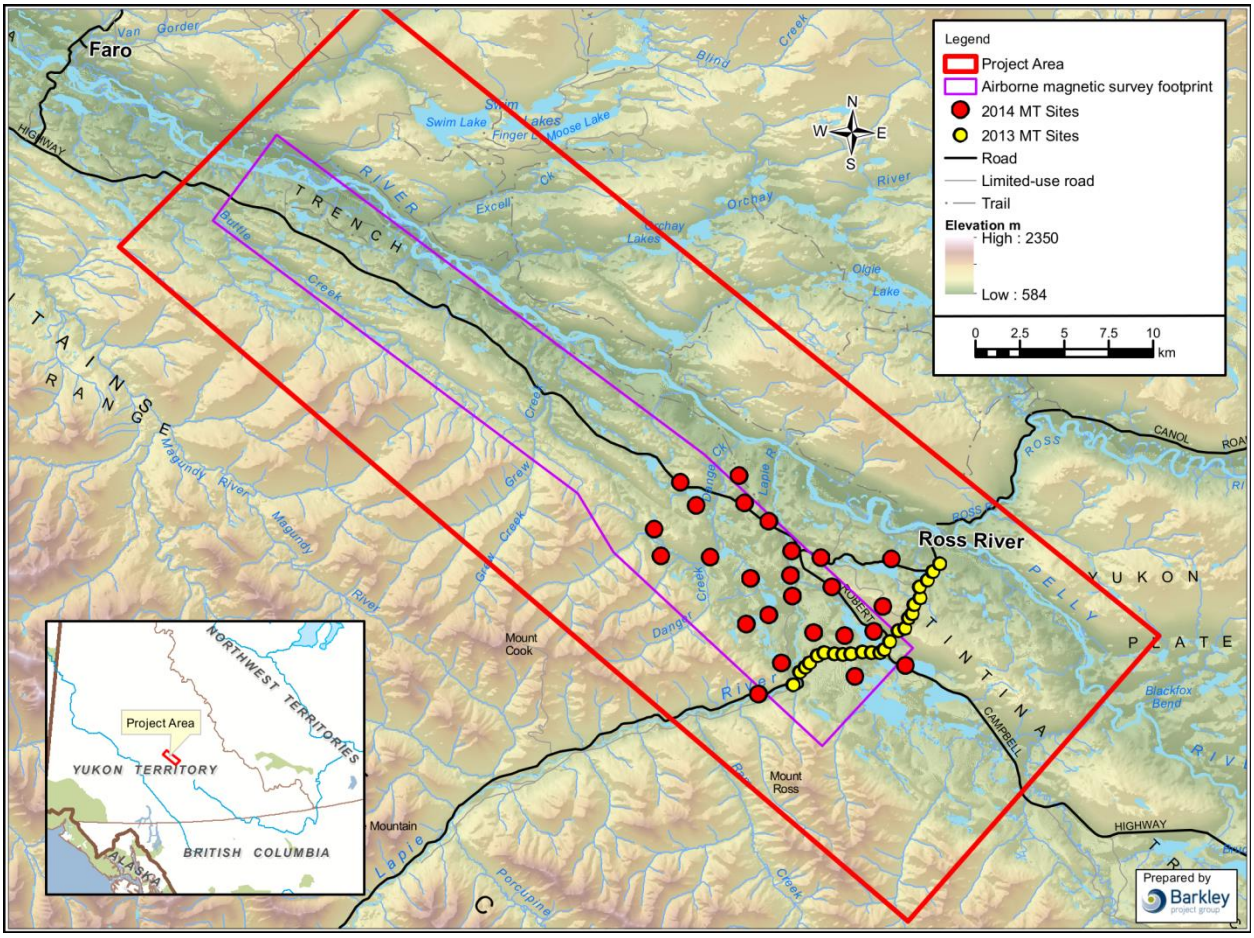

Figure 2. Map showing the footprint of the airborne magnetic survey (purple polygon) within the larger project area (red rectangle). Dots show the locations of the 2014 (red) and 2013 (yellow) MT stations.

Table 2 lists the dates that each team member spent working in the field and the tasks accomplished.

Dates in the field	Organization	Personnel	Tasks
Oct. 2 – 9, 2015	Mira Geoscience	Jeff Witter	• Oversee fieldwork • Collect magnetic rock property data • MT site prep work
Oct. 2 – 8, 2015	University of Nevada, Reno	Nick Hinz & Seth Dee	• Reconnaissance geologic mapping and structural data collection
Oct. 2 – 10 and Oct. 13 – 20, 2015	Snider Geophysics	Aaron Snider	• MT site prep work • Assist with MT data collection
Oct. 5 – 9, 2015	Barkley Project Group	John Ebell	• Oversee and document fieldwork • Liaise with client
Oct. 5 – 9 and Oct. 12 – 16, 2015	Sadlier-Brown Consulting Ltd.	Tim Sadlier-Brown	• MT site prep work • Liaise with YGS
Oct. 15 – 25, 2015	Phoenix Geophysics	MT field crew	• Collect MT data

Table 2. Fieldwork timeline and personnel involved.

Mira Geoscience
...modelling the earth

3. Data Analysis

The three new geoscience datasets collected in the Ross River area (geologic mapping data, magnetic data, and MT data) were analysed by separate parties for this project.

3.1. Magnetic Data

Mira Geoscience compiled and analyzed the field measurements of magnetic susceptibility to characterize the magnetic rock property values of the major bedrock units and glacial till. This was followed by analysis of the airborne magnetic data in 2D map format in which a magnetic lineation map was generated. Lastly, Mira Geoscience performed 3D geophysical inversion modelling of the airborne magnetic data to create a 3D magnetic susceptibility block model that covers the entire footprint of the airborne magnetic survey and extends to a depth of 2 km below sea level (Figure 3). For details, see Appendix 3.

3.2. Geologic Mapping Data

Researchers from the University of Nevada, Reno integrated the new geologic data, obtained through reconnaissance mapping, with the aeromagnetic-based interpretations provided by Mira Geoscience. They also integrated these data with publicly available geologic maps from the Yukon Geological Survey and the Geological Survey of Canada. From this effort, they produced a new digital 1:50,000 scale geologic map of the Ross River project area. Field data on faults, fractures, and folds were analyzed to help characterize the structural framework in the project area (Figure 4). The aim of this effort was to identify which faults are more likely to be permeable compared to those which are less likely to be permeable. Regional data on the bedrock stratigraphy, structural geology, tectonic models, and earthquake seismicity were also compiled from existing geologic maps, published reports, and peer-reviewed papers to characterize the geologic setting. For details, see Appendix 4.

3.3. Magnetotelluric Data

Professor Martyn Unsworth of the University of Alberta combined the MT datasets collected in both 2013 and 2014 and analysed them jointly. He performed a QC check of the data which was followed by generation of 2D apparent resistivity maps. Next, 3D geophysical inversion modelling of MT data from 48 stations was performed which resulted in a 3D resistivity block model of a ~15 km x ~17 km area located west and south of the town of Ross River (Figure 5). This resistivity block model extends to a depth of 5 km below the ground surface. For details, see Appendix 5.

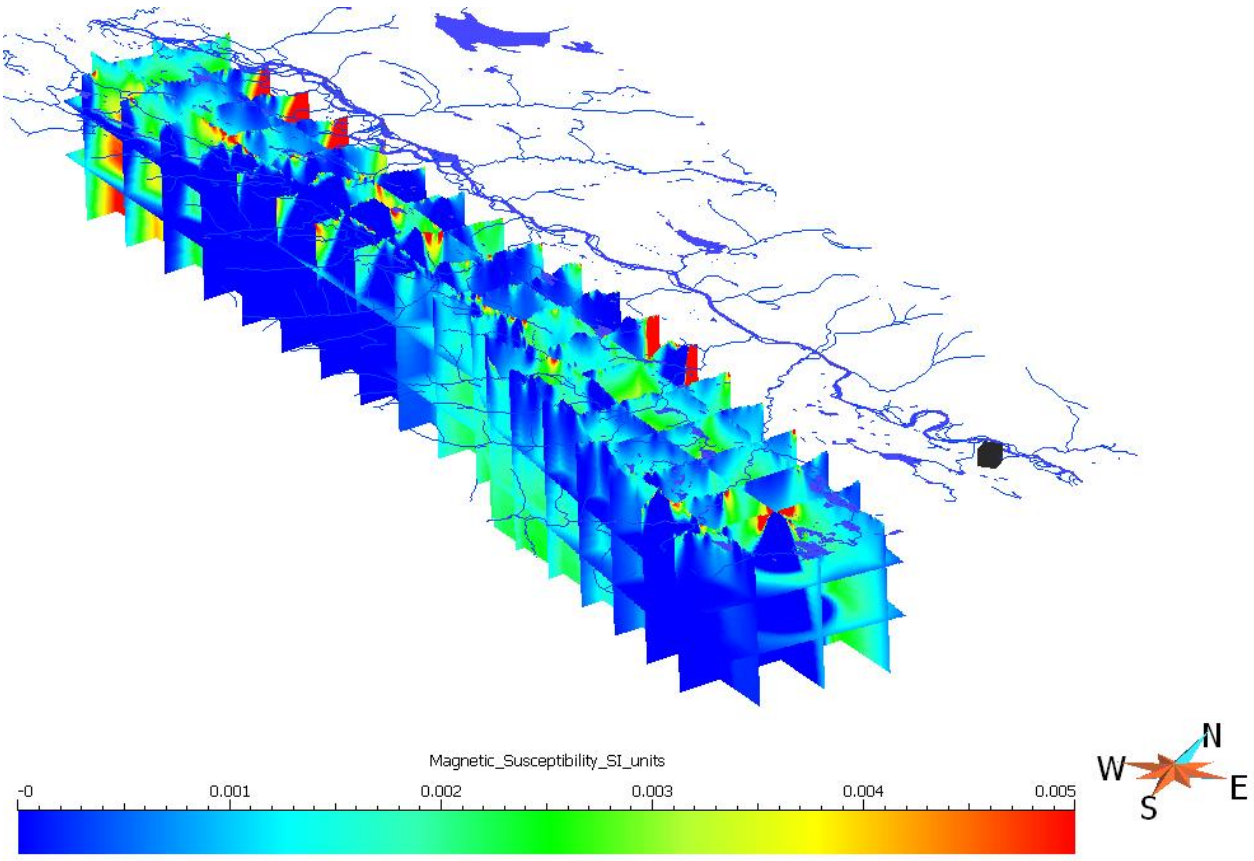

Figure 3. 3D perspective view of horizontal and vertical sections through the magnetic susceptibility model. View looking to the north-northwest. Rivers and lakes are overlain to provide a geographic context. The location of Ross River town is shown by the black cube.

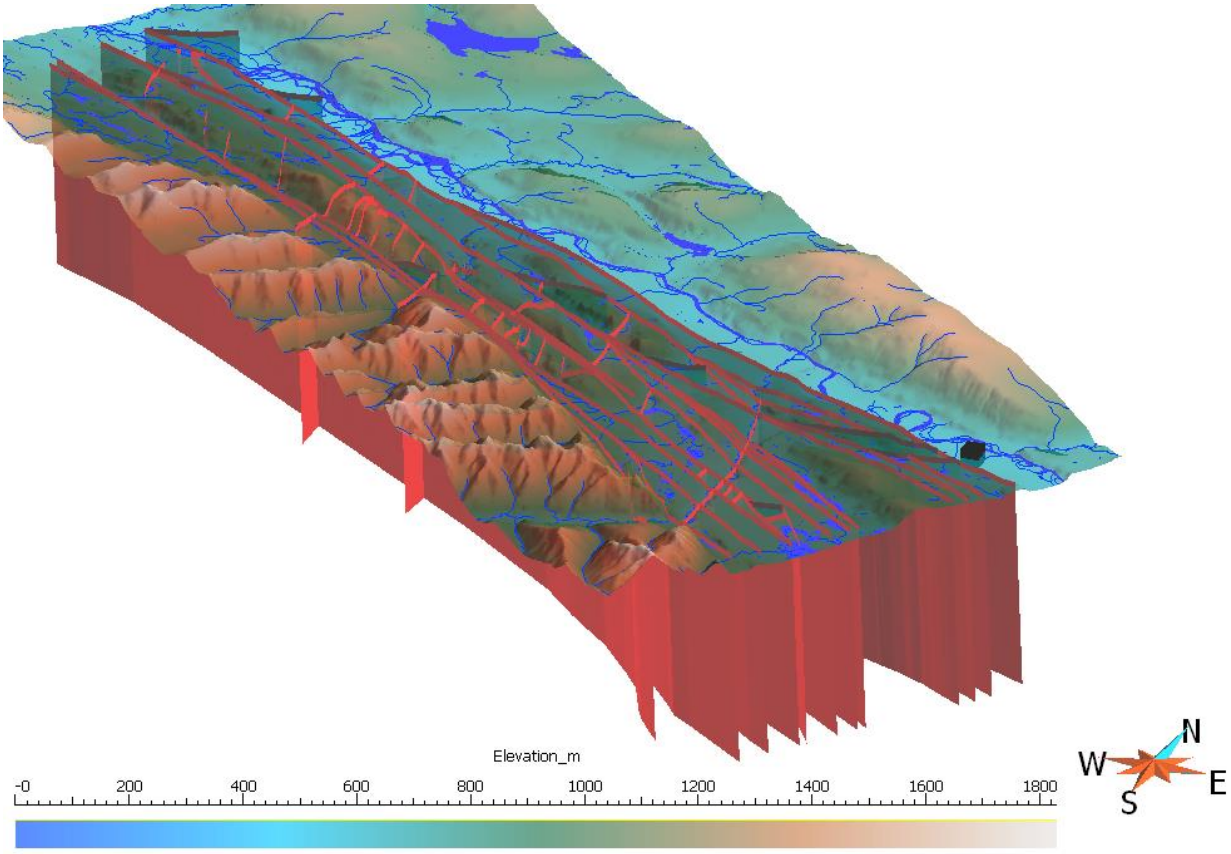

Figure 4. 3D perspective view showing the network of faults (red) compiled for the project by University of Nevada researchers. View looking to the north-northwest. The faults have been extrapolated vertically to a depth of ~3 km below sea level for visualization purposes. Semi-transparent topography and waterbodies have been overlain. The location of Ross River town is shown by the black cube.

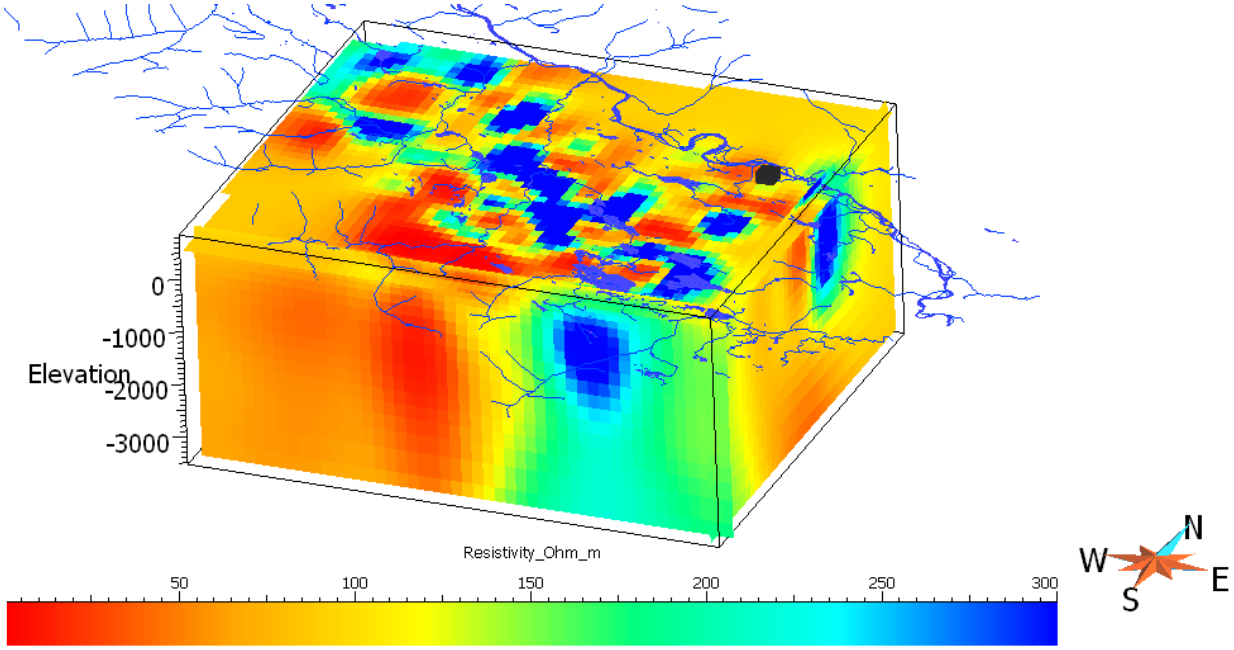

Figure 5. 3D perspective view of the resistivity block model generated from the MT data. View looking to the north-northwest. The elevation scale bar is in metres below sea level. Rivers and lakes are overlain to provide a geographic context. The location of Ross River town is shown by the black cube

Mira Geoscience
...modelling the earth

4. Interpretation of the Geoscience Data

Major conclusions to come out the interpretation of the different geoscience datasets, and what they mean for the geothermal exploration program, are summarized here.

A geologic literature review of the southern Yukon revealed that the rocks in the project area are being compressed by plate tectonic forces in a direction oriented approximately NNE-SSW. The structural analysis of the fold, fracture, and fault measurements made in the field corroborate this conclusion. The new structural measurements suggest that the modern day principle tectonic stress orientation for the Ross River area is NNE-SSW to NE-SW. This is important because faults and fractures oriented parallel or sub-parallel to this direction (e.g. N-S) have the greatest potential to be open and allow fluid flow. Thus, in our exploration program, we have focussed our search for geologic structures that are oriented approximately N-S (Figure 6). We also searched for areas where two faults intersect on the basis that fault intersections may be regions of highly fractured rock, more conducive to fluid flow. Based upon our analysis of the geologic and magnetic data, we have been able to successfully identify many locations within the project area with N-S oriented structures and zones of fault intersections. We have proposed many of these areas as targets for the shallow exploratory drilling program.

Another goal of the exploration effort was to use our understanding of the surface geology in conjunction with the two 3D geophysical models (magnetic and resistivity) in an attempt to improve our understanding of the geometry of the major blocks of bedrock extending from the surface down underground. In this way, we could potentially build a 3D geological model of the project area. The motivation here is that if we understand where all the different rock types are in 3D space as well as the faults that separate them, then we can better test ideas about where geothermal fluids are likely to flow.

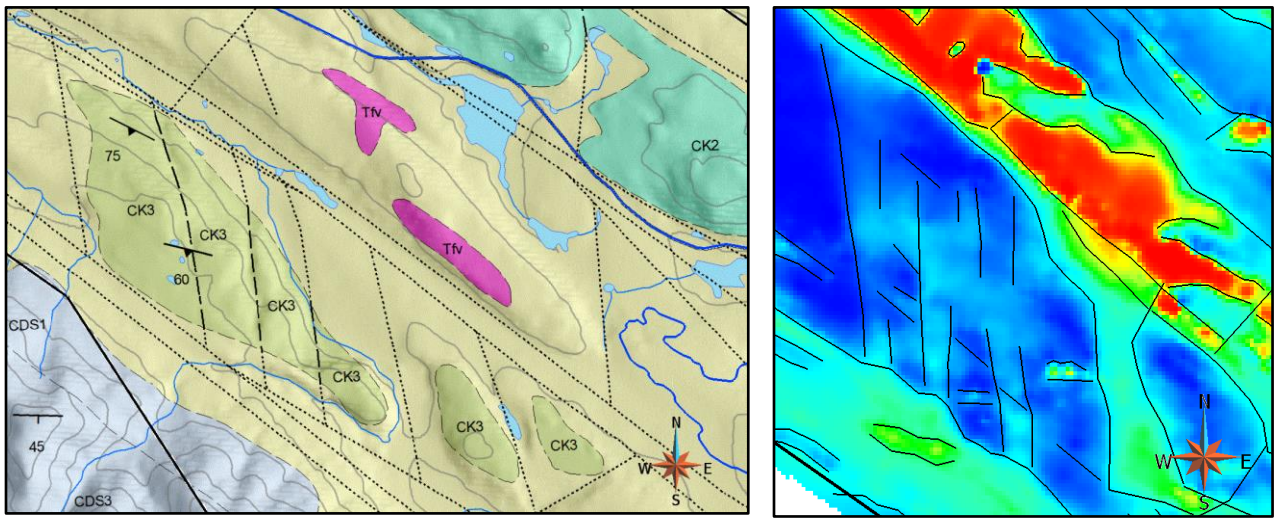

Figure 6. Examples of N-S oriented geologic structures which may be conducive to geothermal fluid flow. Left: N-S structures from the central-south portion of the project area inferred from analysis of the geologic data (geologic map shown as background). Right: N-S structures from the central-north portion of the project area inferred from 2D analysis of the magnetic data (magnetic map as background).

This effort proved to be more challenging than anticipated. First, field measurements showed that the magnetic properties of the principle bedrock units exposed at the surface are, for the most part, quite similar. Thus, it is difficult to clearly differentiate one bedrock type from another based upon the maps of magnetic data or the 3D magnetic model. Interpretation of the geologic maps suggests that there is a pull-apart basin located between the Grew Creek Fault and the Danger Creek Fault (that is filled with Tertiary rocks). As mentioned earlier, this pull-apart basin is an area that has undergone extension and may be more geothermally prospective. Unfortunately, the 3D geometry and boundaries of this pull-apart basin are difficult to discern using the magnetic model. The 3D magnetic model, however, has proven useful to help identify and characterize other rock types in the project area which have stronger magnetic property contrasts, such as Tertiary basalts and reversely magnetized intrusive rocks. Further study of the 3D magnetic model and comparison with exploratory drilling results may allow us to better interpret the magnetic model.

The 3D resistivity model, generated from the MT data, was also utilized in the effort to interpret geology in 3D. The relatively wide spacing of the MT stations (1-2 km) meant that the 3D resistivity model is less sensitive to geologic structure in areas shallower than ~1 km. As a result, 3D mapping of geology using the resistivity model was most useful at greater depths. The 3D resistivity model revealed many areas of low resistivity in the subsurface, particularly to the SW of the Tintina Fault and to the NE of the Danger Creek Fault (Figure 7). These areas of low resistivity can be explained by the presence of graphite and/or sulfide minerals in the rock. Alternatively, the low resistivity signature could be due to highly porous rocks saturated with geothermal waters. Graphitic rock outcrops occur to the SW of the Tintina Fault (unit CDS3: Paleozoic sedimentary rocks) and are likely the cause of the low resistivity zones observed there. The distribution of graphite- and sulfide-bearing rocks on the NE side of the Danger Creek Fault, however, is less clear. Whether the low resistivity zones NE of the Danger Creek Fault represent cold, low resistivity rocks rich in graphite/sulfides or warm, porous rock with geothermal fluids can best be tested with exploratory drilling.

An unexpected outcome of the exploration program is the identification of large bodies of what may be granitic rock deep in the subsurface (Figure 8). Evidence from both the 3D magnetic model and the 3D resistivity model suggest that much of the area between the Tintina Fault and the Danger Creek Fault are likely underlain by large volumes of crystalline bedrock (e.g. granite) at depths greater than 1-2 km beneath the surface. Crystalline bedrock can be important to geothermal exploration for a number of reasons. First, some types of granite contain unusually high concentrations of radioactive elements which produce heat which can drive low temperature geothermal systems. One example of this is the Chena Hot Springs area in central Alaska (Kolker, 2008). It is not known if granitic rock in the Ross River area contains high concentrations of radioactive elements. However, if large bodies of crystalline rock inferred to lie in the Tintina Fault Zone are in actuality highly radiogenic granite, then they may provide a viable geothermal heat source. Furthermore, fractured crystalline rocks can provide

excellent vertical pathways for geothermal fluids (as opposed to clay-rich rocks such as shale). Based upon the 3D geophysical modelling, it appears that several faults within the Tintina Fault Zone slice through the inferred, deep-seated crystalline rock bodies. Such a scenario could potentially create the permeability pathways that could promote deep circulation and heating of geothermal waters.

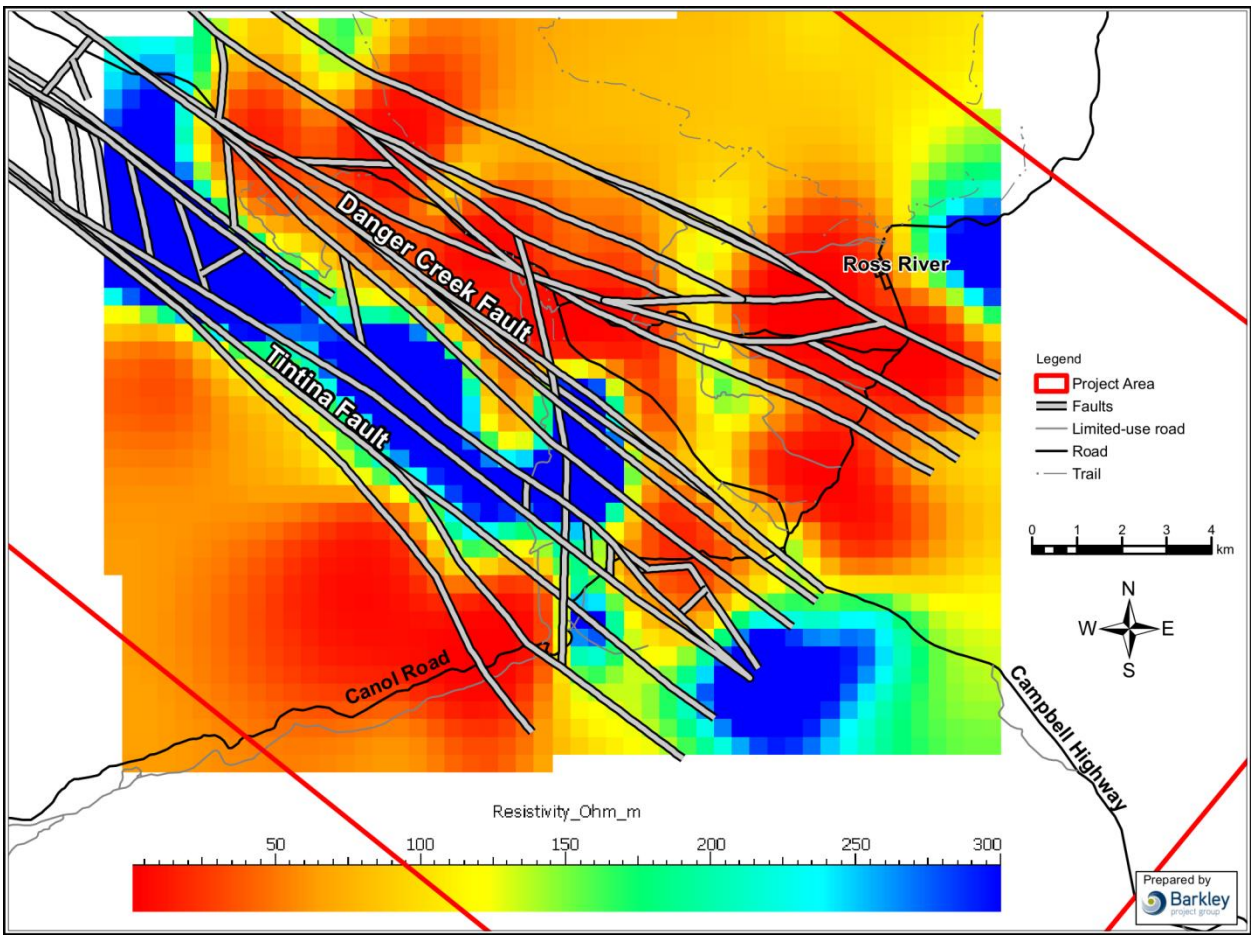

Figure 7. Map view of a horizontal slice of the 3D resistivity model. Slice shown is ~1 km below the ground surface. The color ramp shows areas of high resistivity in blue and areas of low resistivity in red. Faults are overlain (thick grey lines).

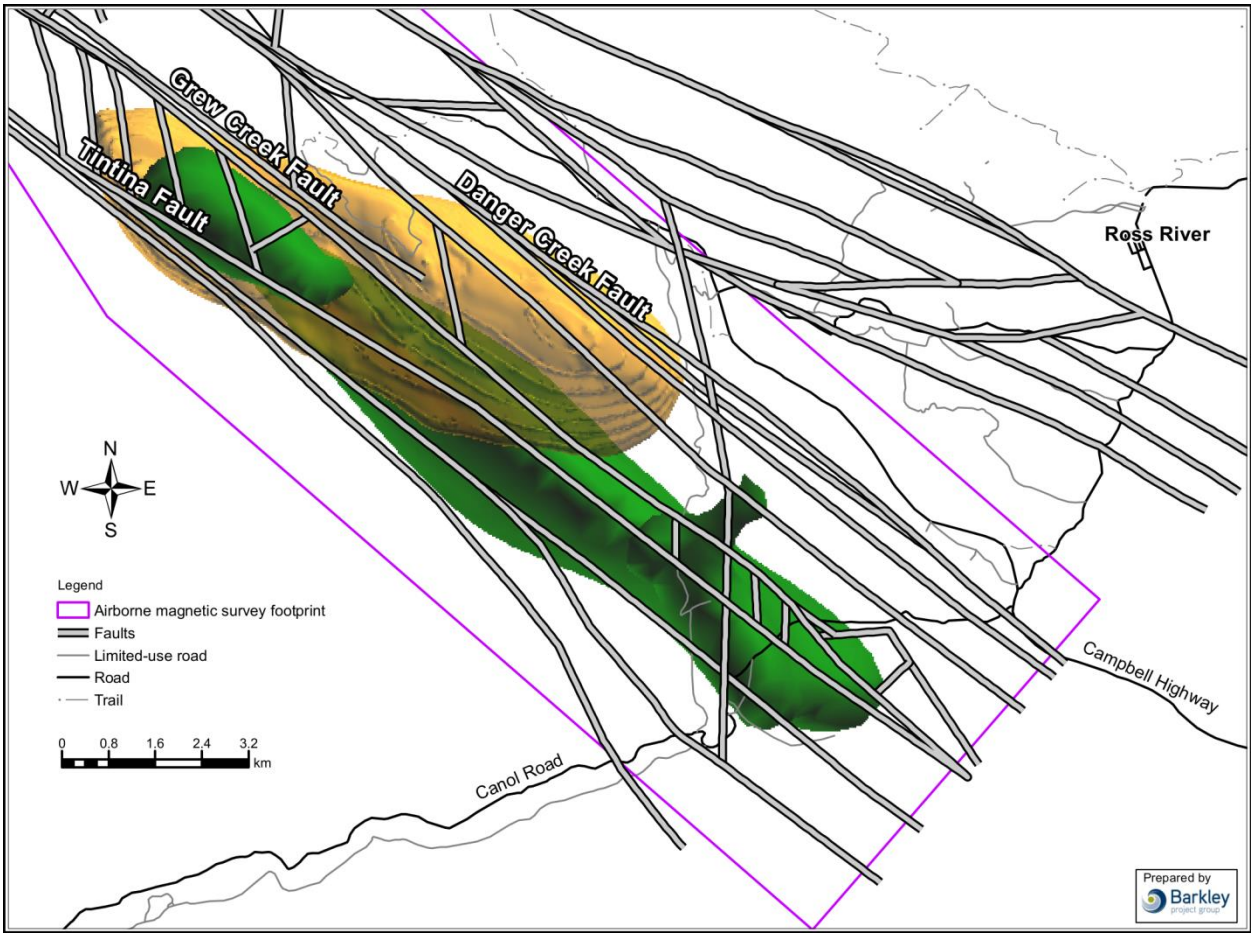

Figure 8. Map view snapshot of the southern half of the airborne magnetic survey (purple polygon) showing the location of some of the inferred deep (>1 km) granite bodies and the many faults (thick grey lines) that cross-cut them. The inferred locations of the granite bodies were derived from the 3D magnetic model (yellow) and the 3D resistivity model (green). Many of the faults shown here may not extend as deep as the granite but the NW-SE trending strands of the Tintina Fault Zone likely do. Extensive faulting through a crystalline rock body would likely enhance vertical permeability and geothermal fluid flow. Additional inferred granite bodies lie to the NW in the northern half of the airborne magnetic survey.

Mira Geoscience
...modelling the earth

5. Conclusions and Recommendations

Overall, the 2014 Ross River exploration program was successful. New geoscience data was collected at the project area in a well-executed field program. Other high quality geoscience data were obtained in a cost-effective manner through purchase from a third party. All of the new geoscience data was analysed and interpreted according to plan. The magnetic and geological information proved particularly useful in this exploration program and the evidence obtained from these datasets was used as criteria to justify the locations of many of the proposed drillsites. In summary, we recommend that this project move forward to the shallow exploratory drilling stage.

It must be noted that none of the methods used in this initial exploration program indicate where it will be “hot” in the subsurface. It is possible that every drilling location proposed here is “cold” and the project may be abandoned after the exploratory holes are drilled. What we have accomplished in the present effort is we have used modern scientific techniques and tapped experts in the field of subsurface exploration to identify what we believe are the locations most likely to exhibit elevated subsurface temperatures. We feel that now it is time to test these locations by drilling.

We recommend the following for the exploratory drilling program:

- Obtain drilling permits from the Yukon government for all of the proposed drilling locations.
- Conduct a site visit to each of the proposed drill sites to determine the exact geographic location of the proposed drilling and record the location with GPS and a labeled, wooden stake.
- Discuss among the project team to decide exactly which sites will be drilled and assign priorities based upon the available geological, geophysical and physiographic observations. Drill as many sites as the 2015 budget will allow.
- Prepare a drill plan and provide it to the drilling contractor prior to drilling.

- Drill 200 – 300 m deep holes to reach well below permafrost and glacial overburden.
- Have a geologist on-site during drilling to examine the drill core/cuttings and record the downhole geology encountered in each hole.
- Measure the magnetic susceptibility of the core/cuttings obtained from each drillhole.
- Collect a water sample from the bottom of each drillhole and have the water chemistry analysed for geothermometry purposes.
- After drilling, install capped tubing to the bottom of each hole to prevent hole collapse and allow downhole temperature readings to equilibrate for a period of weeks-to-months after drilling is complete. Mitigation measures must be taken to avoid freeze up in the portions of the hole that lie in permafrost.
- Measure the temperature profile down each hole multiple times (e.g. after 1 month, 3 months, and 6 months) until the hole has reached thermal equilibrium with the surrounding rocks.
- Evaluate the thermal influence of the last Ice Age on the measured downhole temperature profiles (i.e. the paleoclimatic correction of Majorowicz (2012)).

6. Acknowledgements

We would like to thank Don Murphy and Maurice Colpron from the Yukon Geological Survey for their suggestions, comments, and general support of this geothermal exploration program. We also acknowledge financial support from CanNor, Yukon Energy, the Yukon government, and the Kaska Nation.

Mira Geoscience
...modelling the earth

References

Christie, A.R., Duke, J.L., Rushton, R., 1992, Grew Creek epithermal gold-silver deposit, Tintina Trench, Yukon. *in:* Yukon Geology, Vol. 3, Exploration and Geological Services Division, Yukon, Indian and Northern Affairs, Canada, p. 223-259.

Hyndman, R.D., Flück, P., Mazzotti, S., Lewis, T.J., Ristau, J., Leonard, L., 2005, Current tectonics of the northern Canadian Cordillera. Can. J. Earth Sci., 42, p. 1117-1136.

Kolker, A.M., 2008, Geologic Setting of the Central Alaskan Hot Springs Belt: Implications for Geothermal Resource Capacity and Sustainable Energy Production. Ph.D. Thesis, University of Alaska, Fairbanks, 203 pages.

Leonard, L.J., Mazzotti, S., Hyndman, R.D., 2008, Deformation rates estimated from earthquakes in the northern Cordillera of Canada and eastern Alaska. J. Geophys. Res. v. 113, 18 pages.

Lewis, T.J., Hyndman, R.D., Flück, P., 2003, Heat flow, heat generation, and crustal temperatures in the northern Canadian Cordillera: thermal control of tectonics. J. Geophys. Res., v. 108, no. B6, 18 pages.

Majorowicz, J., 2012, Permafrost at the Ice Base of Recent Pleistocene Glaciations – Inferences from Borehole Temperature Profiles. Bulletin of Geography – Physical Geography Series, No. 5, p. 7-28.

Plouffe, A. and Jackson, L.E., Jr., 1995, Quaternary stratigraphy and till geochemistry in the Tintina Trench, near Faro and Ross River, Yukon Territory. *in:* Drift Exploration in the Canadian Cordillera, Bobrowsky, P.T., Sibbick, S.J., Newell, J.M., and Matysek, P.F., Editors, British Columbia Ministry of Energy, Mines, and Petroleum Resources, Paper 1995-2, p. 53-66.

Yukon Geological Survey, 2014, Update of the Yukon Bedrock Geology Map: Yukon Geological Survey digital data, 1:250,000 scale, http://www.geology.gov.yk.ca/update_yukon_bedrock_geology_map.html

Mira Geoscience
...modelling the earth

Appendix 1: Airborne Magnetic Data Acquisition Report by Precision GeoSurveys

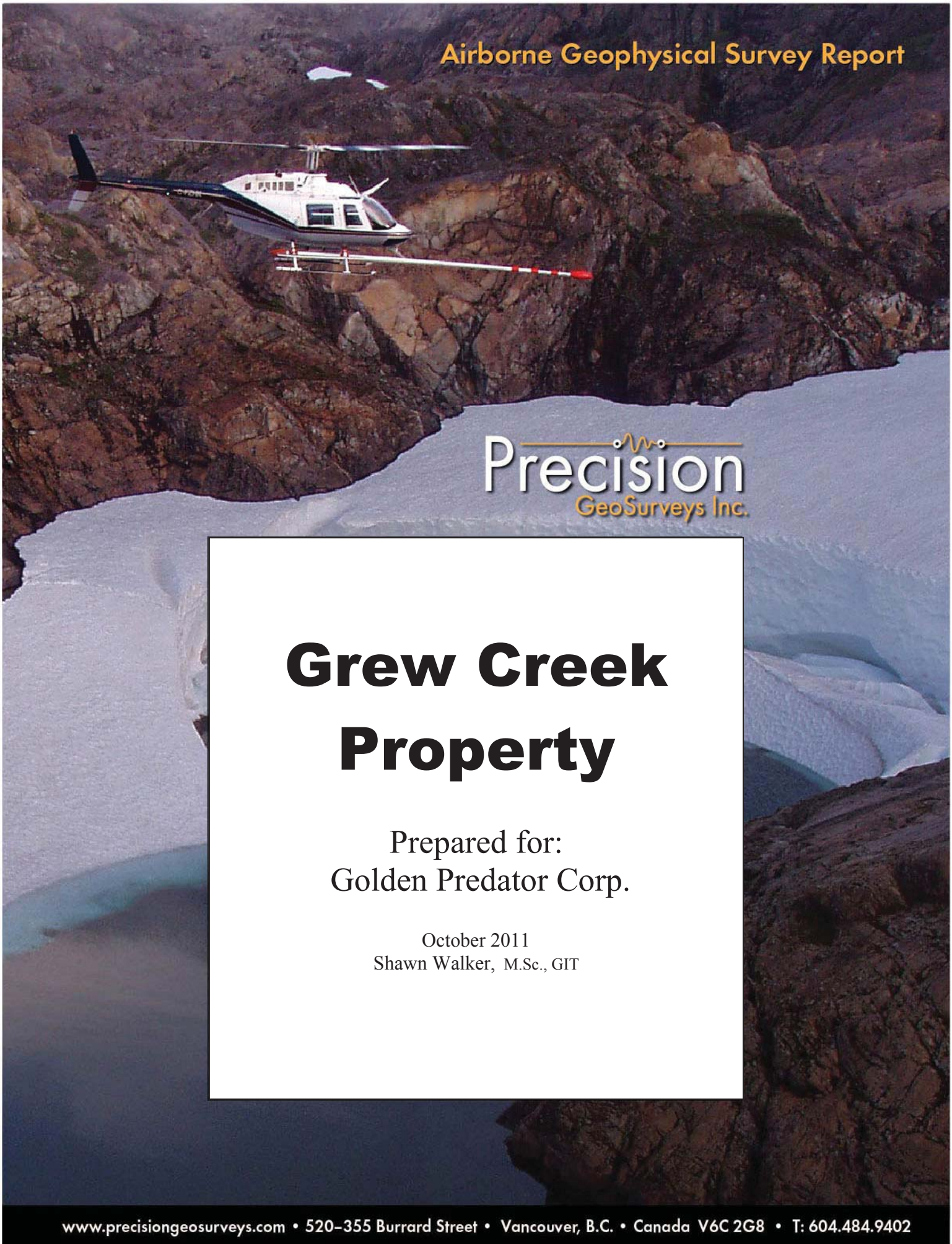

Grew Creek Property

Prepared for:
Golden Predator Corp.

October 2011

Shawn Walker, M.Sc., GIT

www.precisiongeosurveys.com • 520–355 Burrard Street • Vancouver, B.C. • Canada V6C 2G8 • T: 604.484.9402

Table of Contents

1.0 Introduction:

This report outlines the survey operations and data processing actions taken during the airborne geophysical survey flown at Grew Creek. The airborne geophysical survey was flown by Precision GeoSurveys Inc. for Golden Predator Corp. The geophysical survey, carried out between June 18, 2011 and July 23, 2011, saw the acquisition of gamma ray spectrometer data and magnetic data.

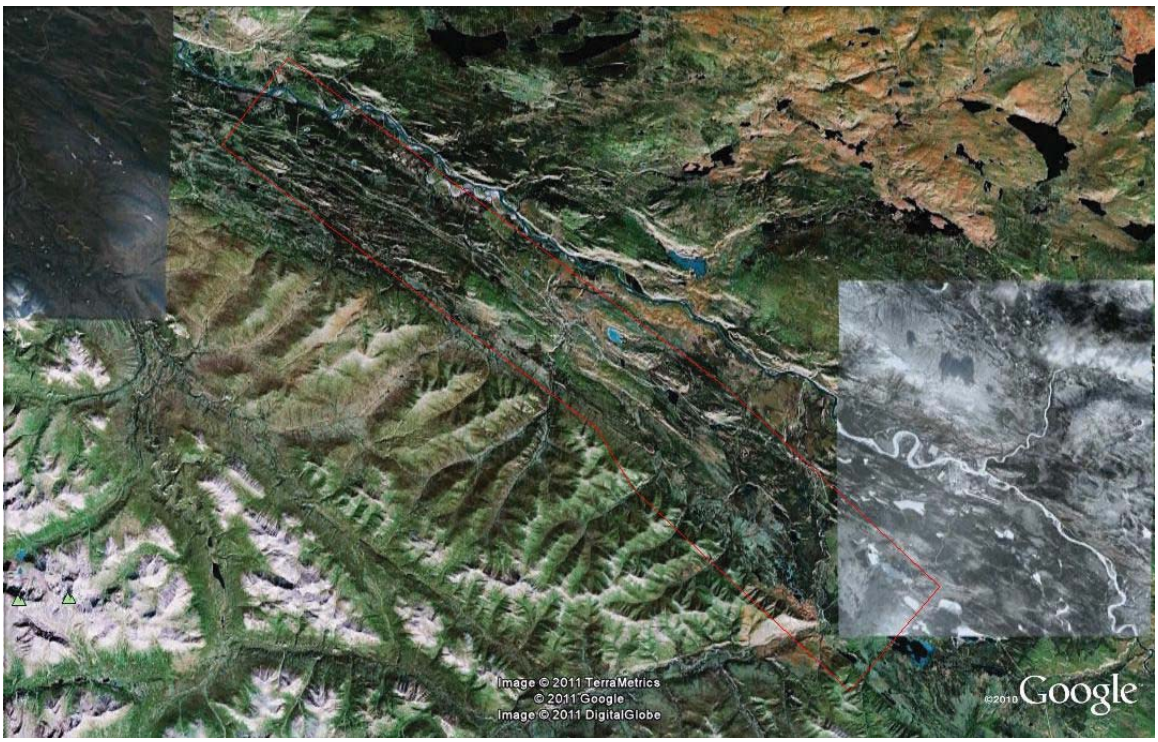

Figure 1: Grew Creek Property (outlined in red) with respect to the Pelly River, YT.

The Grew Creek property lies in the Pelly River valley along the Robert Campbell Highway, YT (Figure 1) and approximately 10 km east of Faro, YT (Figure 2). The survey area itself is approximately 45 km by 7 km. A total of 3310 line kilometers of radiometric and magnetic data were flown for this survey, this total includes tie lines and survey lines. The survey lines were flown at 100 meter spacing's at a 45°/225° heading; the tie lines were flown at 1 km spacing's at a heading of 135°/315° (Figure 3).

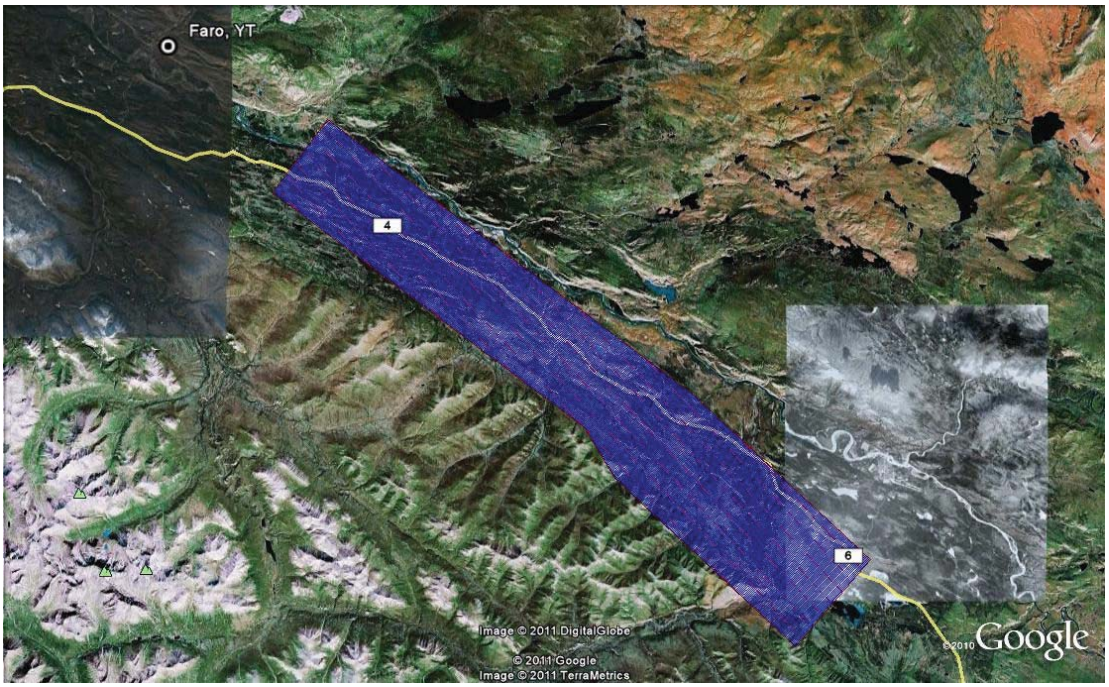

Figure 2: Survey are location relative to Faro,YT. Survey lines are in blue, tie lines are in red and the boundary in dark red in plan view.

Figure 3: Proposed survey basemap of Grew Creek grid showing survey (blue) and tie lines (red) and the boundary (dark red).

1.1 Survey Specifications:

The geodetic system used for this survey is WGS 84 and the area is contained in zone 8N. The survey data acquisition specifications and coordinates for the Grew Creek survey are specified as follows (Table 1 and Table 2).

Survey Block Name	Line Spacing m	Survey Line km	Tie Line km	Total Line km	Survey Line Orientation	Nominal Survey Height m
Grew Creek	100	3008.4	301.2	3310	045 º /225º	35
Total				3310		

Table 1: Grew Creek survey acquisition specifications.

Longitude	Latitude	Easting	Northing
132.4683261	61.9269540	632895.5	6868634
132.5659977	61.8778785	627975.0	6862974
132.7886543	61.9759050	615899.7	6873471
132.8267748	62.0057652	613790.9	6876728
133.2196306	62.1433391	592804.1	6891423
133.1509590	62.1865699	596245.6	6896338
132.6910202	62.0251379	620820.1	6879131

Table 2: Grew Creek survey polygon coordinates using WGS 84 in zone 8N.

2.0 Geophysical Data:

Geophysical data are collected in a variety of ways and are used to aid in the exploration and determination of geology, mineral deposits, oil and gas deposits, contaminated land sites and UXO detection.

For the purposes of this survey, airborne gamma ray spectrometer and magnetic data were collected to serve in the exploration of the Grew Creek property which is host to structurally controlled epithermal gold mineralization.

2.1 Magnetic Data:

Magnetic surveying is probably the most common airborne survey type to be conducted for both mineral and hydrocarbon exploration. The type of survey specifications, instrumentation, and interpretation procedures, depend on the objectives of the survey. Typically magnetic surveys are performed for:

1. Geological Mapping to aid in mapping lithology, structure and alteration in both hard rock environments and for mapping basement lithology, structure and alteration in sedimentary basins or for regional tectonic studies.
2. Depth to Basement mapping for exploration in sedimentary basins or mineralization associated with the basement surface.

2.2 Radiometric Data:

Radiometric surveys detect and map natural radioactive emanations, called gamma rays, from rocks and soils. All detectable gamma radiation from earth materials come from the natural decay products of three primary elements; uranium, thorium, and potassium. The purpose of radiometric surveys is to determine either the absolute or relative amounts of U, Th, and K in surface rocks and soils.

3.0 Survey Operations:

Precision GeoSurveys flew the Grew Creek property using a Bell 206 BIII Jet Ranger (Figure 4). The survey lines were flown at a nominal line spacing of one hundred (100) meters and the tie lines were flown at 1 km spacing for both the spectrometer and magnetometer as they were acquired simultaneously. The average survey elevation was 40 meters vertically above ground. The experience of the pilot helped to ensure that the data quality objectives were met and that the safety of the flight crew was never compromised given the potential risks involved in airborne surveying.

Figure 4: Bell 206 Jet Ranger equipped with mag stinger for magnetic data acquisition.

The base of operations for this survey was the town of Faro, YK located approximately 350 km north-east of Whitehorse, YT on the Robert Campbell Highway. The Precision crew consisted of a total of four members:

Don Intermela and John Witham – Pilots
Mike Jensen – Operator
Shawn Walker – On-site Geophysicist

The survey was started on June 18, 2011 and completed on July 23, 2011. The survey encountered several delays due to equipment issues as well as magnetic storms and inclement weather.

4.0 Equipment:

For this survey, a magnetometer, spectrometer, base station, laser altimeter, and a data acquisition system were required to carry out the survey and collect quality, high resolution data. The survey magnetometer is carried in an approved "stinger" configuration to enhance flight safety and improve data quality in mountainous terrain.

4.1 AGIS:

The Airborne Geophysical Information System, AGIS, (Figure 5), is the main computer used in data recording, data synchronizing, displaying real-time QC data for the

geophysical operator, and generation of navigation information for the pilot display system.

Figure 5: AGIS installed in the Bell 206.

The AGIS was manufactured by Pico Envirotec; therefore the system uses standardized Pico software and external sensors are connected to the system via RS-232 serial communication cables. The AGIS data format is easily converted into Geosoft or ASCII file formats by a supplied conversion program called PEIView. Additional Pico software allows for post real time magnetic compensation and survey quality control procedures.

4.2 Spectrometer:

The IRIS, or Integrated Radiometric Information System is a fully integrated, gamma radiation detection system containing two downward facing NaI detecting crystals for a total volume of 8.4 litres (Figure 6). The IRIS is equipped with upward-shielding high density RayShield® gamma-attenuating material to minimize cosmic and solar gamma noise. Real time data acquisition, navigation and communication tasks are integrated into a single unit that is installed in the rear of the aircraft as indicated below. Information such as total count, counts of various radioelements (K, U, Th, etc.), temperature, barometric pressure, atmospheric humidity and survey altitude can all be monitored on the AGIS screen for immediate QC. All the radiometric data are recorded at 1 Hz.

Figure 6: IRIS strapped into the cargo box of the helicopter.

4.3 Magnetometer:

The magnetometer used by Precision GeoSurveys is a Scintrex cesium vapor CS-3 magnetometer. The system was housed in a front mounted "stinger" (Figure 7). The CS-3 is a high sensitivity/low noise magnetometer with automatic hemisphere switching and a wide voltage range, the static noise rating for the unit is +/- 0.01 nT. On the AGIS screen the operator can view the raw magnetic response, the magnetic fourth difference, aircraft position, and the survey altitude for immediate QC of the magnetic data. The magnetic data are recorded at 10 Hz. A magnetic compensator is also used to remove noise created by the movement of the helicopter as it pitches, rolls and yaws within the Earth's geomagnetic field.

Figure 7: View of the mag stinger.

4.4 Base Station:

For monitoring and recording of the Earth's diurnal magnetic field variation, Precision GeoSurveys uses two base stations: Scintrex proton precession Envi Pro magnetometer and GEM GSM-19T magnetometer. Both base stations are mounted as close to the survey blocks as possible to give accurate magnetic field data. The Envi Pro base station (Figure 8), uses the well proven precession technology to sample at a rate of 0.5 Hz. A GPS is integrated with the system to record real GPS time that is used to correlate with the GPS time collected by the airborne CS-3 magnetometer.

Figure 8: Scintrex Envi Pro proton precession magnetometer.

The GEM GSM-19T magnetometer (Figure 9) also uses the proton precession technology sampling at a rate of 0.5 Hz. The GSM-19T has an accuracy of +/- 0.2 nT at 1 Hz.

Figure 9: GEM GSM-19T proton precession magnetometer.

4.5 Laser Altimeter:

The pilot is provided with terrain guidance and clearance with an Acuity AccuRange AR3000 laser altimeter (Figure 10). This is attached at the aft end of the magnetometer boom. The AR3000 sensor is a time-of-flight sensor that measures distance by a rapidly-modulated and collimated laser beam that creates a dot on the target surface. The maximum range of the laser altimeter is 300 m off of natural surfaces with 90% reflectance and 3 km off special reflectors. Within the sensor unit, reflected signal light is collected by the lens and focused onto a photodiode. Through serial communications and analog outputs, the distance data are transmitted and collected by the AGIS at 10 Hz.

Figure 10: Acuity AccuRange AR3000 laser altimeter.

5.0 Data Processing:

After all the data are collected after a survey flight several procedures are undertaken to ensure that the data meet a high standard of quality. All data were processed using Pico Envirotec software and Geosoft Oasis Montaj geophysical processing software.

5.1 Magnetic Processing:

During aeromagnetic surveying noise is introduced to the magnetic data by the aircraft itself. Movement in the aircraft (roll, pitch and yaw) and the permanent magnetization of the aircraft parts (engine and other ferric objects) are large contributing factors to this noise. To remove this noise a process called magnetic compensation is implemented. The magnetic compensation process starts with a test flight at the beginning of the survey where the aircraft flies in the four orthogonal headings required for the survey (45°/225° and 135°/315° in the case of this survey) at an altitude where there is no ground effect in the magnetic data. In each heading, three specified roll, pitch and yaw maneuvers are performed by the pilot; these maneuvers provide the data that are required to calculate the

necessary parameters for compensating the magnetic data. A computer program called PEIComp is used to create a model for each survey to remove the noise induced by aircraft movement; this model is applied to each survey flight so the data can be further processed.

A lag correction of 0.8 seconds was applied to the total magnetic field data to compensate for the lag in the recording system as the magnetometer sensor flies 6.45 m ahead of the GPS antenna.

A magnetic base station is set up before every flight to ensure that diurnal activity is recorded during the survey flights. In this case, the base station was located close to the river just south of Faro. Base station readings were reviewed at regular intervals to ensure that no data were collected during periods with high diurnal activity (greater than 5 nT per minute). The base station was installed near the survey blocks at a magnetically noise-free area, away from metallic items such as steel objects, vehicles, or power lines. The magnetic variations recorded from the stationary base station are removed from the magnetic data recorded in flight to ensure that the anomalies seen are real and not due to solar activity.

Filtering is also applied to the laser altimeter data as to remove vegetation clutter and to show the actual ground clearance. To remove vegetation clutter a rolling statistic filter was applied to the laser altimeter data and a low pass filter was used to smooth out the laser altimeter profile to remove isolated noise. As a result, filtering the data will yield a more uniform surface in close conformance with the actual terrain.

Some filtering of the magnetic data is also required. A Non Linear filter was used for spike removal. The 1D Non-Linear Filter is ideal for removing very short wavelength, but high amplitude features from data. It is often thought of as a noise spike-rejection filter, but it can also be effective for removing short wavelength geological features, such as signals from surficial features. The 1D Non-Linear Filter is used to locate and remove data that are recognized as noise. The algorithm is 'non- linear' because it looks at each data point and decides if that datum is noise or a valid signal. If the point is noise, it is simply removed and replaced by an estimate based on surrounding data points. Parts of the data that are not considered noise are not modified. The combination of a Non-Linear filter for noise removal and a low pass trend enhancement filter resulted in level data as indicated in the results section of this report. The low pass filters simply smoothes out the magnetic profile to remove isolated noise.

5.2 Radiometric Processing:

Calibrating the spectrometer system in the helicopter is the first and vital step before the airborne radiometric data can be processed. Once calibration of the system has been complete, the radiometric data are processed by windowing the full spectrum to create channels for U, K, Th and total count. A 5-point Hanning filter was applied to the Cosmic window before going any further with processing the radiometric data.

Aircraft background and cosmic stripping corrections were applied to all three elements, upward uranium channels, and total count using the following formula:

$$C_{ac} = C_{lt} - (a_c + b_c * \mathrm{Cos}_f)$$

where: C_{ac} is the background and cosmic corrected channel
C_{lt} is the live time corrected channel
a_c is the aircraft background for this channel
b_c is the cosmic stripping coefficient for this channel
Cos_f is the filtered cosmic channel

The radon backgrounds are first removed followed by compton stripping. Spectral overlap corrections are applied on to potassium, uranium, and thorium as part of the compton stripping process. This is done by using the striping ratios that have been calculated for the spectrometer by prior calibration, this breaks the corrected elemental values down into the apparent radioelement concentrations. Lastly, attenuation corrections are applied to the data which involves nominal survey altitude corrections, in this case 34 metres is applied to total count, potassium, uranium, and thorium data.

With all corrections applied to the radiometric data, the final step is to convert the corrected potassium, uranium, and thorium to apparent radioelement concentrations using the following formula:

$$eE = C_{cor} / s$$

where: eE is the element concentration K(%) and equivalent element concentration of U(ppm) & Th(ppm)
s is the experimentally determined sensitivity
Ccor is the fully corrected channel

Finally, the natural air absorption dose rate is determined using the following formula:

$$E = 13.08 * K + 5.43 * eU + 2.69 * eTh$$

where: E is the absorption dose rate in nG/h
K is the concentration of potassium (%)
eU is the equivalent concentration of uranium (ppm)
eTh is the equivalent concentration of thorium (ppm)

To calculate for radiometric ratios it follows the guidelines in the IAEA report. Due to statistical uncertainties in the individual radioelement measurements, some care was taken in the calculation of the ratio in order to obtain statistically significant values. Following IAEA guidelines, the method of determining ratios of the eU/eTh, eU/K and eTh/K was as follows:

1. Any data points where the potassium concentration was less than 0.25 were neglected.
2. The element with the lowest corrected count rate was determined.
3. The element concentrations of adjacent points on either side of each data point were summed until they exceeded a certain threshold value. This threshold was set to be equivalent to 100 counts of the element with the lowest count rate. Additional minimum thresholds of 1.6% for Potassium, 20 ppm for thorium, and 30 ppm for uranium were set up to insure meaningful ratios.
4. The ratios were calculated using the accumulated sums.

With this method, the errors associated with the calculated ratios will be similar for all data points.

5.3 Final Data Format

Abbreviations used in the GDB files are listed in the following table:

Channel	Units	Description
X	m	UTM Easting - WGS84 Zone 7 North
Y	m	UTM Northing - WGS84 Zone 7 North
Galt_m	m	GPS height - WGS84 Zone 7 North
Lalt	m	Laser Altimeter readings
DTM	m	Digital Terrain Model
GPStime	Hours:min:secs	GPS time
basemag	nT	Base station diurnal data
mag	nT	Total Magnetic Intensity
BaltLC	m	Barometric Altitude
Baro_mb	millibar	Atmospheric Pressure
BAROmg_kP	KiloPascal	Atmospheric Pressure
BstpLC	m	Barometric Altitude (Pres and Temp Corrected)
RaltLC	m	Laser altimeter - Aircraft/sensor height
TempLC	Degrees C	Air Temperature
COSFILT	counts/sec	Spectrometer - Filtered Cosmic
TCcor	µR	Dose Rate Equivalent
Kcor	%	Equivalent Concentration - Potassium
Ucor	ppm	Equivalent Concentration - Uranium
THcor	ppm	Equivalent Concentration - Thorium
UpU_cps	counts/sec	Spectrometer RAW Counts - Upward Uranium
UPUTEMP	counts/sec	Spectrometer - Filtered Upward Uranium
THKratio		Spectrometer - eTh/%K ratio
UKratio		Spectrometer - eU/%K ratio
UTHratio		Spectrometer - eU/eTh ratio
Date	yyyy/mm/dd	Local Flight Date

Table 3: Grew Creek survey channel abbreviations.

The file format will be provided in two (2) formats, the first will be a .GDB file for use in Geosoft Oasis Montaj, the second format will be a .XYZ file, this is text file. A complete file provided in each format will contain both magnetic and radiometric data.

Appendix A

Equipment Specifications

Scintrex Envi Pro Proton Magnetometer with Integrated GPS (Base Station)

Total Field Operating Range	23,000 to 100,000 nT (gamma)
Total Field Absolute Accuracy	±1 nT (gamma)
Sensitivity	0.1 nT (gamma) at 2 second sampling rate
Tuning/ Sampling	Fully solid state. Manual or automatic, keyboard selectable Cycling (Reading) Rates 0.5, 1, 2, or 3 seconds
Gradiometer Option	Includes a second sensor, 0.5m (20 inch) staff extender and processor module
Gradient Tolerance	> 7000 nT (gamma)/m
'Walking' Mode	Continuous reading, cycling as fast as 0.5 seconds
Supplied GPS Accuracy	+/- 1m (Autonomous), < 1m WAAS Connects to most external GPS receivers with NMEA & PPS output
Standard Memory	**Total Field Measurements**: 84,000 readings **Gradiometer Measurements**: 67,000 readings **Base Station Measurements**: 500,000 readings
Real-Time Clock	1 second resolution, ± 1 second stability over 24 hours or GPS time
Digital Data Output	RS-232C, USB Adapter
Power Supply	Rechargeable, 2.9 Ah, lead-acid dry cell battery 12 Volts External 12 Volt input for base station operations
Operating Temperature	40°C to +60°C (-40°F to 140°F)
Dimensions and Weight	**Console**: 250mm x 152mm x 55mm (10" x 6" x 2.25") 2.45 kg (5.4 lbs) with rechargeable battery **Magnetic** 70mm d x 175mm (2.75"d x 7") **Sensor**: 1 kg (2.2 lbs) **Gradiometer** 70mm d x 675mm (2.75"d x 26.5") **Sensor**: (with staff extender) 1.15 kg (2.5 lbs) **Sensor Staff**: 25mm d x 2m (1"d x 76") 0.8 kg (1.75 lbs)

GEM GSM-19T Proton Precession Magnetometer (Base Station)

Configuration Options	15
Cycle Time	999 to 0.5 sec
Environmental	-40 to 60 ° Celsius
Gradient Tolerance	7,000 nT/m
Magnetic Readings	299,593
Operating Range	10, 000 to 120,000 nT
Power	12 V @ 0.62 A
Sensitivity	0.1 nT @ 1 sec
Weight (Console/ Sensor)	3.2 Kg
Integrated GPS	Yes

Scintrex CS-3 Survey Magnetometer

Operating Principal	Self-oscillation split-beam Cesium Vapor (non-radioactive Cs-133)
Operating Rage	15,000 to 105,000 nT
Gradient Tolerance	40,000 nT/metre
Operating Zones	10° to 85° and 95° to 170°
Hemisphere Switching	a) Automatic b) Electronic control actuated by the control voltage levels (TTL/CMOS) c) Manual
Sensitivity	0.0006 nT √Hz rms.
Noise Envelope	Typically 0.002 nT P-P, 0.1 to 1 Hz bandwidth
Heading Error	+/- 0.25 nT (inside the optical axis to the field direction angle range 15° to 75° and 105° to 165°)
Absolute Accuracy	<2.5 nT throughout range
Output	a) continuous signal at the Larmor frequency which is proportional to the magnetic field (proportionality constant 3.49857 Hz/nT) sine wave signal amplitude modulated on the power supply voltage b) square wave signal at the I/O connector, TTL/CMOS compatible
Information Bandwidth	Only limited by the magnetometer processor used
Sensor Head	Diameter: 63 mm (2.5”) Length: 160 mm (6.3”) Weight: 1.15 kg (2.6 lb)
Sensor Electronics	Diameter: 63 mm (2.5”) Length: 350 mm (13.8”) Weight: 1.5 kg (3.3 lb)
Cable, Sensor to Sensor Electronics	3m (9’ 8”), lengths up to 5m (16’ 4”) available
Operating Temperature	-40°C to +50°C
Humidity	Up to 100%, splash proof
Supply Power	24 to 35 Volts DC
Supply Current	Approx. 1.5A at start up, decreasing to 0.5A at 20°C
Power Up Time	Less than 15 minutes at -30°C

RMS Herz TOTEM-2A Multi-channel VLF Electromagnetic System

Primary Source	Magnetic field component radiated from remote or local VLF radio transmitters (one or two simultaneously)
Parameters Measured	Total field, vertical quadrature, horizontal quadrature and gradient
Frequency Range	15 kHz to 25 kHz; front panel selectable for each channel in 100 Hz steps
Sensitivity Range	130 mV m to 100 mV m at 20 kHz, 3 db down at 14 kHz and 24 kHz
VLF Signal Bandpass	-3 dB at +80 Hz; < 4% variation at +50 Hz
Adjacent Channel Rejection	300 to 800 Hz = 20 to 32 dB; 800 to 1500 Hz = 32 to 40 dB; > 1500 Hz > 40 dB (for < 2% noise envelope)
Out of Band Rejection	10 kHz to 2.5 kHz = 5 x 10-4 Am to 5 x 10 -1 Am < 2.5 kHz rising at 12 db octave; 30 kHz to 60 kHz = 5 x 10-4 Am to 8 x 10-3 Am > 60 kHz rising at 6 dB octave (for no overload condition)
Output Filter	Time constant 1 sec. for 0% to 50% or 10% to 90%, noise bandwidth 0.3 Hz (second order LP)
Internal Noise	1.3 mV m rms (ambient noise will exceed this)
Electric Field Rejection	< 0.5% error for 20 m tow cable
Sferics Filter	Reduces noise contribution of impulse filter
Controls	Power switch, frequency selector switches (Line and Ortho), meter switch (total quad), and sferics filter switch
Displays	Meters (Line and Ortho), sferics light, overload light

Pico Envirotec AGIS data recorder system
(for Navigation, Gamma spectrometer, VLF-EM and Magnetometer Data Acquisition)

Functions	Airborne Geophysical Information System (AGIS) with integrated Global Positioning System Receiver (GPS) and all necessary navigation guidance software. Inputs for geophysical sensors - portable gamma ray spectrometer GRS-10, MMS4 Magnetometer, Totem 2A EM, A/D converter, temperature probe, humidity probe, barometric pressure probe, and laser altimeter. Output for the 2 line Pilot Indicator
Display	Touch screen with display of 800 x 600 pixels; customized keypad and operator keyboard. Multi-screen options for real-time viewing of all data inputs, fiducial points, flight line tracking, and GPS channels by operator.
GPS Navigation	Garmin 12-channel, WAAS-enabled
Data Sampling	Sensor dependent
Data Synchronization	Synchronized to GPS position
Data File	PEI Binary data format
Storage	80 GB
Supplied Software	**PEIView:** Allows fast data Quality Control (QC) **Data Format:** Geosoft GBN and ASCII output **PEIConv**: For survey preparation and survey plot after data acquisition
Software	**Calibration:** High voltage adjustment, linearity correction coefficients calculation, and communication test support **Real Time Data Collection:** Automatic Gain real time control on natural isotopes and PC based test and calibration software suite
Power Requirements	24 to 32 VDC
Temperature	Operating:-10 to +55 deg C; storage:-20 to +70 deg C

Appendix B

Maps

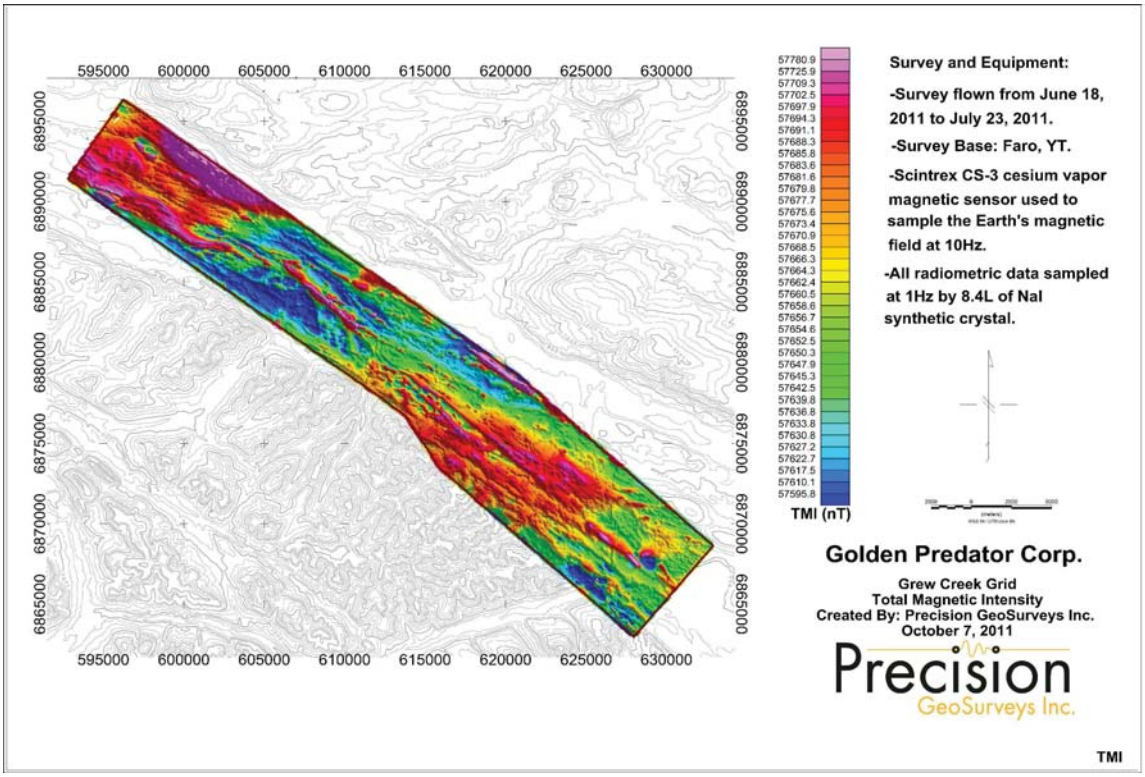

Map 1: Grew Creek Grid - Total Magnetic Intensity.

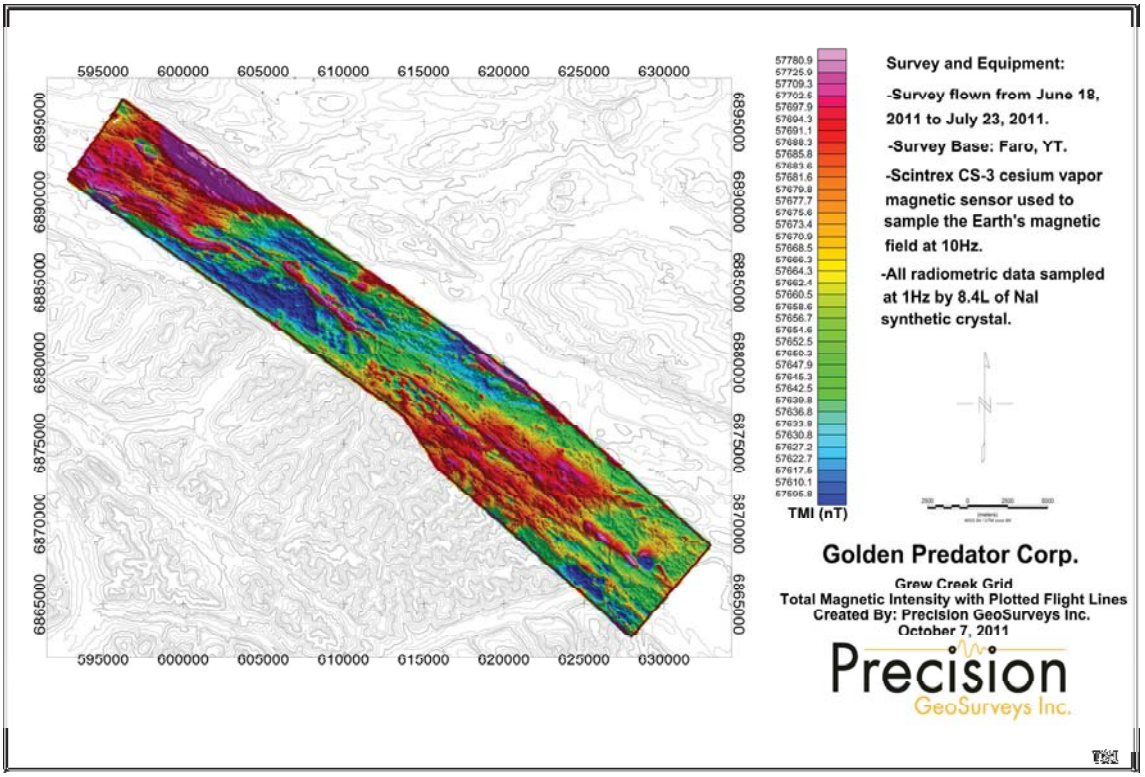

Map 2: Grew Creek Grid - Total Magnetic Intensity with plotted flight lines.

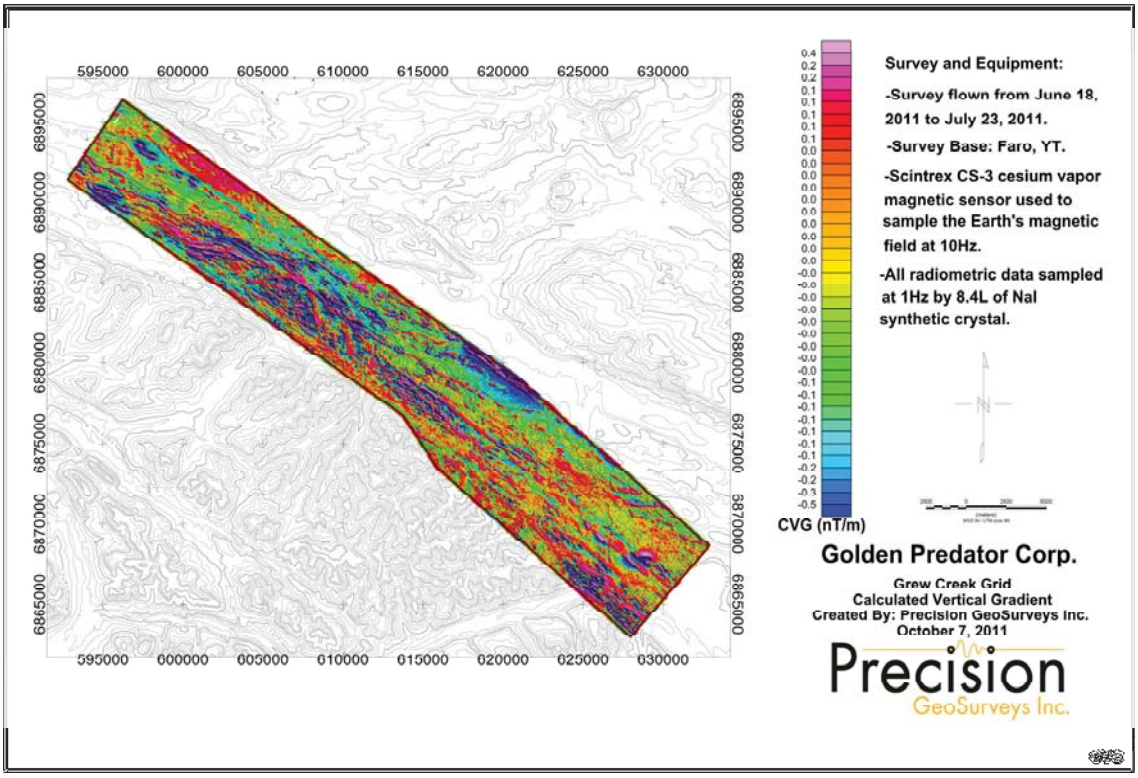

Map 3: Grew Creek Grid - Calculated Vertical Gradient.

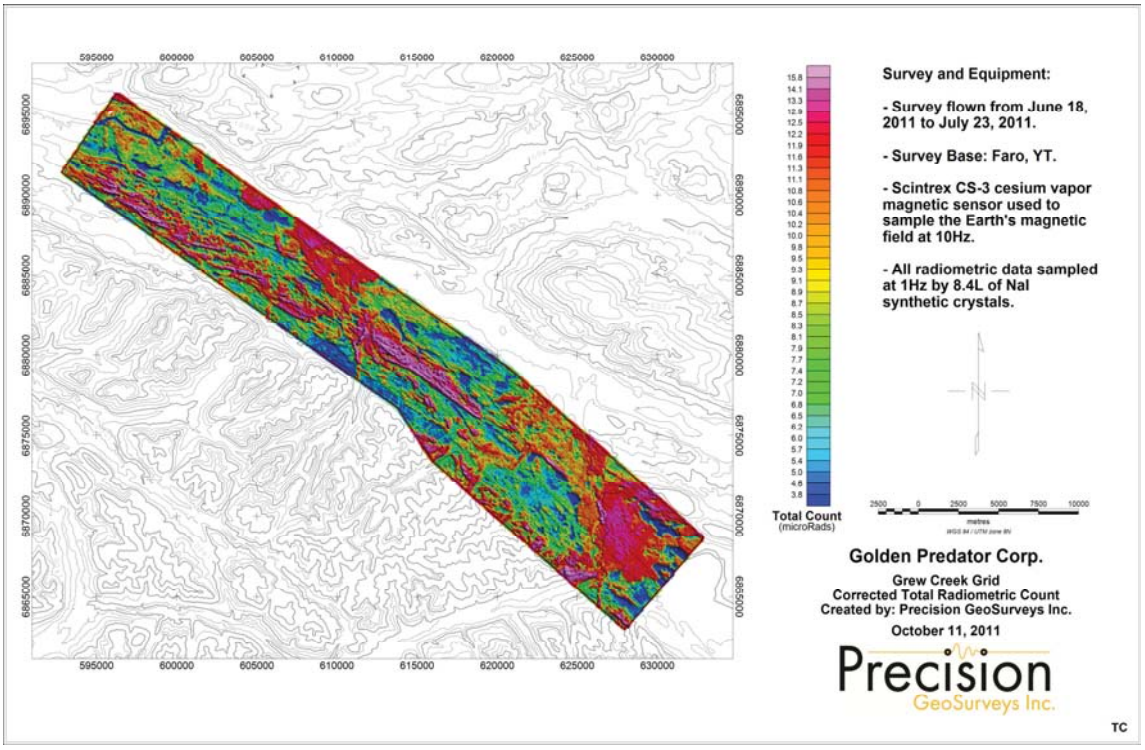

Map 4: Grew Creek Grid - Corrected Total Radiometric Count

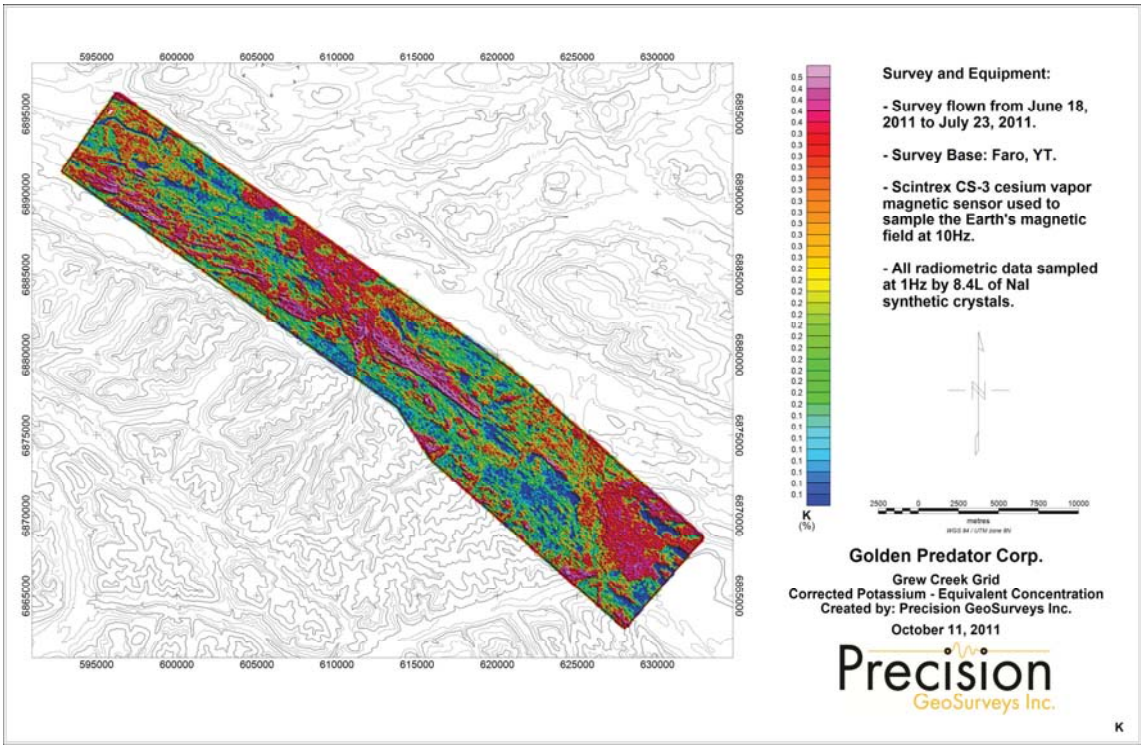

Map 5: Grew Creek Grid - Corrected Potassium

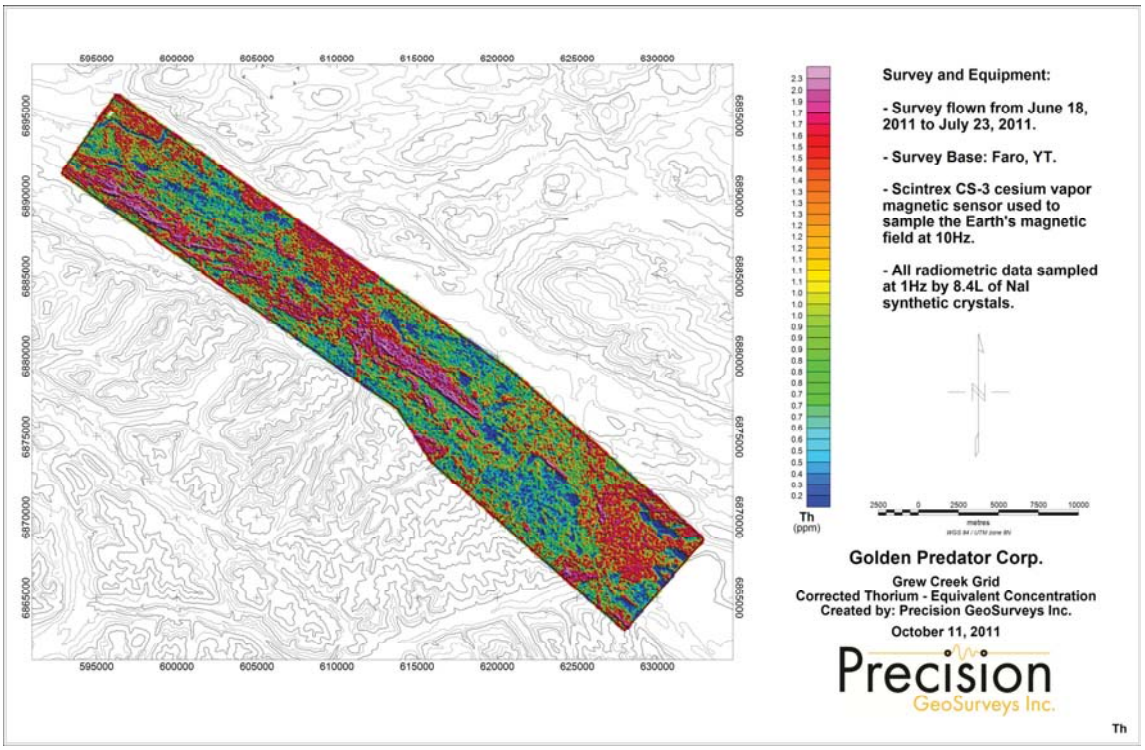

Map 6: Grew Creek Grid - Corrected Thorium

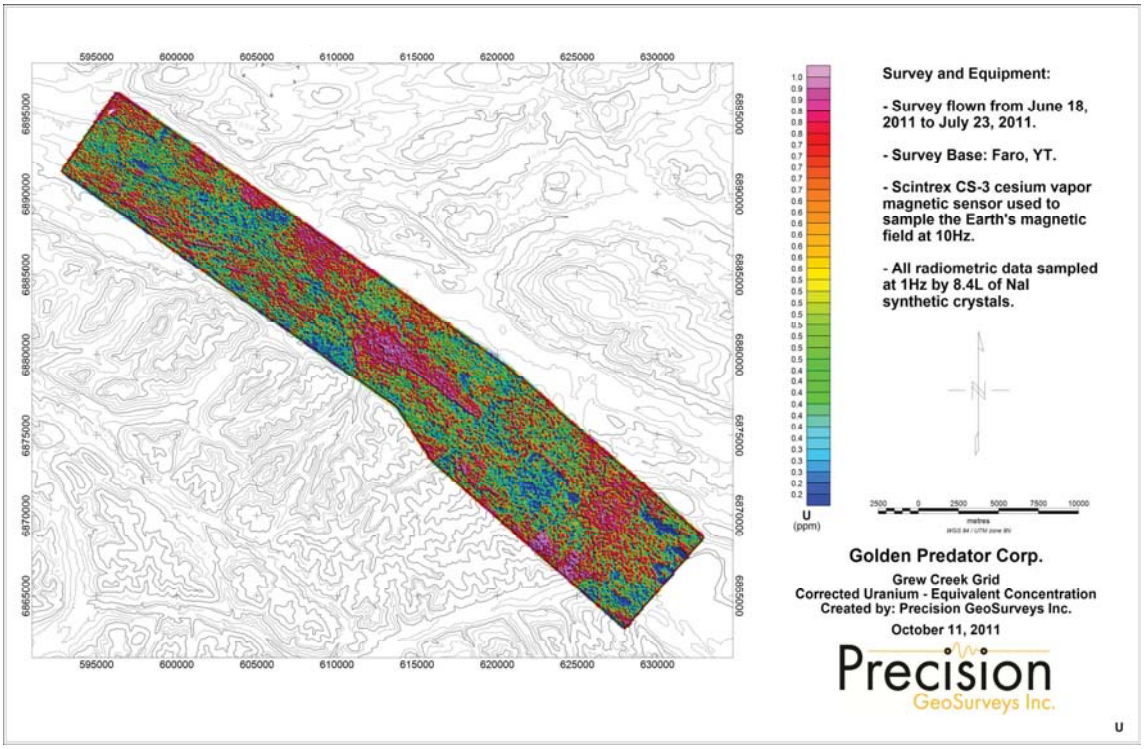

Map 7: Grew Creek Grid - Corrected Uranium

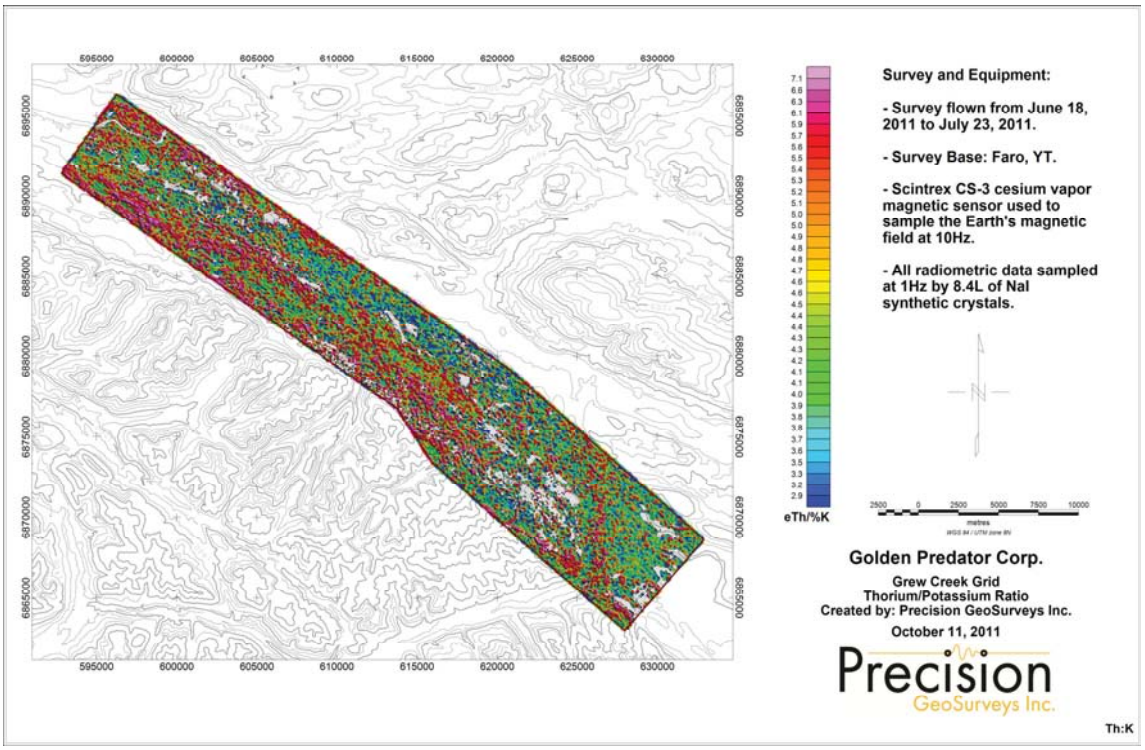

Map 8: Grew Creek Grid - Thorium/Potassium Ratio

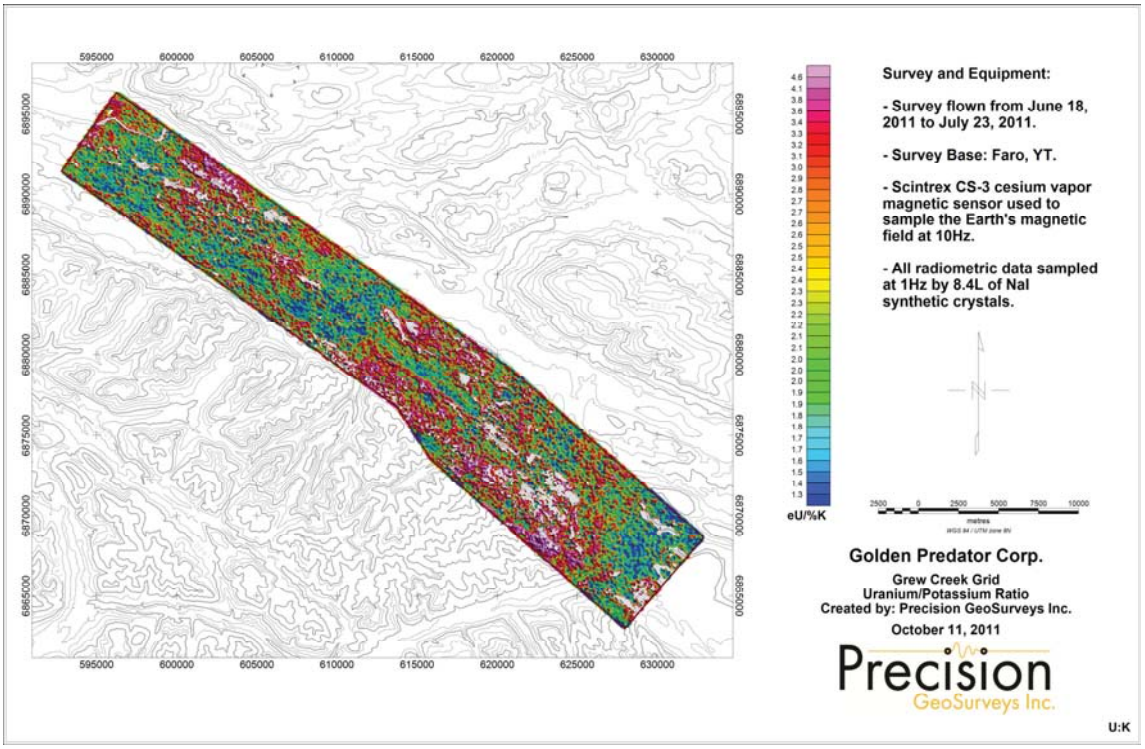

Map 9: Grew Creek Grid - Uranium/Potassium Ratio

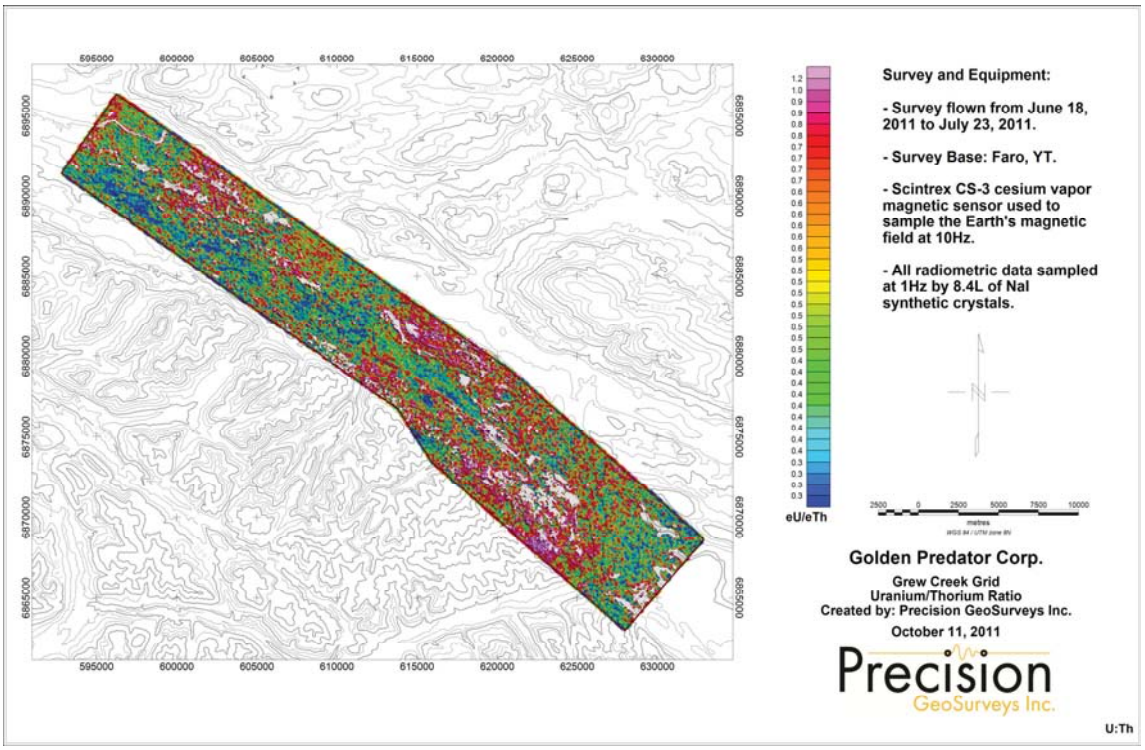

Map 10: Grew Creek Grid - Uranium/Thorium Ratio

Mira Geoscience
...modelling the earth

Appendix 2: Magnetotelluric Data Acquisition Report by Phoenix Geophysics

PHOENIX GEOPHYSICS LIMITED

3781 Victoria Park Avenue
Unit 3
Toronto, ON M1W3K5
CANADA

Phone (1)-416-491-7340

Fax (1)-416-491-7372

MT Survey at Ross River, Yukon as the continuation of MT work performed in 2013

REPORT

On the MT data acquisition and processing on Ross River valley.
November 2014

Contents

Chapter 1 Introduction

Phoenix Geophysics Limited was contracted in October 2014 by Dena Nezziddi Development Corporation to acquire Magnetotelluric (MT) soundings on the Ross River valley area in Yukon.

Murat Urakov, from the Phoenix data acquisition team, left Toronto on October 15 for Whitehorse, he met Tim Sadlier-Brown and he retrieved the equipment. On the next day he drove to Faro and did all the equipment calibration and testing.
Caroline Finateu arrived to Faro on the same day.

Production started on October 17 2014

Working Lines

This project was the continuation of the 2013 survey at Ross River area. The sounding positions were predefined and distributed through all over the graben with an approximate spacing between sites of approx. 1 to 1.5 km, for a more regional study and regional understanding.

The sounding positions were marked with stakes and flag tapes, mentioning the site name. This was very convenient to locate and identify the sites.

The daily production target was set at 3 to 4 sites per day. The soundings were performed overnight for an average duration of 17 to 21 hours.

Phoenix Geophysics Data Acquisition Team

To assure reliable and high-quality data, Phoenix Geophysics provided a highly experienced survey team in geophysical surveys and Phoenix equipment:

- Ms. Caroline Finateu, Chief Geophysicist, in charge of data processing, quality control, geophysical operations and reporting.
- Mr. Murat Urakov, Senior Geophysicist, in charge of data processing, quality control, and geophysical operations.

Geophysical Equipment

Phoenix provided a fully functional MT/AMT satellite-synchronized system with a complete set of magnetic and electric sensors (see Figure 1 and Figure 2):

- 5 MTU-5A receivers, each with five broadband channels for MT and AMT.
- 10 MTC-50H magnetic coil sensors for MT.
- 5 MTC-80H magnetic coil sensors for MT (to measure vertical component Hz)
- 25 non-polarizing electrodes.
- Electrode and sensor cables, GPS antennas, accessories, computers, etc.

All receivers are synchronized with GPS time signals. Therefore, all receivers record synchronous signals on both the electric and the magnetic channels.

Figure 1: MTU-5A receiver

Figure 2: MTC-50H and MTC-80H magnetic sensors, and the new PE-5 electrodes

All equipment was tested in Toronto at Phoenix Geophysics headquarters and successfully passed our factory tests. The equipment was then retested and calibrated directly at the survey area. This operation allowed us to ensure the equipment was not damaged during transportation. The equipment passed all tests in the field and was ready to be used in production.

The equipment test consists of one full calibration of the receivers and sensors at every frequency. The calibration response curves indicate the proper working status and the response limits of the equipment.

Figure 3 and Figure 4 show the typical calibration responses for the instruments.

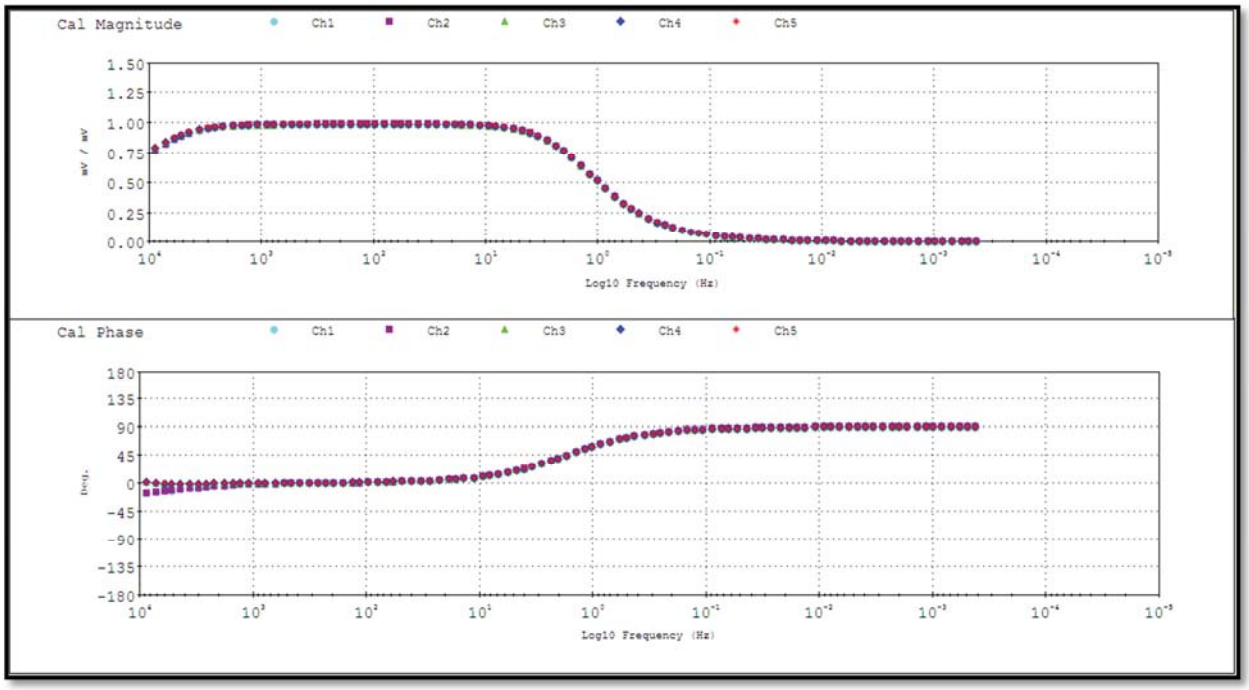

Figure 3: Typical calibration curves for MTU-5A receiver.

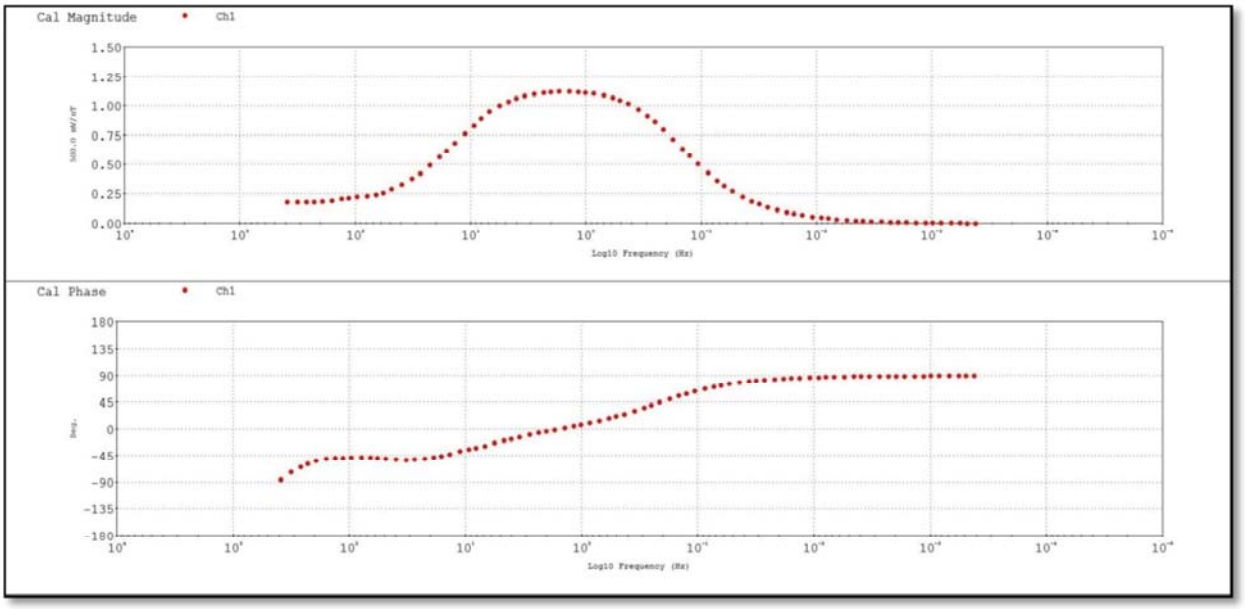

Figure 4: Typical calibration curves for MTC-50H and MTC-80H magnetic sensors.

Quality Control

The Ross River 2014 survey went smoothly; we were even able to record more sites than expected, within the scheduled time window. The mobilization and demobilization of the equipment presented no hurdles and were accomplished without delays.

Overall, the data quality is pretty good and we accomplished a total of 25 sites while we were expecting to record 18 sites.
Figure 5 shows a typical apparent resistivity and phase curves from this survey.

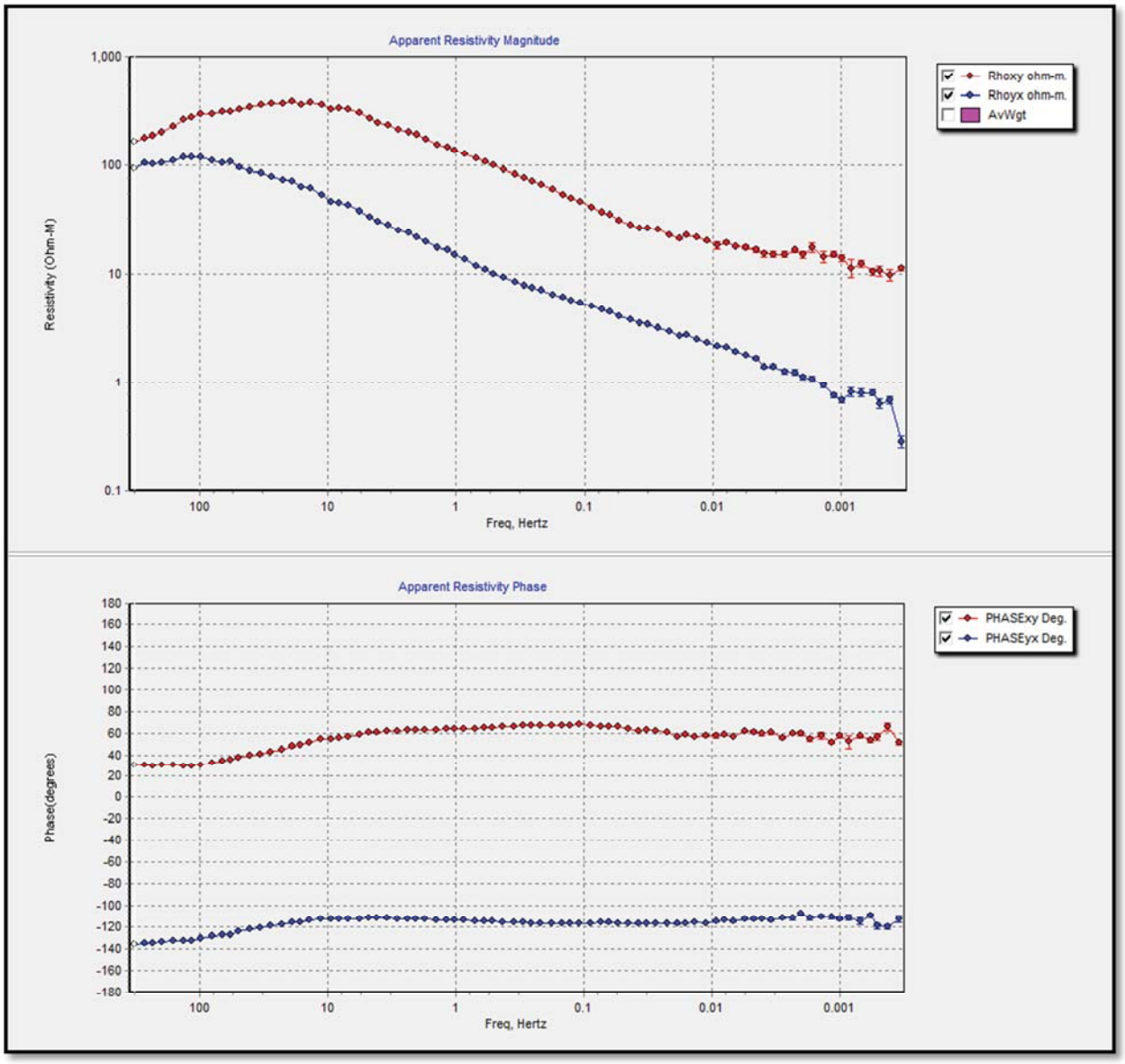

Figure 5: Apparent resistivity and Phase curves of site RR1416

The only site with very bad data quality is site 1417 (Figure 6). This site was located at approx. 100 m from a cellphone tower; there was no point to repeat it.

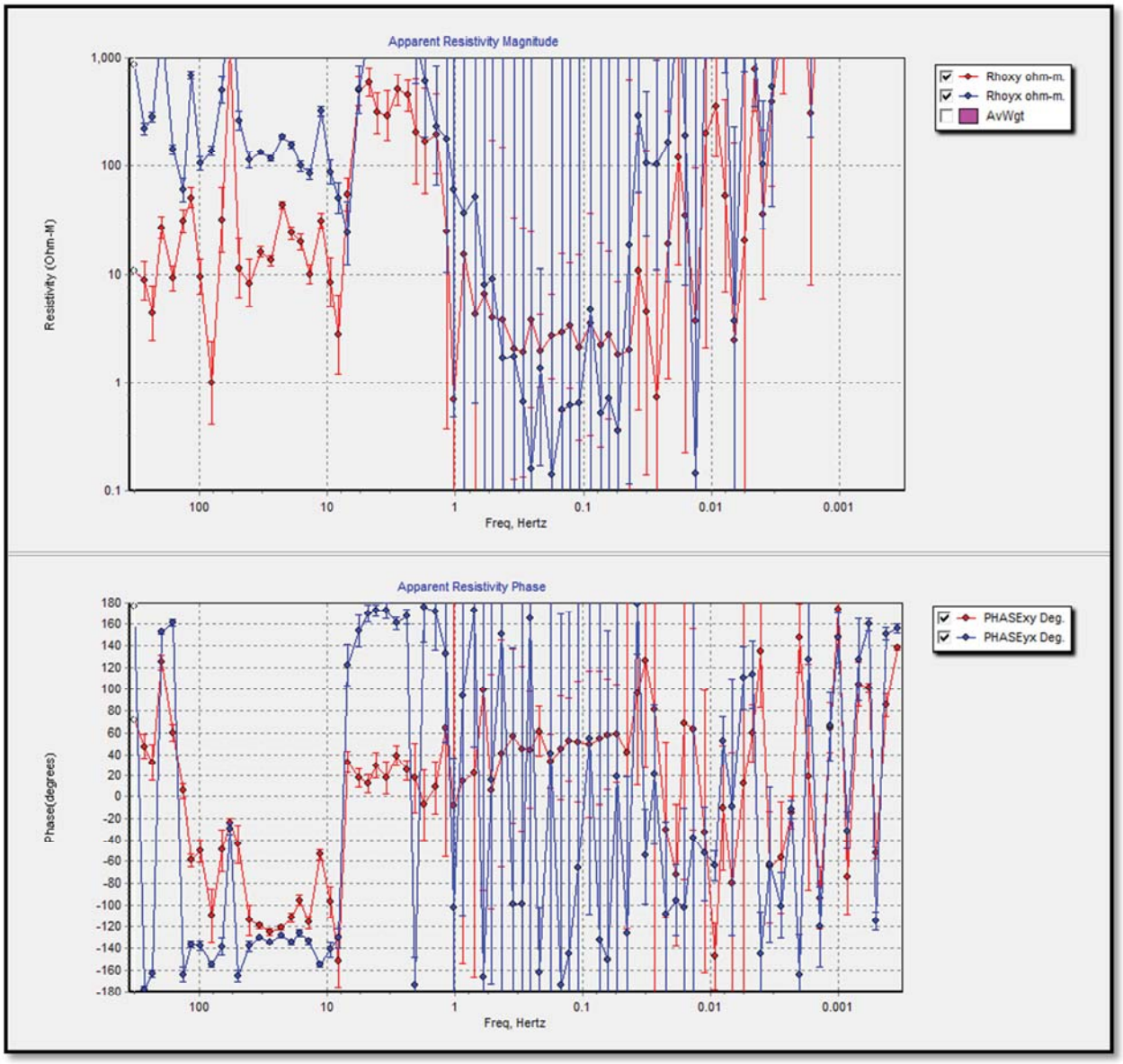

Figure 6: Apparent resistivity and Phase curves of site RR1417

Chapter 2 Acquisition

MT Acquisition

MT acquisition settings

The gain was set to Normal for the electrical and the magnetic channels. With these settings of gains the saturation was within 0.3 – 3 percent.
The coupling was set to DC for both E and H channels.
The low pass filter was set to 0 (weakest since the contact resistance was mostly below 1 kΩ.

Overnight MT

The overnight soundings are about 17-21 hours long.
All start time have been settled so the MUT-5A starts recording as soon as the box is turned on. This way, the field technicians do not leave the site until the box starts recording.

Due to the very quiet environment, no remote reference station was installed.

The Ex and Ey dipole length was set to 100 meter length on all sites, with some variations to accommodate the landscape.

Ex and Hx azimuths were set to 0 degree, with some changes again to adapt to some landscape constraint. North reference was set to Magnetic North.

We were able to set up 3 to 4 sites per day.

Note that we used a helicopter to access sites RR1418, RR1419, RR1420, RR1421, RR1422 and RR1423.

Acknowledgements

We wish to express our thanks and appreciation to

- Aaron Snider and Tim Sadlier-Brown who coordinated the survey, did the sites scooting and prepared all e-lines' path.
- John Ebell and Tim who made that project possible and coordinated it.
- Dena Nezziddi Development Corporation and their collaboration for providing field helpers.
- Gordon, Howard and Tyler (alias Cowboy), our local helpers for their perfect organization and management of the whole field operation, their precious help and joy of life.

We would like to mention that the helpers' team was one of the best we have ever had.

Chapter 3 Daily Report

DATE	LOCATION	ACTION
October 15, 2014	Toronto Whitehorse	Murat Urakov flew from Toronto to Whitehorse and retrieved the equipment
October 16, 2014	Vancouver Whitehorse Faro	Caroline Finateu flew from Vancouver to Whitehorse Murat Urakov drove to Faro. Calibration of MT equipment
October 17, 2014	Whitehorse Faro Ross River	Caroline Finateu joined the field Set-up of sites: RR1405, RR1414, RR1415
October 18, 2014	Faro Ross River	Pick-up of sites: RR1405, RR1414, RR1415 Set-up of sites : RR1406, RR1407, RR1411, RR1412
October 19, 2014	Faro Ross River	Pick-up of sites: RR1406, RR1407, RR1411, RR1412 Set-up of sites : RR1408, RR1409, RR1410
October 20, 2014	Faro Ross River	Pick-up of sites: RR1408, RR1409, RR1410 Set-up of sites : RR1401, RR1403, RR1404, RR1413
October 21, 2014	Faro Ross River	Pick-up of sites: RR1401, RR1403, RR1404, RR1413 Set-up of sites : RR1402, RR1416, and RR1419, RR1421 with helicopter
October 22, 2014	Faro Ross River	Pick-up of sites: RR1402, RR1416, and RR1419, RR1421 with helicopter Set-up of sites : RR1418, RR1420, RR1422, RR1423 with helicopter
October 23, 2014	Faro Ross River	Pick-up of sites: RR1418, RR1420, RR1422, RR1423 with helicopter Set-up of sites : RR1417, RR1424, RR1425
October 24, 2014	Faro Ross River Whitehorse	Pick-up of sites : RR1417, RR1424, RR1425 Equipment is retrieved from the field, cleaned and packed. Caroline Finateu and Murat Urakov drove to Whitehorse and sent the equipment back to Toronto.
October 25, 2014	Whitehorse Toronto	Caroline Finateu and Murat Urakov flew back to Toronto

Chapter 4 Data Pre-Processing

Please note that in this section, we have re-used illustrations and text from a previous report ***on a different survey***. The techniques used for processing data are the same for most surveys. ***The figures in this chapter are not derived from Ross River data***, but are reproduced simply to illustrate the techniques.

Cultural Noise Filtering

In both acquisition and processing, filtering of various sorts is used to reduce as much as possible the effect of natural and human-generated noise. The different digital filters used include the comb filter and the low-pass filter. Cross-power editing is also used.

Comb Filter

This filter is also called the “Power Line Filter,” and it is set up according to the local power line frequency, 50 or 60 Hz. This filter is set up before the acquisition of the data. In our case it was set up to 60 Hz.

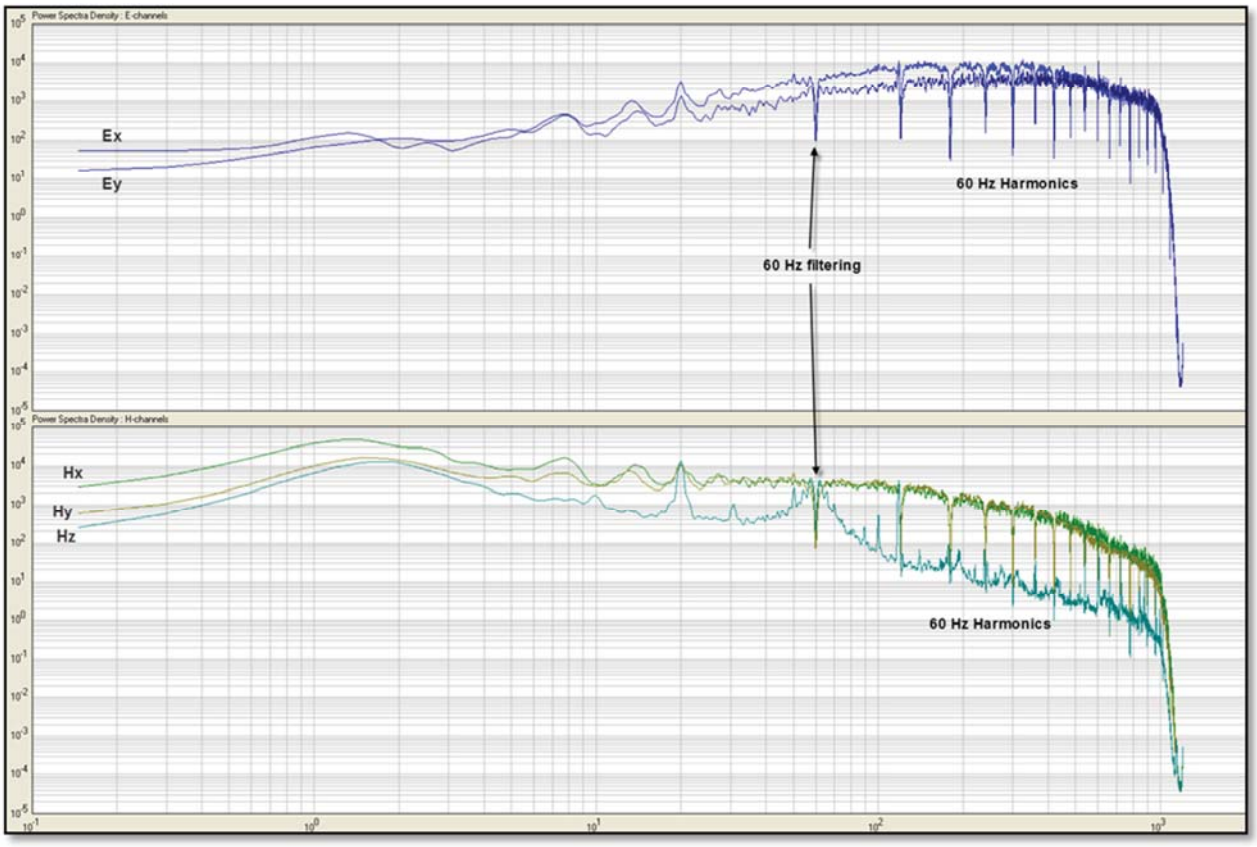

Figure 7: Power spectrum of an MT site, showing the filtering at 60 Hz and all associated harmonics.

Low Pass Filter

The low pass filter allows optimization for AMT data, in the presence or absence of VLF noise and over a wide range of electrode contact resistance. This filter is set up before the acquisition of data.

Cross-power Editing

Cross-power editing is performed after data acquisition. Each point (i.e. each discrete frequency) on the resistivity and phase spectra is the average of many cross-powers (40 in the Ross River survey, and in the following example), where each cross-power is derived from a time-series segment and assigned a weight based on a user-selectable weighting function. Usually, only some parts of the records will be affected by sporadic noise, which means only some cross-powers will not be correct. The goal of editing the cross-powers is to determine which cross-powers are adversely affecting the data and to delete[1] them, thus considerably improving the data quality.

Figure *8* shows the data with no editing.

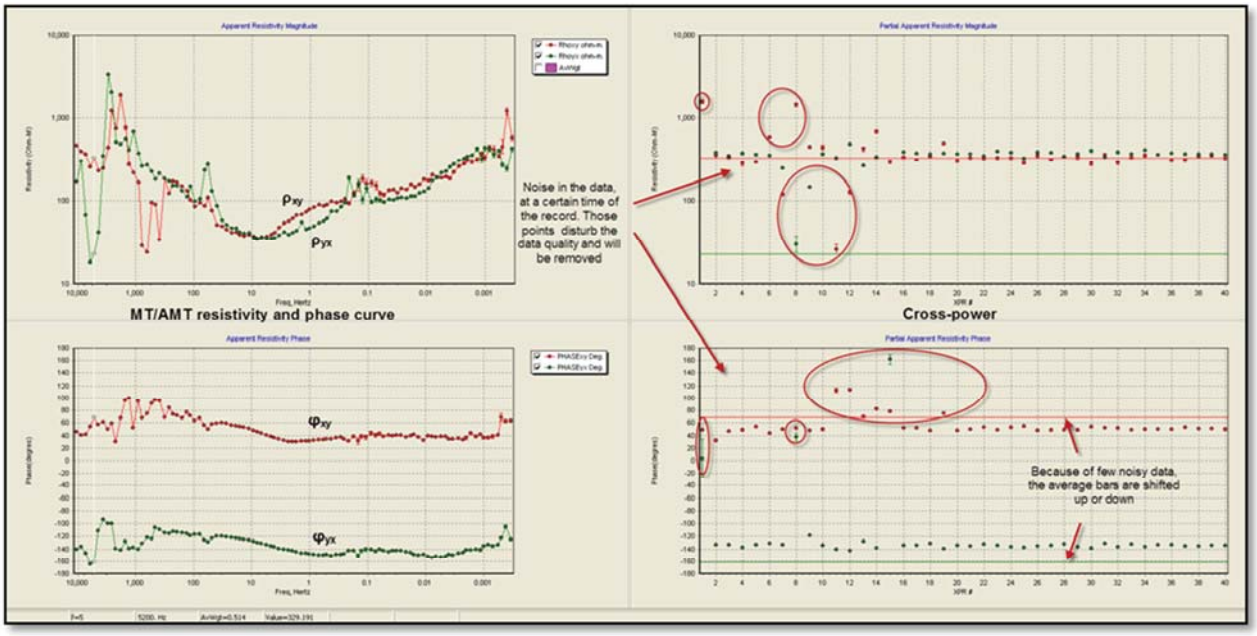

Figure 8: MT/AMT site before cross-power editing.

The resistivity and phase spectra (left) show some noisy data, especially at high frequencies. The cross-power panel (right) shows the 40 successive estimates at a single frequency, obtained during the sounding. Some estimates deviate from the average trend. These deviations are due to intermittent random noise. These bad data move the average value (used to plot the corresponding data point on the resistivity and phase curves) up or down. The editing goal is to spot these out-of-range cross-powers and delete them. The result is that the average value then trends through the less noise-contaminated responses for resistivity and phase, as shown in Figure *9*. Editing is often a critical step in the pre-processing, and it requires experience and accuracy.

After the cross-power editing, an EDI file is generated that can be used by any processing software.

[1] A "deleted" cross-power is actually masked (ignored in the calculations); it is not permanently deleted.

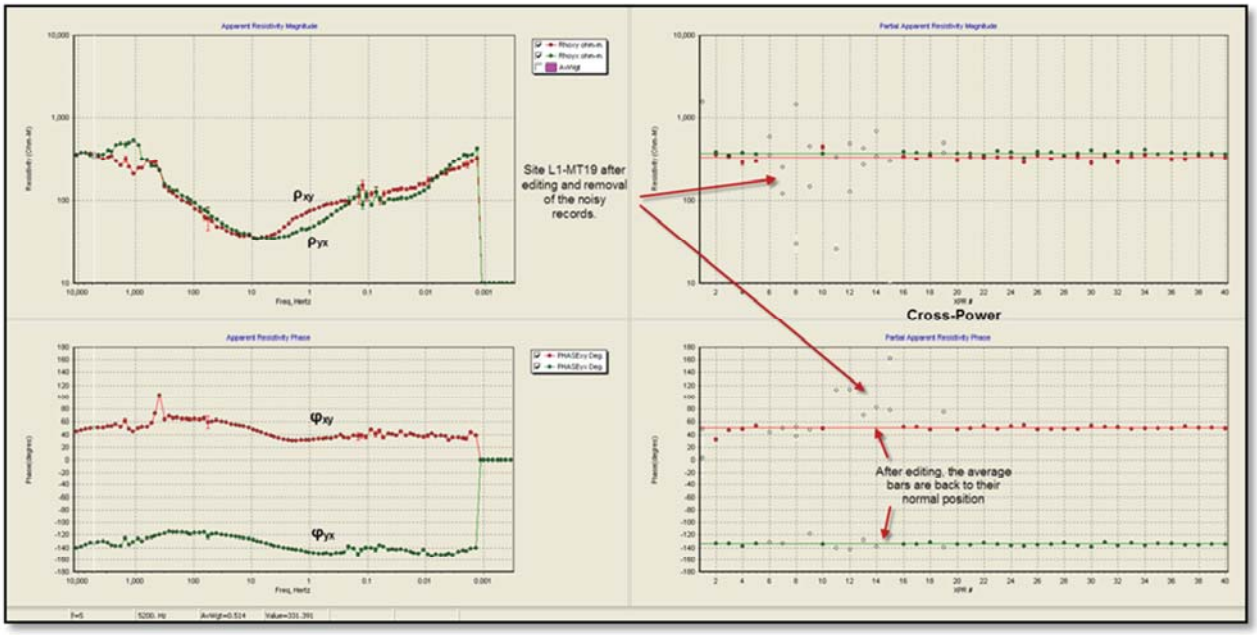

Figure 9: Same MT/AMT site after cross-power editing.

Mira Geoscience
...modelling the earth

Appendix 3: Magnetic Data Analysis and Interpretation Report by Mira Geoscience

Mira Geoscience
...modelling the earth

409 Granville Street, Suite 512 B
Vancouver, BC
Canada V6C 1T2

Tel: (778) 329-0430
info@miragеoscience.com
www.miragеoscience.com

Interpretation of Airborne Magnetic Data for the Ross River Geothermal Exploration Project

Prepared for: Dena Nezziddi Development Corp.

Project #4300

February 5, 2015

Mira Geoscience
...modelling the earth

Table of Contents

Mira Geoscience
...modelling the earth

List of Figures

Mira Geoscience
...modelling the earth

1. Introduction

Mira Geoscience was contracted by the Dena Nezziddi Development Corp. in September 2014 to be part of a geoscience team exploring for geothermal energy resources on Kaska First Nation traditional lands. The project area lies within the Tintina Fault Zone between the townships of Ross River and Faro in the south central Yukon (Figure 1). Various geoscience datasets have been collected by other parties who are part of the project team and these include reconnaissance geological and structural mapping, an airborne magnetic survey, and a magnetotelluric survey.

The role of Mira Geoscience in this project is to analyse, model, and interpret the airborne magnetic survey data as well as integrate the other geoscience datasets into a 3D model of the subsurface to help identify drilling targets. The specific scope of work reported on here includes:

- Analysis of magnetic susceptibility measurements collected from bedrock in the project area
- 2D analysis and interpretation of the airborne magnetic survey data
- 3D analysis, modelling, and interpretation of the airborne magnetic survey data

All data analysis and modelling were performed using a coordinate system and datum of UTM WGS84 zone 8N. This report concludes with a list of proposed exploratory drilling locations based on the interpretation work performed by Mira Geoscience. This report forms part of a larger document which describes the 2014 geothermal exploration effort in the Ross River area.

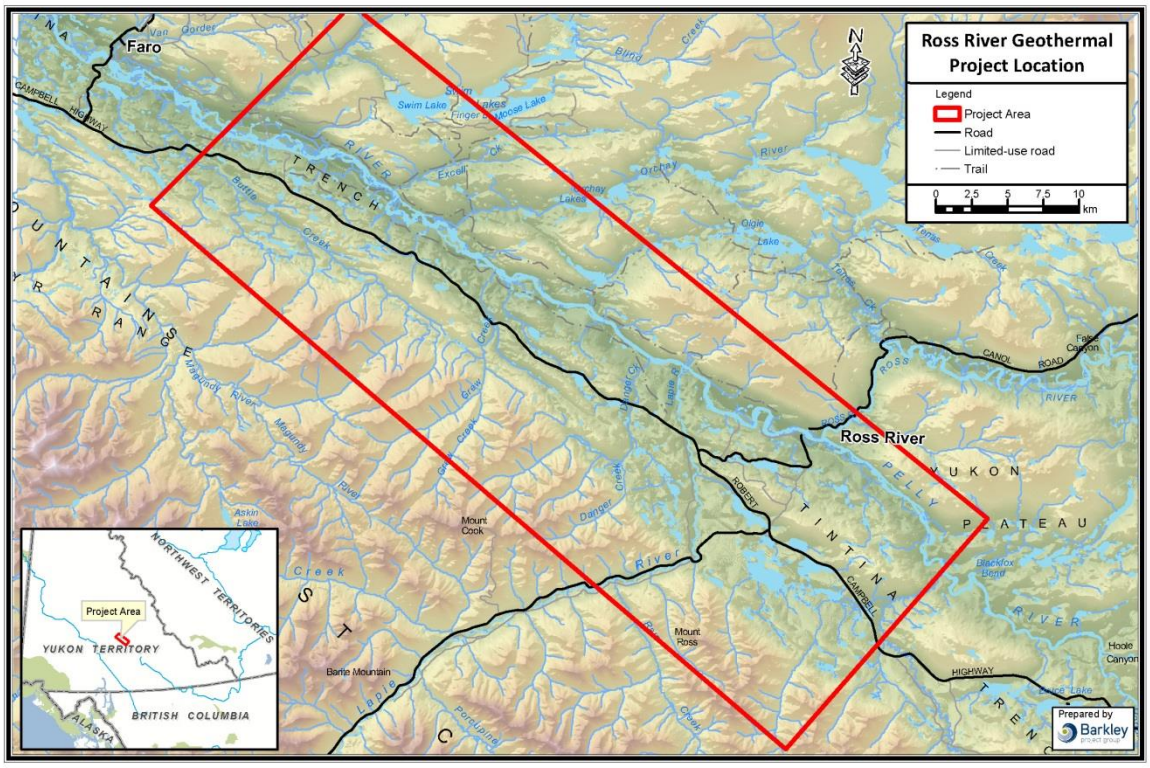

Figure 1. Location map for the Ross River geothermal project in the south central Yukon. The project area is outlined in red.

1.1. Airborne Magnetic Survey

Airborne magnetic survey data that covers a portion of the project area were purchased by the Dena Nezziddi Development Corp. from Golden Predator Corp. in September 2014. The footprint of the magnetic survey area is oriented NW-SE, lies within the Tintina Fault Zone, and is located to the west of the town of Ross River (Figure 2). The magnetic survey area is ~45 km long x ~8 km wide and was collected by Precision GeoSurveys Inc. in the summer of 2011. The topography within the survey area ranges from 600 m to 1600 m above sea level. A total of 3310 line kilometers of magnetic data were collected along NE-SW oriented survey lines spaced 100 m apart with

perpendicular tie lies spaced 1 km apart. The data were collected by helicopter with a front mounted “stinger” at a nominal sensor height of 35 m above the ground.

Mira Geoscience was provided with the complete magnetic survey database from Precision GeoSurveys. An initial review showed the magnetic data to be of high quality. However, we did identify minor errors in some of the laser altimetry and GPS elevation data collected during the magnetic survey. Precision GeoSurveys corrected the laser altimetry errors. The errors in the GPS elevation data, however, are not correctable. These errors are restricted to small areas along the mountainous southwestern edge of the survey area. Apparently, poor GPS signal in this mountainous terrain resulted in erroneous GPS elevation data. The poor quality GPS data do not affect our ability to analyze and interpret the rest of the magnetic data.

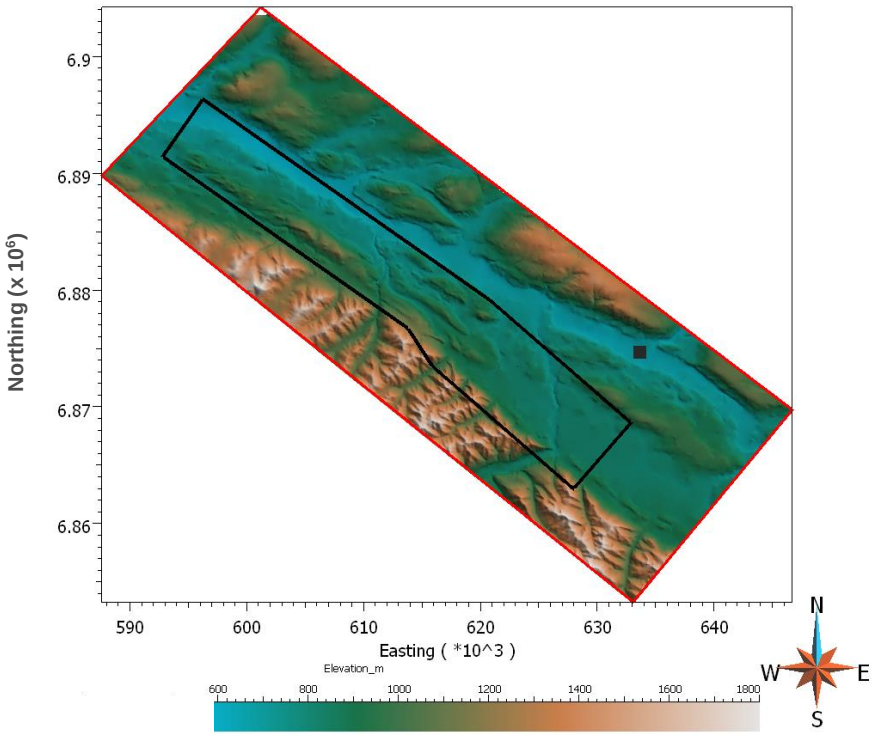

Figure 2. Map showing the footprint of the airborne magnetic survey (black polygon) within the larger project area (red box). The background is shaded relief topography with the color bar showing elevation in metres above sea level. The location of Ross River town is shown by the black square. All coordinates are in UTM WGS84 zone 8N.

2. Magnetic Susceptibility Field Data

In early October 2014, Mira Geoscience began work on this project by conducting a brief field campaign to measure the magnetic properties of the principal bedrock units within the project area. This effort was performed to support the subsequent magnetic modelling and interpretation portions of this project. By measuring the magnetic properties of the rocks in the field, we were able to use actual field measurements to "ground truth" our magnetic modelling effort which supports a more geologically-based interpretation.

We measured magnetic susceptibility in the field using a handheld KT-10 magnetic susceptibility meter from Terraplus Inc. Magnetic susceptibility was measured at 45 locations within the project area. Several closely spaced measurements were taken at each location to assess the local variability in the magnetic susceptibility of each rock unit. The geographic location and rock type were recorded for each measurement. In many cases, a representative rock sample was also obtained. Appendix 1 lists the magnetic susceptibility data collected in the field.

Magnetic susceptibility measurements were collected from ten different bedrock units that fall within the footprint of the airborne magnetic survey (Figure 3). A few opportunistic measurements were taken outside of the magnetic survey area, but these were on bedrock units that also outcrop within the magnetic survey area. A number of measurements were made on Quaternary glacial deposits as well to assess the magnetic susceptibility of the glacial cover.

Overall, the measured magnetic susceptibility values in the project area are quite low and generally range from 10^{-5} to 10^{-3} SI units (Figure 4). The lowest value is 1.8×10^{-5} SI measured on an outcrop of Paleozoic limestone (bedrock unit CK2). The highest measured value is 1.6×10^{-2} SI obtained on a rare outcropping Tertiary basaltic dike (within bedrock unit ITR3). This high value is not spatially representative of the majority of Tertiary sedimentary and volcanic rocks in unit ITR3 and is not shown in Figure 4.

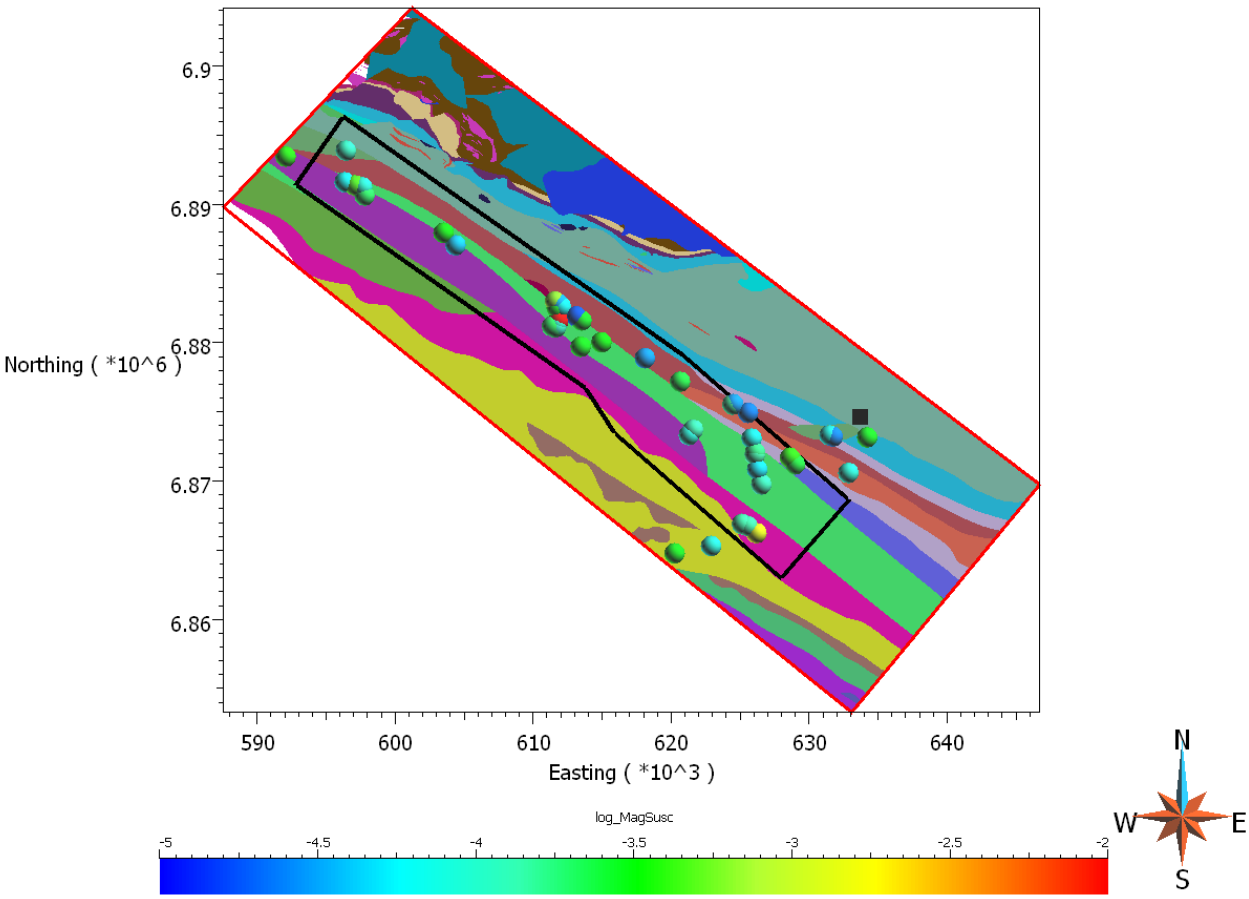

Figure 3. Map showing the geographic distribution of magnetic susceptibility field measurements. The project area is outlined in red while the footprint of the airborne magnetic survey is shown as a black polygon. Spheres denote the locations of magnetic susceptibility measurements and they are colored according to the log of the magnetic susceptibility shown on the color bar. Most of the susceptibility values are ~10^{-4} SI (blue-green). The backdrop shows colored polygons which represent the different bedrock units from the 2014 Yukon Geological Survey 1:250,000 scale geologic map. Our magnetic susceptibility field measurements cover most of the bedrock units within the magnetic survey footprint. The location of Ross River is shown by the black square.

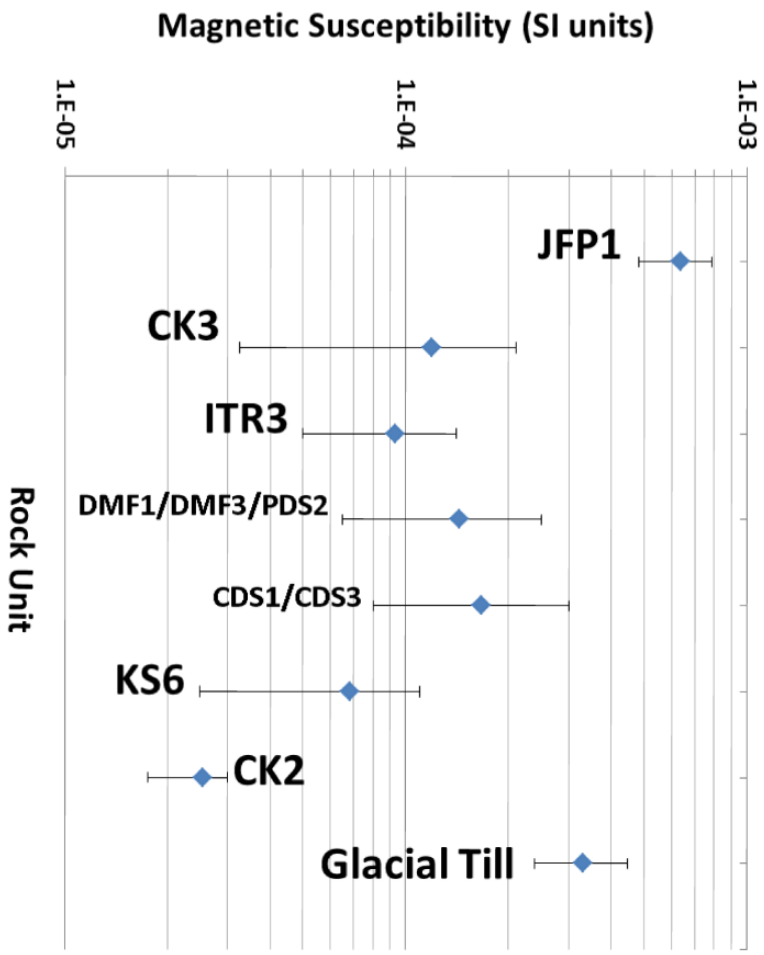

Figure 4. Summary of magnetic susceptibility values measured in the field and grouped by major rock type. Blue diamonds represent the average magnetic susceptibility for the given rock type. The horizontal bars span the entire range of magnetic susceptibility values encountered. Some rock types have been grouped due to similarity in lithology. Definitions of the bedrock codes can be found in Appendix 1.

The rock type with the lowest average magnetic susceptibility is Paleozoic limestone (CK2; 2.5 x 10^{-5} SI). The rock type with the highest magnetic susceptibitity is an outcrop of serpentinized basalt (JFP1; 6.3 x 10^{-4} SI). All of the other bedrock units cluster around a magnetic susceptibility value of 1 x 10^{-4} SI. These other bedrock units include Paleozoic sedimentary rocks (CK3, CDS1, CDS3), Tertiary volcanic and sedimentary

rocks (ITR3), Paleozoic metamorphosed sedimentary rocks (DMF1, DMF3, PSD2), and Cretaceous sedimentary rocks (KS6). Interestingly, with a value of 3.3 x 10^{-4} SI, the magnetic susceptibility of glacial till is higher than all of the bedrock units (except JFP1). Our measured values for bedrock magnetic susceptibility are in agreement with expected values for the different rock types encountered; however, many of them fall at the low end of their normal range (Figure 5).

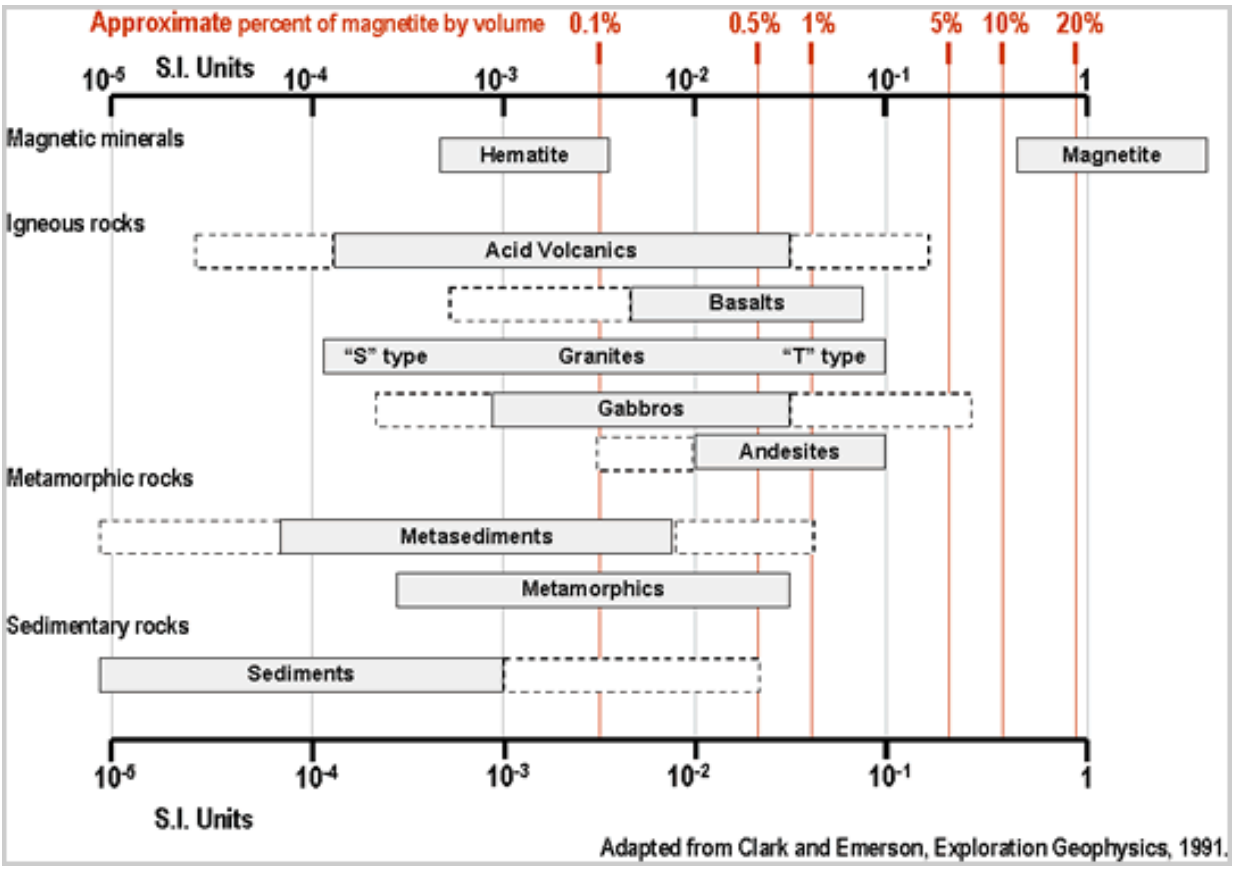

Figure 5. Generally accepted ranges of magnetic susceptibility for the different rock types. Obtained from www.eos.ubc.ca

Mira Geoscience
...modelling the earth

3. 2D Interpretation of the Magnetic Survey Data

The airborne magnetic survey data were initially analyzed and interpreted using a 2D map-based approach. The purpose of this effort is to identify areas with anomalously high or low magnetic signatures as well as map out lineations in the magnetic survey data which may represent geologic structure. Our 2D map-based interpretation included traditional magnetic data filtering and a structural interpretation as well as a simple comparison between a geologic map and the magnetic highs / lows.

3.1. Magnetic Data Filtering

The airborne magnetic survey data were provided in the form of total magnetic intensity (TMI) data along the flight lines. These data were then gridded using a 30 m cell size and the Reduction to Pole (RTP) filter applied. The first vertical derivative (1VD) and total horizontal derivative (THD) were calculated from the TMI-RTP gridded dataset. The filtered magnetic maps are shown in Figure 6 (TMI), Figure 7 (TMI-RTP), Figure 8 (TMI-RTP-1VD), and Figure 9 (TMI-RTP-THD).

Using the Natural Resources Canada Magnetic Field Calculator (IGRF 2010 Model), a field amplitude of 57695 nT was calculated for the date and location of this magnetic survey. When the IGRF correction is applied to the TMI data (i.e. ambient field intensity subtracted), the residual has a range from -150 to 200 nT. About 80% of the data, however, span the much more restricted range of -20 to 60 nT. This restricted range is a reflection of the overall lack of significant magnetic variability in the rocks within the survey footprint. This is also the reason why the TMI map in Figure 6 is mostly green (i.e. limited variation).

3.2. 2D Interpretation

The various filtered magnetic maps were structurally interpreted to identify linear or curvilinear features that mark the edges of magnetic domains (Figure 10). These interpreted curvilinears may represent geological/structural features such as faults or

contacts between different rock units. In order to ascertain if a specific interpreted magnetic feature is likely a fault or not, comparison with a geologic map and other geoscience data is needed.

As part of this 2D interpretation we cross-checked the magnetic map with the 2014 Yukon Geological Survey geologic map to test whether the observed magnetic highs and lows correspond to magnetic and non-magnetic rock types mapped in the field (Figure 11). For the majority of the survey area bedrock type is difficult to discern due to limited variation in the measured magnetic data. However, the most obvious magnetic highs either coincide with outcropping magnetic rock (e.g. Tertiary basalt) or close to outcrop of magnetic rock (e.g. Paleozoic eclogite). Similarly, the primary magnetic lows correspond to Paleozoic sedimentary rocks which we confirmed with field measurements to have low magnetic susceptibility. One striking magnetic low, found at the far SE end of the survey area, remains unexplained due to a lack of nearby outcrops.

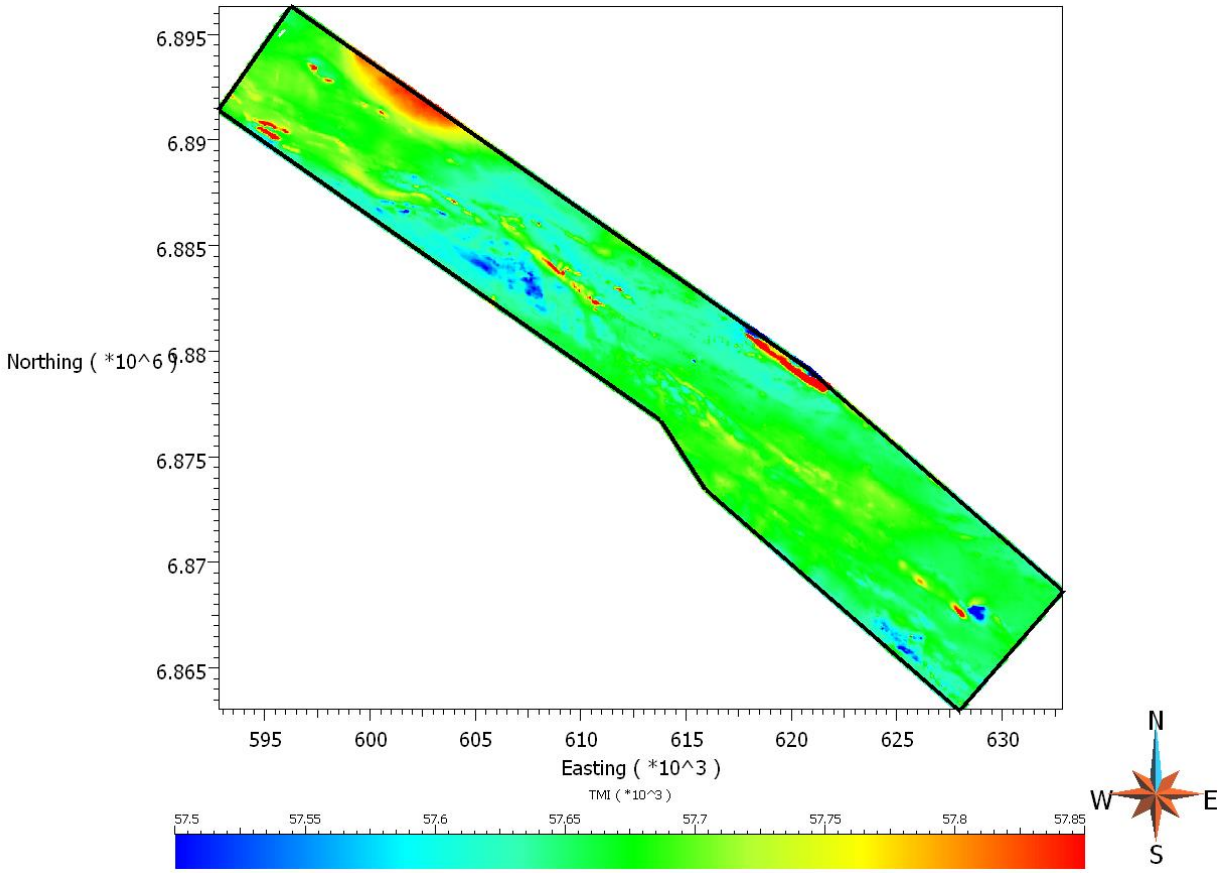

Figure 6. Map showing the Total Magnetic Intensity (TMI) for the survey area. The color bar covers the range 57,500 – 57,850 nT.

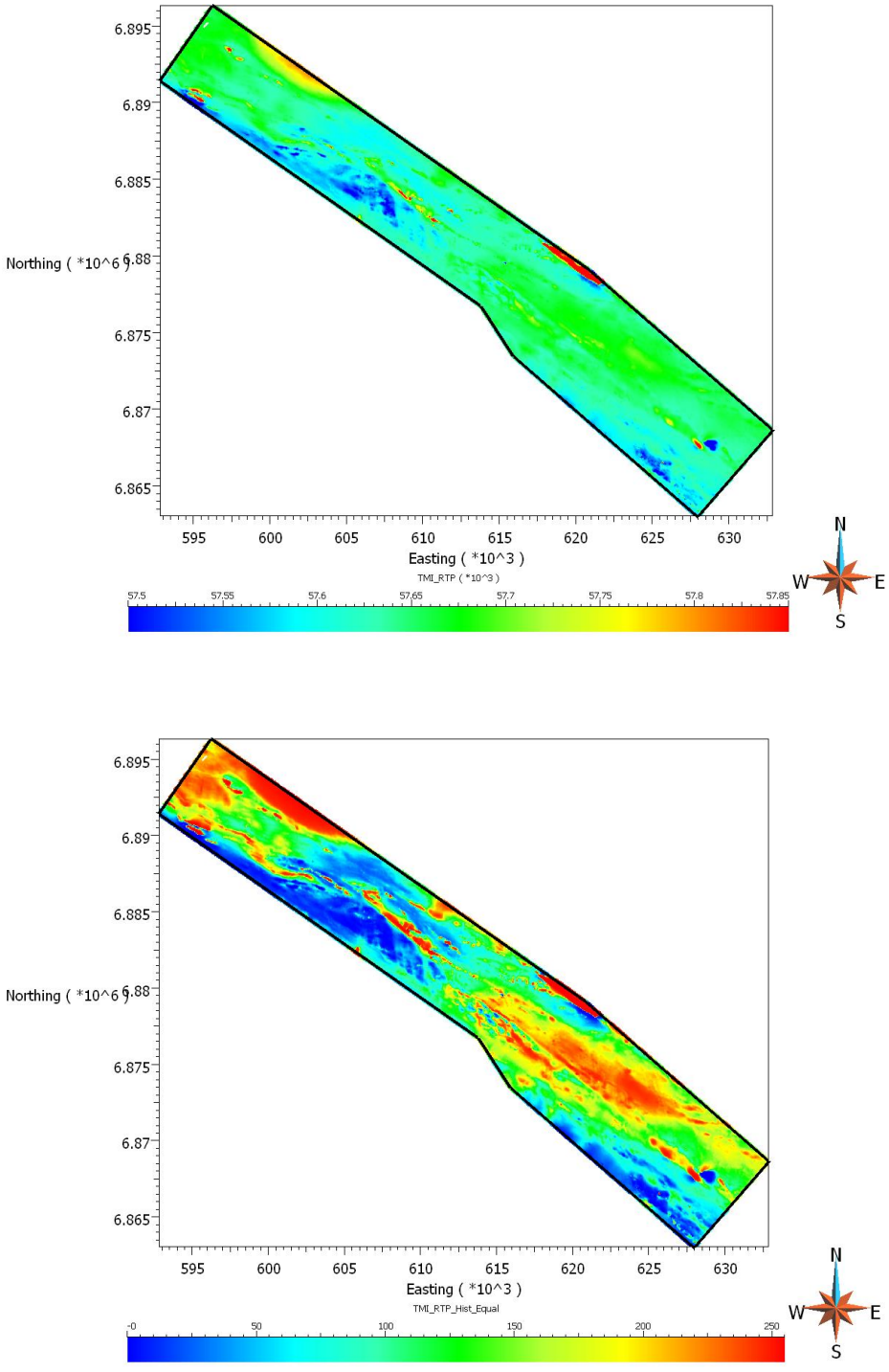

Figure 7. Upper panel: Map showing the Total Magnetic Intensity Reduced-to-Pole (TMI-RTP) for the survey area. The color bar is in units of nT. Lower panel: Same as the upper panel but plotted with histogram equalization to visually enhance the variation in the data.

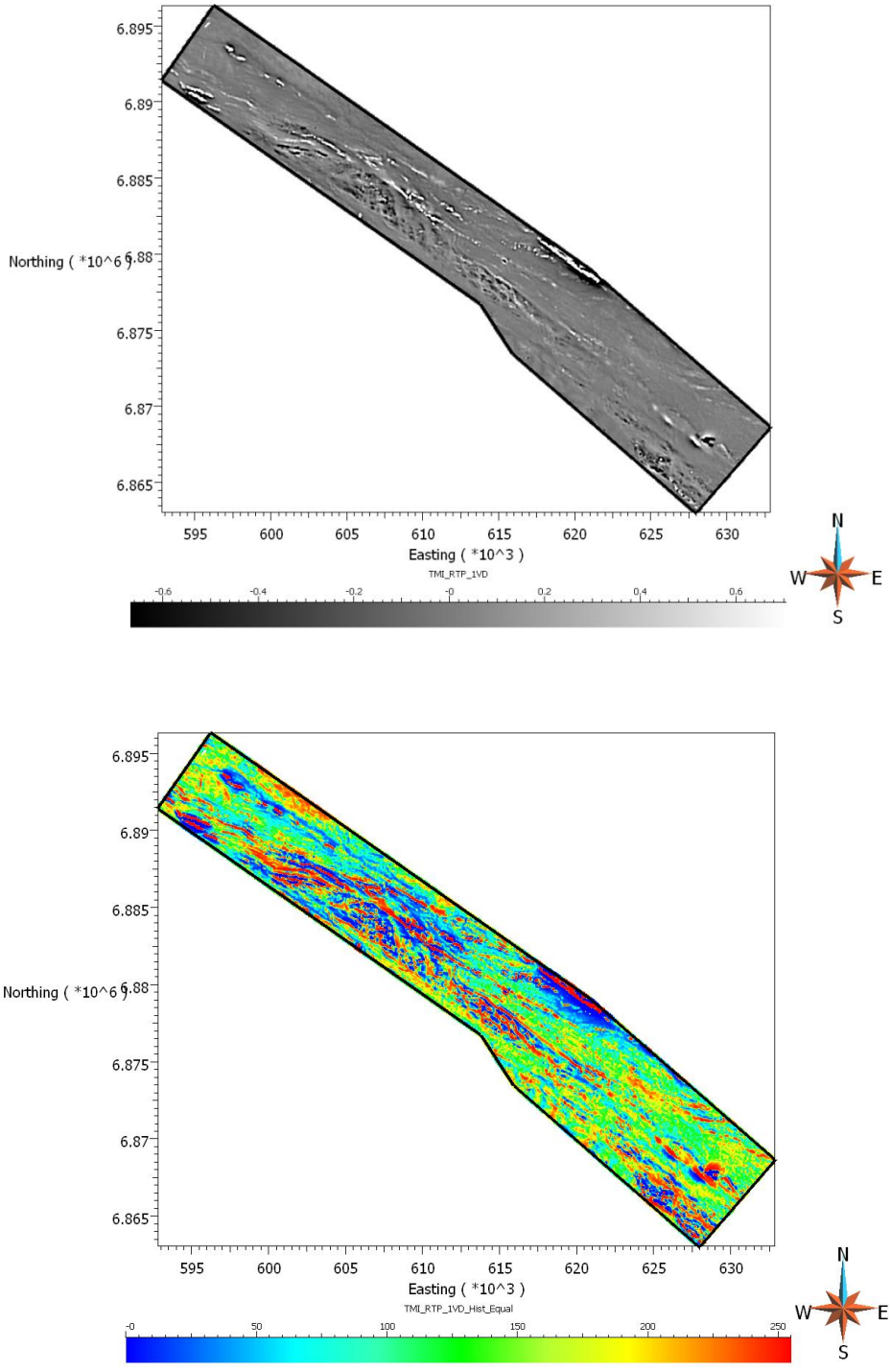

Figure 8. Upper panel: Map showing the First Vertical Derivative of the Total Magnetic Intensity Reduced-to-Pole (TMI-RTP-1VD) for the survey area. The greyscale bar is in units of nT/m. Lower panel: Same as the upper panel but plotted with histogram equalization to visually enhance the variation in the data.

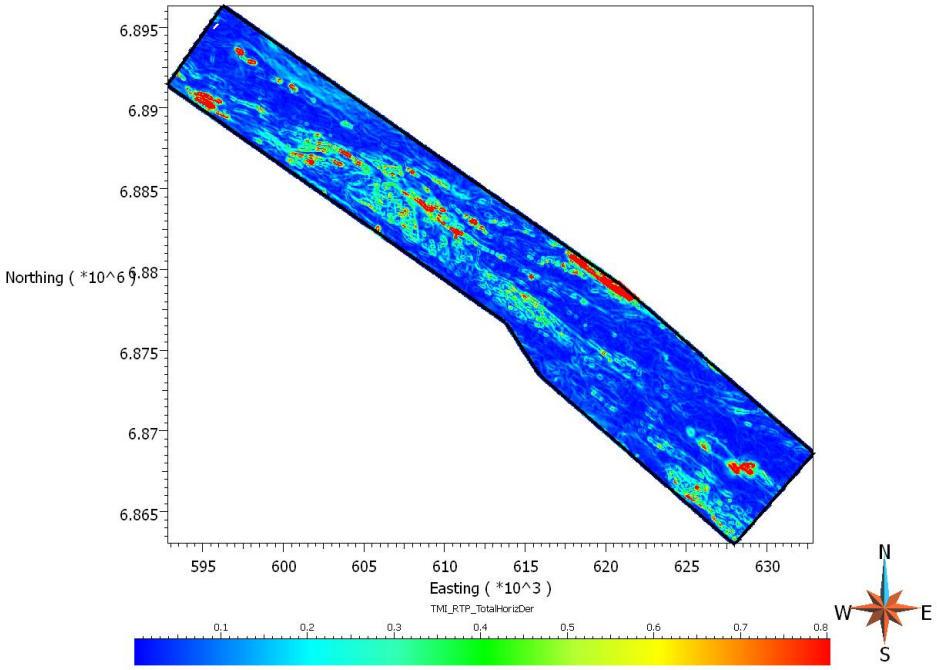

Figure 9. Map showing the Total Horizontal Derivative of the Total Magnetic Intensity Reduced-to-Pole (TMI-RTP-THD) for the survey area.

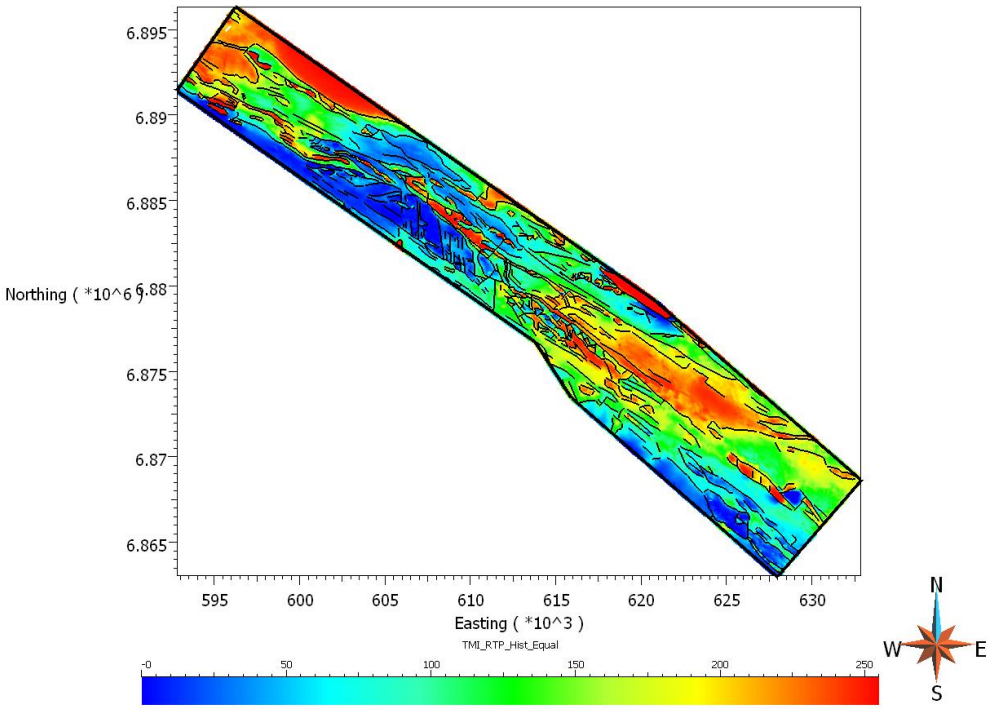

Figure 10. Histogram equalized TMI-RTP map with the magnetic interpretation lines overlain.

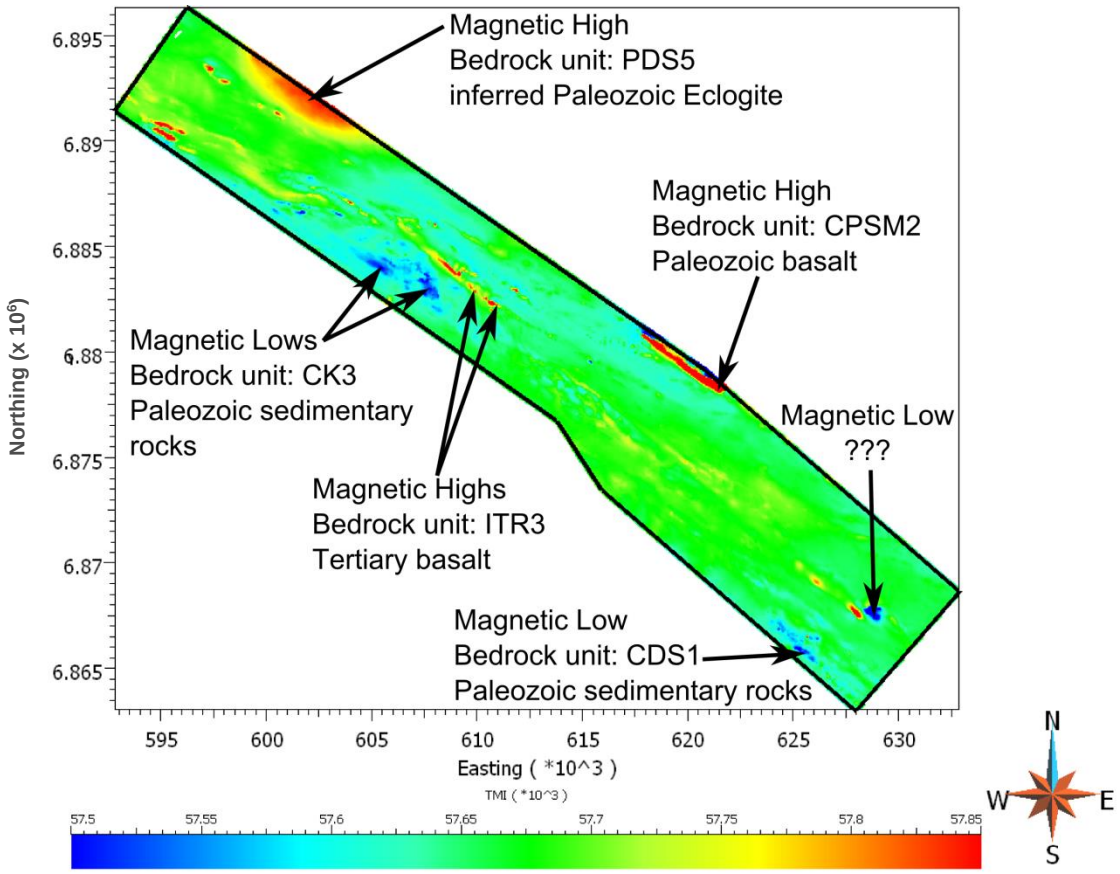

Figure 11. TMI map annotated with interpretations of various magnetic highs and lows based upon comparison with the 2014 Yukon Geological Survey bedrock geology map.

Mira Geoscience
...modelling the earth

4. 3D Modelling and Interpretation of the Magnetic Survey Data

Geophysical inversion can be a useful exploration tool because it turns magnetic data (in 2D map form, measured in units of nanotesla or nT) into a 3D subsurface distribution of magnetic susceptibility (in SI units). This is helpful for geologic interpretation of the subsurface because magnetic susceptibility is a physical property associated with the rocks themselves. In certain circumstances, the subsurface shapes of different rock domains can be modelled in 3D using the 2D magnetic data, provided the rock domains have distinct magnetic signatures. For this approach to be most effective, strong contrasts in the magnetic properties of the rocks are needed. According to the field measurements of magnetic susceptibility (Section 2), most of the major rock types in the study area are weakly magnetic with little or no susceptibility contrast between them. As a result, 3D modelling of the major lithologic domains, with each rock unit assigned a magnetic susceptibility value based upon the field measurements (as was originally intended for this project) will not adequately explain the aeromagnetic data. Therefore, we have chosen to perform 3D inversion of the magnetic data in an unconstrained manner to answer the following question instead: What is a 3D subsurface distribution of magnetic susceptibility that reproduces the measured magnetic data? From this result, we can infer what rock types and structural relations might be expected in the subsurface in different parts of the survey area.

4.1. 3D Modelling Methodology

We performed geophysical inversion of the airborne magnetic survey data using VPmg software from Fullagar Geophysics, dynamically linked to the GOCAD Mining Suite software. The geophysical inversion was performed without constraints, which means that specific geologic or physical property information was not utilized as *a priori* inputs to the geophysical modelling process.

The magnetic susceptibility model we generated extends from the ground surface to a depth of 2000 m below sea level and is divided into ~4.5 million cells. The horizontal (x,

y) cell size was set at 50 m. The vertical (z) cell size was set at 30 m at the surface but the vertical cells increased in size by a factor of 1.1 moving downwards. This selection of cell sizes kept the total number of cells in the model at a manageable level so that the inversion could be performed using the available computer resources.

Input data for the geophysical inversion modelling included: public domain topographic data with ~30 m spatial resolution and the airborne magnetic data gridded to 30 m cells. As a starting point for the modelling, the magnetic susceptibility was set at 10^{-4} SI in the entire model volume and negative susceptibility values were not allowed. The actual flight height of the magnetic sensor (measured with laser altimetry by Precision GeoSurveys) was incorporated into the modelling to take into account areas where the actual flight height diverged from the nominal flight height of 35 m above the ground.

4.2. Interpretation of 3D Magnetic Susceptibility Model

3D perspective views of the magnetic susceptibility model result are shown in Figure 12 and Figure 13 . In general, the modelled susceptibilities vary from 0 to 10^{-2} SI with an average of 10^{-3} SI. This is higher than the average of the magnetic susceptibility field measurements (~10^{-4} SI) which suggests that either the majority of the field measurements were made on rock types with low values or some subsurface rock units (i.e. not exposed) have higher susceptibilities than those measured. Our interpretation is that both are likely.

Prior to interpreting the geophysical model result, it is important to identify the parts of the model which fit the magnetic data well and which parts do not. Areas of the model which do not fit the data need to be interpreted with care and/or require further investigation. The standard approach to assessing how well the model fits the data is to compare the observed magnetic data (i.e. the measurements made in the airborne magnetic survey) with the magnetic data calculated from the 3D susceptibility model. This is done by computing the residual between the observed and calculated magnetic response. The residual is derived simply by taking the difference between the observed

and calculated values. Plots showing the observed magnetic data, the magnetic data calculated from the 3D susceptibility model, and the residual are shown in Figures 14, 15 and 16. An overall misfit value for the entire model, called the RMS misfit, has also been calculated and has a value of 12 nT. The RMS misfit is considered acceptable since it is less than 5% of the overall range in the observed magnetic data (~350 nT).

Spatially, the fit of the susceptibility model is quite good over the majority of the survey area as shown in Figure 16. However, the fit is poor in four areas (labeled in Figure 16). We suspect that the poor fit observed at areas #1 and #2 are caused by an inability to match the near zero magnetic susceptibility values in Paleozoic sedimentary rocks that outcrop there. Negative susceptibilities are needed here to improve the fit. In constrast, poor misfit in area #3 is likely due to difficulty in reproducing high magnetic susceptibility values associated with the Paleozoic basalt in that area. Area #4 appears to be more interesting. The striking low magnetic anomaly (see Figure 11) and the distinct cylindrical shape of the “zero susceptibility zone” beneath this anomaly in the 3D model (see Figure 18 and Figure 19) suggest that this is a zone affected by magnetic remanence. The likely geological explanation is that a reversely magnetized intrusion is creating the observed anomaly. Reversely magnetized intrusions could also explain the poor fit in areas #1 and #2. Further investigations and specific modelling of magnetic remanence are outside the scope of this study.

Overall, the 3D susceptibility model matches well with some of the observed geology in the near surface. For example, areas of elevated susceptibility in the model coincide with outcrops of Tertiary basalt (within rock unit ITR3) as well as mapped Paleozoic mafic rocks (unit CPSM2) as similarly noted in Figure 11. Other, generally northwest-trending susceptibility highs in the near surface within rock unit ITR3 may indicate additional as yet unmapped mafic volcanic rocks in the area covered by Quaternary glacial deposits.

Major NW-SE trending divisions between the primary bedrock units (e.g. CK3, CK2, ITR3, and CDS1) that are present in geologic maps of the area are not consistent along

the entire length of the 3D magnetic model. Susceptibility boundaries between the mapped bedrock units are readily discernable in the central-NW portion of the 3D susceptibility model (Figure 17). However, these boundaries are less well-defined in the NW and SE sectors of the susceptibility model. Furthermore, clear variations in susceptibility are observed along strike within the bedrock units. The most obvious example is the large susceptibility low in the central-NW portion of the survey area (Figure 18 and Figure 19) which is flanked to the NW and SE by zones of higher susceptibility. These along-strike variations in susceptibility may be due to small differences in magnetic mineral content within the primary bedrock units. However, an alternative explanation is that the NW-SE change in magnetic susceptibility may reflect a structural or lithological contact (Figure 18 and Figure 19).

Areas of elevated magnetic susceptibility are found at depth at the NW end and in the central SE portion of the 3D model (Figure 18 and Figure 19). Such elevated susceptibility is required to match the observed magnetic data obtained in the airborne survey. In the unconstrained model shown, elevated susceptibility (~5 x 10^{-3} SI units) extends from sea level to the bottom of the model (at 2 km below sea level). Rock types that have this susceptibility include: gabbro, I-type granites, metasedimentary rocks, or metamorphic rocks, all of which are possible in the Tintina Fault Zone. We suggest that granite or gabbro intruded at depth within the Tintina Fault Zone may be the most likely of the options because of the history of igneous activity in the Grew Creek area as well as the abundant evidence for along-fault extension in the past.

It is important to note that geophysical inversion modelling is hampered by non-uniqueness, which means that the model result shown in the figures here is not the only one which can explain the data. Other susceptibility models are possible. By incorporating more geoscience data to better constrain the model result, uncertainty can be reduced and a better geologic understanding of the subsurface can be obtained.

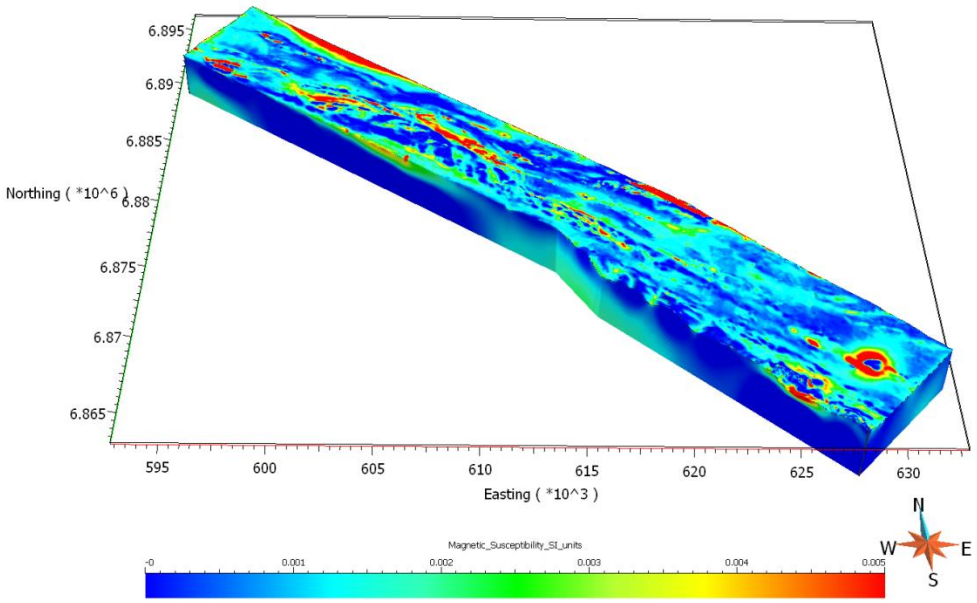

Figure 12. 3D perspective view of the entire magnetic susceptibility block model. The color bar covers the range from 0 to 5 x 10^{-3} SI units.

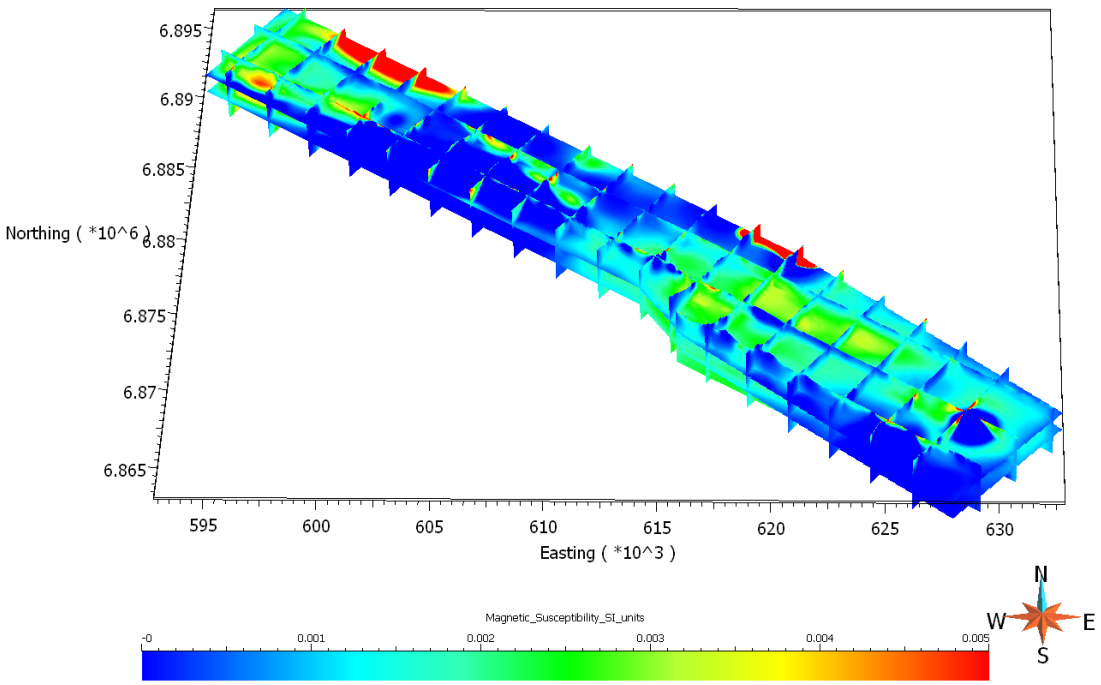

Figure 13. 3D perspective view of horizontal and vertical sections through the magnetic susceptibility model. The color bar covers the range from 0 to 5 x 10^{-3} SI units.

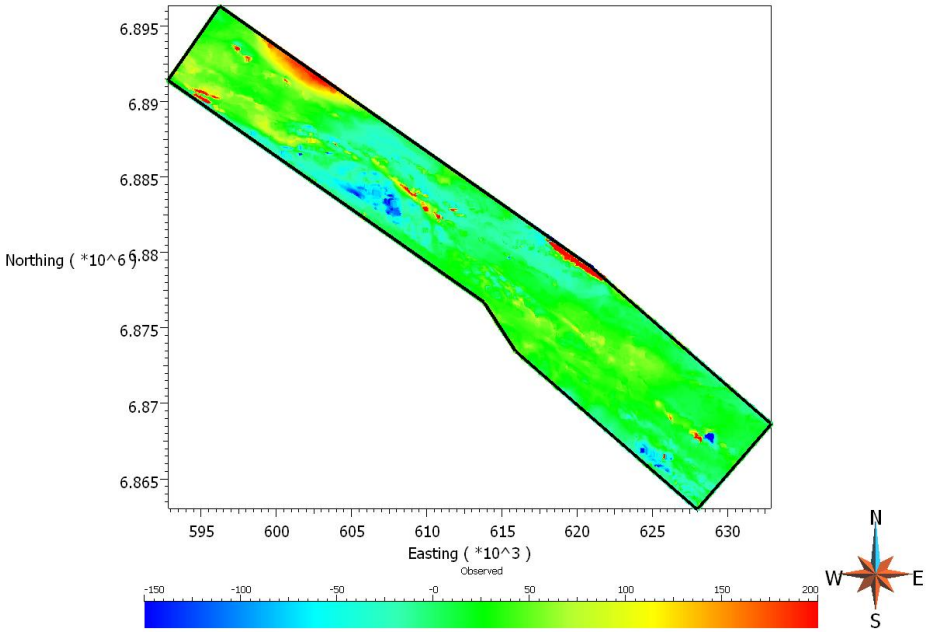

Figure 14. Observed magnetic data collected in the airborne survey. Color bar is in units of nT.

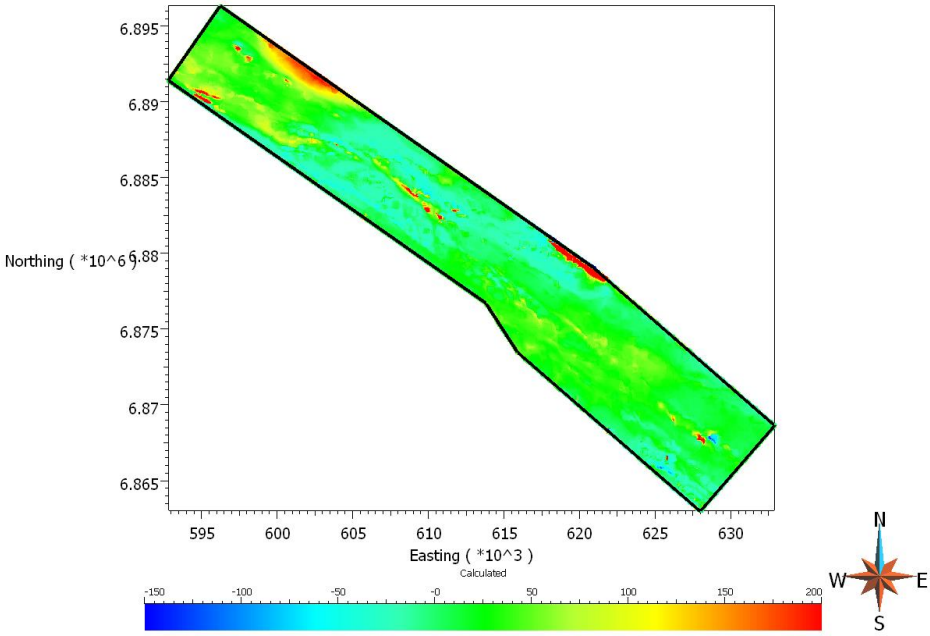

Figure 15. Magnetic data calculated from the 3D susceptibility model. Color bar is in units of nT.

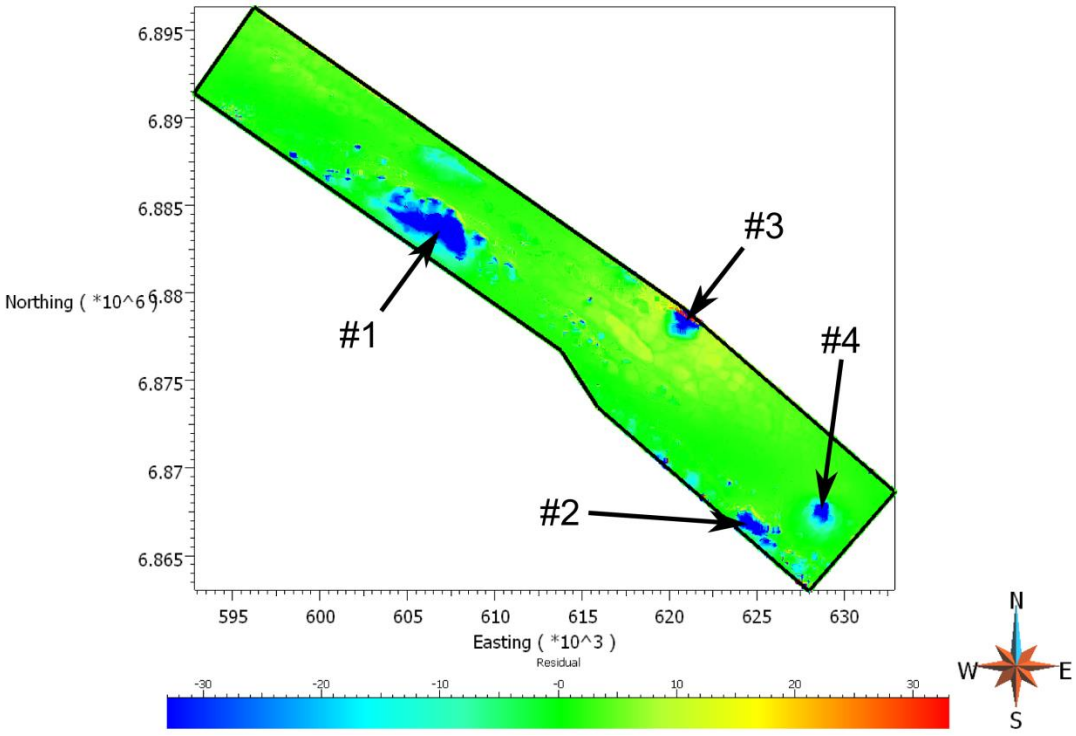

Figure 16. Residual between the observed and calculated magnetic data (e.g. observed – calculated). The fit is good (i.e. green) over the majority of the survey area. Fit is poor in four labeled areas. Color bar is in units of nT. See text for discussion.

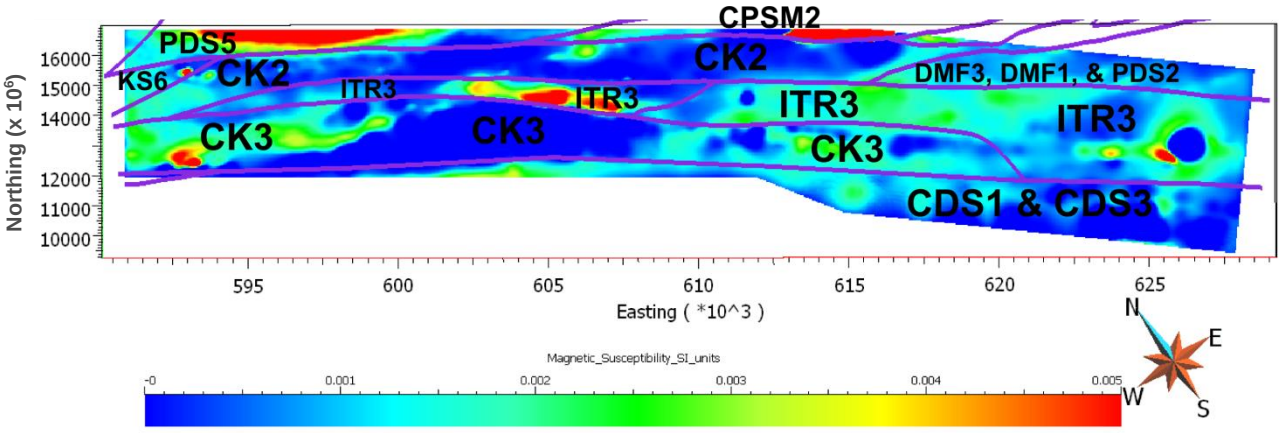

Figure 17. Horizontal slice through the magnetic susceptibility model positioned at an elevation of 500 m above sea level. Major faults from the 2014 Yukon Geological Survey 1:250K map are overlain as purple lines. Along-strike variations in magnetic susceptibility occur within the primary bedrock units. Bedrock unit labels are defined in Appendix 1. Color bar covers the range from 0 to 5 x 10^{-3} SI units.

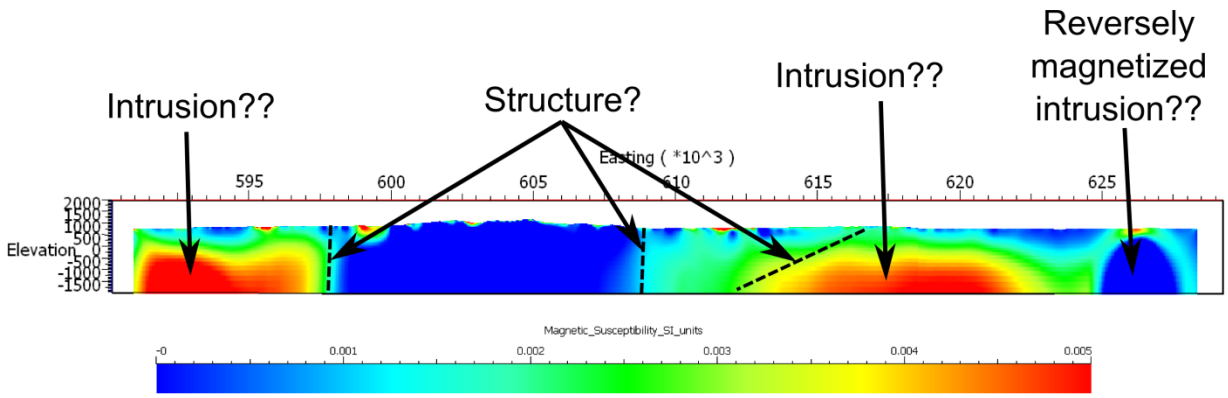

Figure 18. Example of a NW-SE trending cross-section through the magnetic susceptibility model positioned near the centre of the survey area. View looking to the NE. Color bar covers the range from 0 to 5 x 10^{-3} SI units. The bottom of the model cross-section lies at 2000 m below sea level.

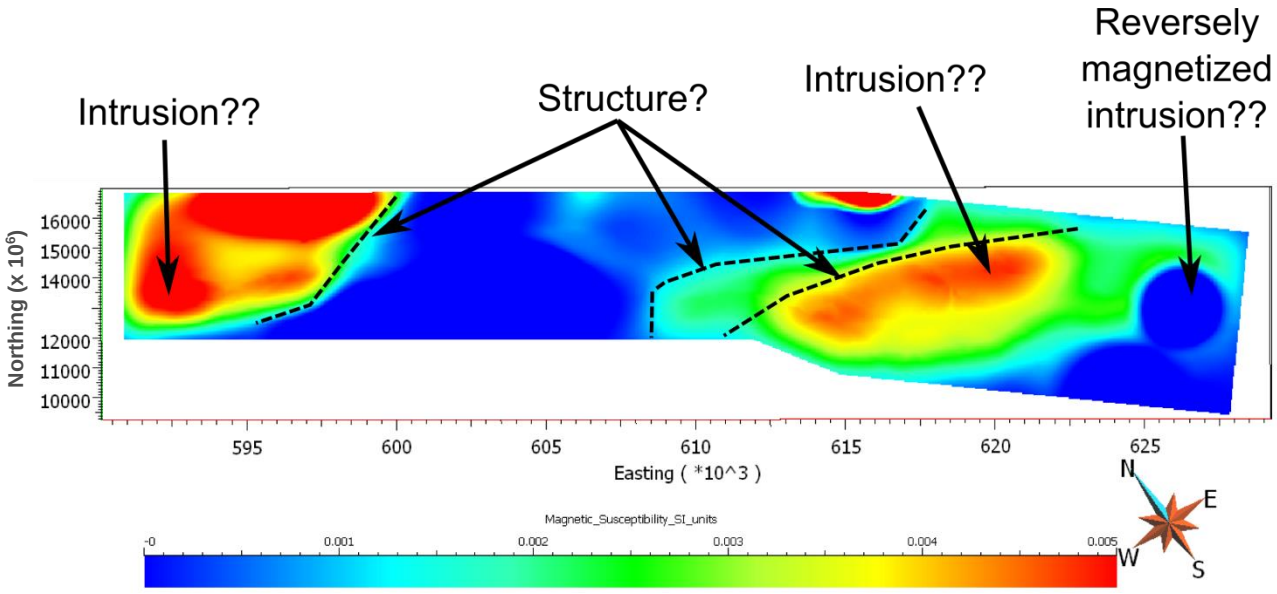

Figure 19. Horizontal slice through the magnetic susceptibility model positioned at an elevation of 1000 m below sea level. Color bar covers the range from 0 to 5 x 10^{-3} SI units.

4.3. Glacial Till Modelling

The majority of the magnetic survey area is covered by Quaternary glacial deposits with outcrops of bedrock generally restricted to zones of elevated topography. Based upon measurements made by Plouffe (1995), the thickness of till deposits in the Ross River region may be on the order of 50 m, however, the spatial variations in thickness are unknown. Our field measurements of magnetic susceptibility suggest that the magnetic signature of glacial till is higher than nearly all of the bedrock units that lie beneath it (Figure 4). Thus an effort to use the magnetic data to model the thickness variations of the till might be possible. If successful, estimates of till thickness in specific locations would be useful for two reasons: 1) it could assist with the geologic interpretation of the magnetic data and 2) it is important information for the planning of exploratory drillholes.

We attempted to model till thickness over the entire magnetic survey area using VPmg software from Fullagar Geophysics dynamically linked to GOCAD Mining Suite software. Areas of outcropping bedrock were fixed with a zero till thickness and average (homogeneous) values of magnetic susceptibility were set for the till (3.3×10^{-4} SI) and generic “bedrock” (1×10^{-4} SI) units. This modelling effort was unsuccessful and we believe it was not successful for two primary reasons. First, the magnetic susceptibility contrast between till and bedrock is too small. Second, the till is expected to be on the order of 50 m thick but the magnetic data were collected at a line spacing of 100 m. Attempting to resolve geologic features that are smaller than the line spacing of the data is difficult.

Once exploratory drilling targets are selected, a renewed effort at till thickness modelling focused specifically on the drill target areas may be warranted. However, it would be most successful in areas where the susceptibility contrast is greatest, such as where till (3.3×10^{-4} SI) overlies the limestone bedrock unit CK2 (2.5×10^{-5} SI). Gravity data could be more effective at mapping till thickness since till is less dense than bedrock.

5. Summary

Airborne magnetic survey data, collected in the south-central Yukon between the towns of Faro and Ross River, were analysed and interpreted as part of a larger exploration effort for geothermal energy resources. The airborne magnetic data was provided to the Dena Nezziddi Development Corp. by Golden Predator Corp.

The airborne magnetic survey data covered an area ~45 km x ~ 8 km oriented NW-SE within the Tintina Fault Zone. These data were supplemented by magnetic susceptibility measurements on bedrock outcrops. The magnetic susceptibility values measured are quite low having the range 10^{-5} to 10^{-3} SI units. These values are consistent with the rock types encountered in the area (e.g. sedimentary rocks). Distinct magnetic susceptibility contrasts between bedrock types are lacking.

Various filtered magnetic maps (e.g. 1st vertical derivative) were generated and interpreted to create a magnetic lineaments map. Many of the lineaments likely represent geologic structure; however, to confirm this, detailed comparison with mapped geology is necessary. Principal magnetic lineation directions are: NW-SE, N-S, and ESE-WNW. The N-S lineations (faults?) are most abundant in the Grew Creek area. In addition, several magnetic highs and lows observed on the magnetic maps are consistent with mapped rock units that have the appropriate magnetic properties.

Unconstrained 3D geophysical inversion was performed on the airborne magnetic data and a 3D magnetic susceptibility block model was generated. This model has a horizontal spatial resolution of 50 m and reaches a depth of 2 km below sea level. The fit of the model to the observed data was generally acceptable. However, the fit was poor in four areas, three of which are likely affected by remanence. Reversely magnetized igneous intrusions are the likely explanation for the remanence.

In the shallow subsurface, the 3D magnetic susceptibility model correlates well with magnetic rock units mapped at the surface (e.g. Tertiary basalt) and points to other areas where there may be additional mafic (i.e. magnetic) rocks that are buried under

glacial cover. Overall, the magnetic model does a poor job of mapping out the primary bedrock units because of a lack of distinct susceptibility contrast between the units.

At depth, the magnetic model highlights two areas of elevated magnetic susceptibility: one at the NW end of the survey area and the other in the central-SE. We interpret these bodies to possibly represent Tertiary igneous rocks (granite or gabbro) which have intruded into the Tintina Fault Zone but did not reach the surface. Structurally, we have identified a significant discontinuity in the magnetic susceptibility in the central-NW portion of the model which separates high values to the NW from much lower values to the SE. Such a proposed structure is difficult to reconcile with mapped geology because it cross-cuts the Tintina Fault Zone. Similar, but less distinct, magnetic discontinuities have also been identified in the central-SE portion of the magnetic model.

An attempt was made to model the thickness variations of the glacial till using the magnetic data constrained with both magnetic susceptibility measurements and outcrop. This effort was not successful due to a weak susceptibility contrast and the relatively thin till overburden (0 m to ~50 m).

Target locations were selected for exploratory temperature-gradient drilling based upon the interpretation of the magnetic data in combination with available geologic data. These targets remain confidential at the request of the client.

Mira Geoscience
...modelling the earth

References

Plouffe, A. and Jackson, L.E., Jr., 1995, Quaternary stratigraphy and till geochemistry in the Tintina Trench, near Faro and Ross River, Yukon Territory. *in:* Drift Exploration in the Canadian Cordillera, Bobrowsky, P.T., Sibbick, S.J., Newell, J.M., and Matysek, P.F., Editors, British Columbia Ministry of Energy, Mines, and Petroleum Resources, Paper 1995-2, p. 53-66.

Yukon Geological Survey, 2014, Update of the Yukon Bedrock Geology Map: Yukon Geologogical Survey digital data, 1:250,000 scale, http://www.geology.gov.yk.ca/update_ yukon_bedrock_geology_map.html

Mira Geoscience
...modelling the earth

Appendix 1: Magnetic Susceptibility Data

Magnetic susceptibility data was collected in the field within the Ross River geothermal project area. Definitions of the bedrock types at each measurement locality are provided below. Bedrock type is listed according to the 2014 Yukon Geological Survey 1:250,000 geologic map. In the event that bedrock was not measured, the measured rock type is indicated (e.g. glacial till). In a few instances, only one measurement of magnetic susceptibility was made at a given locality – in these cases, the minimum and maximum values were not determined and are labeled "n.d."

	UTM WGS84				Mag Susc (SI x 10^{-3})		
ID	Easting (m)	Northing (m)	Elevation (m)	Bedrock Type	Min.	Max.	Average
1	613443	6879712	853	Glacial erratic	0.297	0.297	0.297
2	613118	6881918	824	CK2	0.015	0.020	0.018
3	611359	6881202	849	CK3	0.150	0.220	0.210
4	611567	6881094	780	CK3	0.170	0.230	0.200
5	611668	6881147	778	ITR3	0.070	0.160	0.100
6	611729	6881373	770	ITR3	0.050	0.150	0.100
7	611851	6881637	750	ITR3	7.000	24.000	15.500
8	624513	6875553	772	CK2	0.020	0.040	0.030
9	624437	6875515	766	DMF3	0.130	0.170	0.150
10	625831	6873069	741	DMF1	0.040	0.090	0.065
11	626082	6872067	742	DMF1	0.160	0.170	0.165
12	626069	6871899	746	ITR3	0.080	0.170	0.140
13	628989	6871203	813	PDS2	0.200	0.300	0.250
14	626180	6866227	794	CDS1	0.500	2.000	1.500
15	622893	6865300	861	CDS3	0.070	0.090	0.080
16	620246	6864775	841	CDS3	0.200	0.400	0.300
17	625510	6866751	941	CDS1	0.110	0.170	0.140
18	632843	6870582	936	DMF3	0.070	0.100	0.085
19	634208	6873154	742	Quaternary fine-grained lake sediments	0.255	0.332	0.294
20	631704	6873221	803	KS6	0.016	0.045	0.025
21	631476	6873292	806	KS6	0.060	0.080	0.070
22	625125	6866891	986	CDS1	n.d.	n.d.	0.140
23	596424	6893881	618	KS6	0.090	0.130	0.110

24	597608	6891247	802	ITR3	0.061	0.114	0.088
25	628607	6871693	863	Glacial till	0.272	0.485	0.379
26	620645	6877175	802	Glacial till	0.141	0.337	0.239
27	618098	6878880	804	CK2	0.020	0.045	0.030
28	614946	6880027	792	Glacial till	0.270	0.354	0.312
29	611714	6882497	753	Glacial till	0.175	0.409	0.292
30	597058	6891373	796	Glacial till	0.334	0.560	0.447
31	592065	6893452	743	Glacial till	0.172	0.556	0.364
32	596340	6891595	759	CK3	0.040	0.229	0.060
33	603502	6887933	829	Glacial till	0.237	0.386	0.312
34	604376	6887037	849	CK3	0.020	0.060	0.040
35	612017	6882590	775	ITR3	0.050	0.070	0.060
36	611765	6882854	762	CK3	0.018	0.047	0.033
37	611585	6882985	768	JFP1	0.481	0.785	0.633
38	625569	6874926	754	CK2	0.020	0.028	0.024
39	613503	6881610	788	Glacial till	0.200	0.369	0.285
40	597784	6890638	800	CK3	0.156	0.256	0.206
41	621585	6873713	821	ITR3	n.d.	n.d.	0.125
42	621290	6873327	840	CK3	n.d.	n.d.	0.080
43	626237	6870826	775	ITR3	n.d.	n.d.	0.050
44	626237	6870826	775	ITR3	n.d.	n.d.	0.050
45	626537	6869742	761	ITR3	0.090	0.138	0.120

Bedrock Type	Rock Description
CK2	Paleozoic limestone
CK3	Paleozoic volcaniclastic/sandstone/conglomerate/shale sedimentary rock
ITR3	Eocene sediments/volcanics siltstone/congl./sandstone/basalt/rhyolite/porphyry
DMF3	Paleozoic metamorphic carbonaceous phyllite
DMF1	Paleozoic metamorphic phyllite schist
PDS2	Paleozoic metamorphic marble & carbonaceous schist
CDS1	Paleozoic sedimentary shale/siltstone/limestone
CDS3	Paleozoic sedimentary shale/slate/quartzite/limestone
KS6	Cretaceous mudstone/conglomerate
JFP1	Jurassic sedimentary conglomerate/chert/quartzite/serpentinite
PDS5	Paleozoic metamorphic quartzite, amphibolite, and eclogite
CPSM2	Paleozoic volcanics, basalt, and chert

Appendix 2: List of Deliverables

Deliverable	File Format	Description
Report	.pdf	Summary report describing the project objectives, procedures used, results, interpretation, and conclusions.
3D magnetic susceptibility inversion model	ASCII .txt file	Block model of magnetic susceptibility that extends over the entire magnetic survey area from the ground surface down to 2000 m below sea level
Iso-surfaces of constant magnetic susceptibility	.DXF files	Iso-surfaces are for the following magnetic susceptibility values: 0.0001, 0.0005, 0.001, 0.003, 0.004, 0.005, and 0.01 SI units
Horizontal slices through the 3D magnetic susceptibility model at constant elevation	Geosoft 2D binary grid files	Horizontal slices are at the following elevations: -2000 m, -1500 m, -1000 m, -250 m, -500 m, 0 m, +250 m, +500 m, +750 m, and +1000 m relative to sea level

NW-SE oriented longitudinal sections through the 3D magnetic susceptibility model	ASCII .txt files with four columns of data: X, Y, Z, MagSusc	Seven longitudinal sections spaced approximately 1.2 km apart. Locations are shown graphically below. Data points in the sections are spaced 50 m apart horizontally and 30 m apart vertically.
NE-SW oriented cross-sections through the 3D magnetic susceptibility model	ASCII .txt files with four columns of data: X, Y, Z, MagSusc	Nineteen cross-sections spaced about 2.5 km apart. Locations are shown graphically below. Data points in the sections are spaced 50 m apart horizontally and 30 m apart vertically.
2D maps of filtered magnetic data	Geosoft 2D binary grid files	The following maps are provided: TMI, TMI-RTP, TMI-RTP (with Histogram Equalization), TMI-RTP-1VD, TMI-RTP-1VD (with Historgram Equalization), TMI-RTP-Total Horizontal Derivative
Interpretation of 2D magnetic maps	.DXF file	Ross_River_Mag_Interp.dxf

All deliverables are provided in UTM WGS84 zone 8N

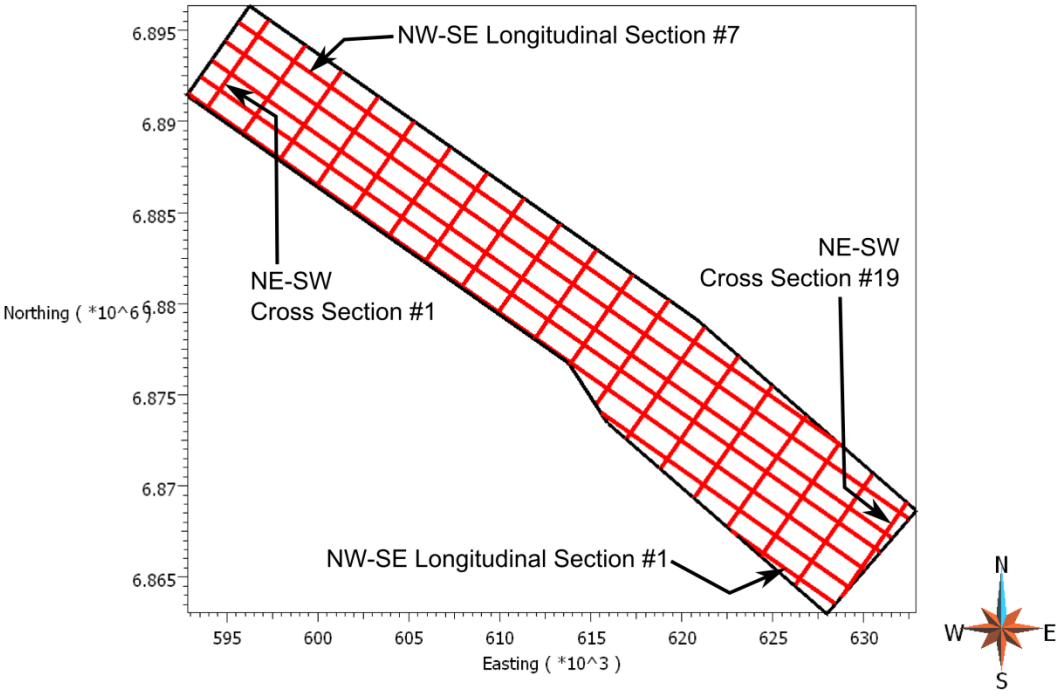

Graphical depiction of the relative locations of the seven NW-SE oriented longitudinal sections and the 19 NE-SW oriented cross-sections. The black polygon is the outline of the magnetic survey area. The exact 3D coordinates of the magnetic susceptibility data in the sections are recorded for each data point within the ASCII .txt files.

Mira Geoscience
...modelling the earth

Appendix 4: Structural Geology Data Analysis and Interpretation Report by University of Nevada, Reno

FINAL REPORT

GEOLOGIC ASSESSMENT OF THE GEOTHERMAL POTENTIAL OF THE ROSS RIVER AREA, YUKON, CANADA

Prepared for:
Dena Nezziddi Development Corporation
Ross River, Yukon
Y0B 1S0

Prepared by:
Nicholas Hinz and Seth Dee
Nevada Bureau of Mines and Geology, University of Nevada, Reno, NV 89557

February 2015

INTRODUCTION

Geologic investigations were conducted in conjunction with concurrent geophysical studies collectively designed to assess the geothermal potential across the Ross River project area in the Yukon, Canada. Investigation findings will guide anticipated future exploration phases, including the selection of drill targets for temperature gradient drilling. The Ross River project area is rectangular in shape, 20 km-wide by 60 km-long, and elongate northwest-southeast along the Tintina fault zone (Fig. 1). Reconnaissance geologic field mapping was conducted over a one week period in October, 2014. The new field data was integrated with new aeromagnetic-based interpretations provided by Mira Geosciences and from existing publically available geologic maps from the Yukon Geological Survey and the Canadian Geological Survey to produce a digital 1:50,000 scale geologic map of the Ross River project area (Plate 1). Field data on faults, fractures, and folds were analyzed to help characterize the structural framework. Regional data on the bedrock stratigraphy, structural geology, tectonic models, and earthquake seismicity was compiled from existing geologic maps, published reports, and peer-reviewed papers to characterize the geologic setting. The current tectonic stress fields and crustal strain rates in the region are of particular relevance to the assessment of the geothermal potential of bedrock structures within the Ross River project area. This report summarizes the structural and stratigraphic framework of the Ross River project area, characterizes the geologic setting, geothermal potential, and provides guidance for the anticipated temperature gradient drilling program.

BACKGROUND ON GEOLOGIC SETTINGS OF GEOTHERMAL RESOURCES

Geothermal energy is thermal energy generated and stored in the Earth. Thermal energy naturally radiates outward from the Earth's hot core and mantle through the crust. The temperature difference between the ground surface and the base of the Earth's crust determines the geothermal gradient. Geothermal systems are characterized by locally elevated geothermal gradients and enhanced permeability (i.e., fluid flow) in the upper few kilometers of the crust. Elevated geothermal gradients are related to one or more of the following attributes: 1) absolute crustal thickness (thinner crust facilitates higher geothermal gradient), 2) thermal conductivity of lithologic units (the ability of a specific rock type to conduct heat transfer), 3) convection of fluids along faults, fractures, and/or through lithologic units with naturally high permeability (convection is a more efficient mode of heat transfer than conduction), and 4) heat from magma in the crust (active volcanic regions). Geothermal power is generated by the extraction of hot fluids through wells installed to depths ranging from less than 1 km to more than 2 km. In summary, geothermal systems require a combination of heat, permeability, and fluids. Even when heat is present, finding permeability has been one of the greatest challenges to geothermal exploration as attested by numerous hot dry wells drilled around the world.

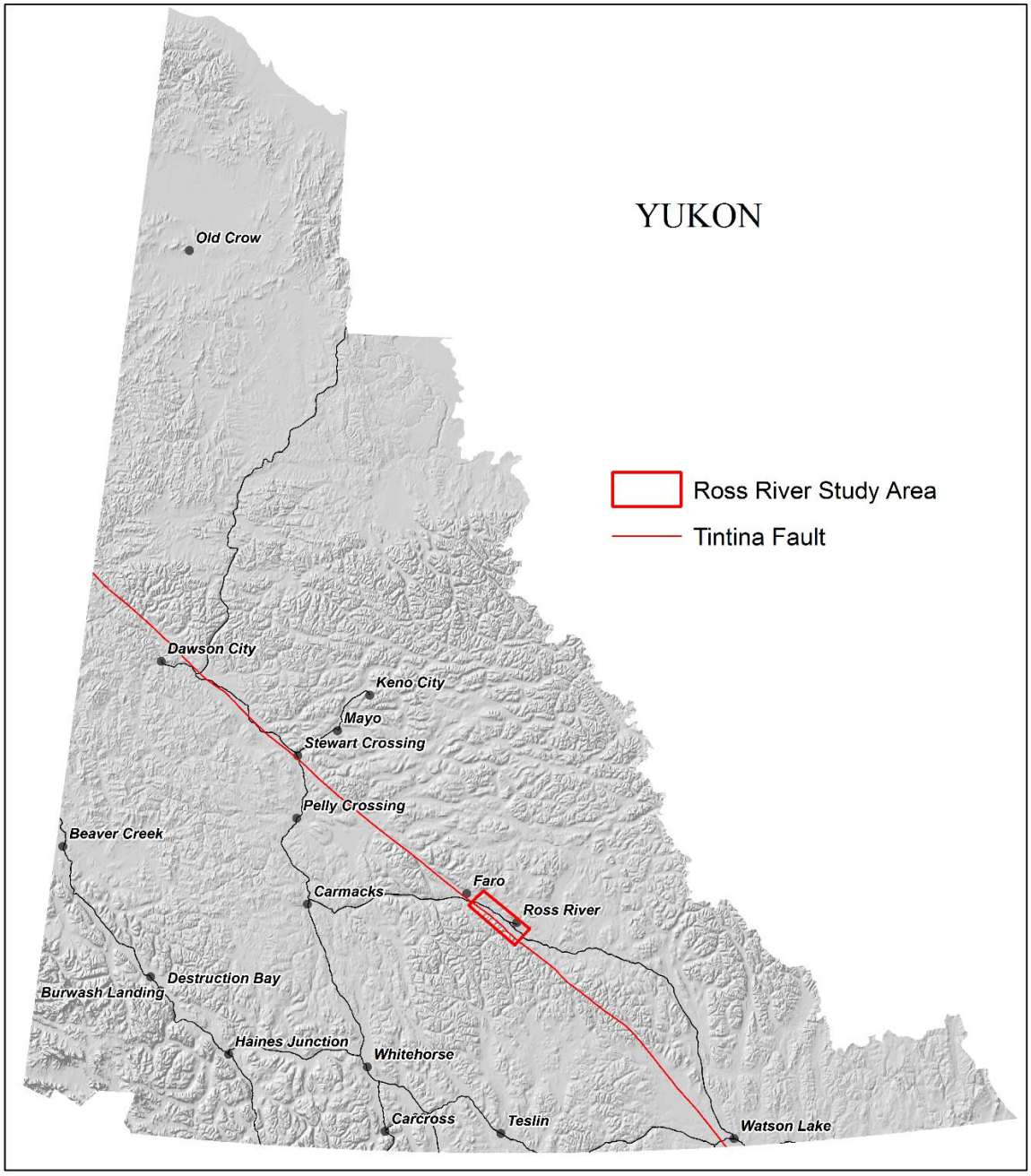

Figure 1. Location map of the Ross River project area on a shaded relief map of the Yukon.

GEOTHERMAL RESOURCE POTENTIAL IN THE ROSS RIVER AREA

Given the geographic position of the Ross River area it is unlikely that a potential undiscovered geothermal resources will be related to magmatic heat. The Ross River area is located northeast of the northwest-trending northern Cordilleran volcanic province (NCVP) that runs west of the Tintina fault zone (Edwards and Russell, 2000). Furthermore, many of the Quaternary volcanic centers in the NCVP are comprised of basaltic magmas sourced from the base of the crust and

therefore provide little heat to drive geothermal activity. Magmatically heated geothermal systems around the world are typically associated with upper crustal magmatism.

Potential geothermal resources for the Ross River area include structurally controlled systems, radiogenic granites (such as at Chena Hot Springs, AK), or possibly deep stratigraphic resources.

- Structurally Controlled Systems: Over the past decade research has greatly advanced the understanding of amagmatic structurally controlled geothermal systems. Notably: (1) All of these systems are associated with steeply dipping faults with complex fault and fracture networks that facilitate deep convection of geothermal fluids, and are associated with specific structural settings, such as terminations of major normal faults, accommodation zones, pull-aparts in strike-slip faults, displacement transfer zones, or step-overs in range-front faults (Faulds et al., 2011, 2015); (2) Quaternary faults typically lie within or near most of the geothermal systems (Bell and Ramelli, 2007); and (3) With respect to the Great Basin, the density of geothermal systems correlates positively with tectonic strain rates, particularly extensional strain (Faulds et al, 2012, 2015). Furthermore, many of these systems are blind; of the more than 400 known geothermal systems in the Great Basin region, USA, >40% are blind and have no active surface manifestations such as hot springs or fumaroles (Faulds et al., 2011; Faulds and Hinz, 2015).
- Radiogenic granites: Anomalously radioactive plutons can produce sufficient heat through decay of the radiogenic minerals to drive geothermal activity. One such example is Chena Hot Springs, located near Fairbanks, Alaska in the central Alaskan hot springs belt. Chena has had an operating 0.7 MW power plant since 2006 (Kolker, 2008). However, few radiogenic resources have been developed globally as permeability has been an issue, possibly due to an unfavorable present-day tectonic setting.
- Deep Stratigraphic Reservoirs: The potential for "deep stratigraphic reservoirs" has acquired recent attention in North America and elsewhere in the world, (e.g., Hurter and Schellschmidt, 2003; Porro et al., 2012; Barkaoui et al., 2014; Busby, 2014). Recent studies indicate the best conditions for economically viable development are associated with thick sedimentary basins with low-thermal-conductivity sedimentary cap rocks overlying permeable host rocks (e.g. carbonates) and co-located with areas of high heat flow (Allis et al., 2012; Kirby, 2012). In basins that have been studied thus far in the Great Basin region, the theoretical optimum depth for economical production is 3 to 4 km-deep. For example, in Steptoe Valley in eastern Nevada, a 130 km^2 reservoir with appropriate depth and temperature may hold upwards of 500 MWe of geothermal resource potential (Allis et al., 2012; Hinz et al., 2015). The cost of drilling deep test holes alone makes exploration for these resources challenging. However, exploration of deep "hot" stratigraphic resources has mostly focused on higher enthalpy resources for power production, but shallow "warm" stratigraphic reservoirs can be economically viable for direct use applications (heating of buildings, etc.).

GEOLOGIC SETTING OF THE ROSS RIVER AREA

The Ross River project area straddles the northwest-striking Tintina fault zone (Fig. 1, Plate 1). The Tintina fault joins the northern Rocky Mountain trench near the Yukon/British Columbia border forming a 2000 km-long structure that separates dominantly autochthonous (native) North American rocks to the east and dominantly allochthonous (accreted) terranes to the west. The autochthonous rocks east of the Tintina fault include late Proterozoic to Paleozoic metamorphic rocks and Paleozoic to middle Mesozoic sedimentary and volcanic rocks. The allochthonous rocks west of the Tintina fault include Paleozoic to middle Mesozoic sedimentary rocks. Cretaceous granitic plutons intrude both the autochthonous strata and accreted strata to either side of the Tintina fault. Early Tertiary volcanic and sedimentary rocks locally fill pull-apart basins within the Tintina trench and rest unconformably on Paleozoic strata. Quaternary surficial deposits cover the valley floors and lower hillslopes and include unconsolidated glacial and fluvial deposits that range from several meters to more than 50 meters thick.

Tectonic History

The Proterozoic and Paleozoic strata east of the Tintina fault were deformed during multiple orogenic events in the Paleozoic (Cook, 1992). Active plate convergence and subduction dominated the western margin of North America throughout the Mesozoic, deforming all pre-Tertiary strata. Dextral-oblique subduction along western North America in the Mesozoic and early Cenozoic drove large intra-orogenic strike-slip faults such as the Denali and Tintina faults that translated large crustal blocks at least 400 to 500 km northwestward along each fault (Murphy and Mortensen, 2003). Early Tertiary strata were locally deposited during periods of transtension in pull-apart basins along the Tintina fault zone and subsequently deformed through later transpression (e.g., Till et al., 2007; Stroshein, 2008). Motion along the Tintina fault waned by the middle Tertiary, probably in relation to the shift from subduction to mainly strike-slip plate boundary along the western margin of the northern Cordillera in the late Eocene (e.g., Engebretson et al., 1995).

Present-day Tectonics

It is not known if the Tintina fault has remained active in the late Tertiary and Quaternary. Quaternary fault scarps have not been identified along the fault, although thorough paleoseismic studies (e.g. LiDAR analysis and paleoseismic trenching) have not been conducted along this fault. Regional earthquake seismicity and geodetic data help to characterize potential for activity on the Tintina fault and help define the regional tectonic stress field.

The distribution of historic seismicity across the Yukon is primarily focused in two areas: 1) in the southwest along the highly active Denali, St. Elias, and Duke River dextral fault zones; and 2) in the Richardson and Mackenzie Mountains along the Yukon/NWT border region (Fig. 2; Leonard et al., 2008). A third area of concentrated low level seismicity, north of Dawson City is related to the Dawson Thrust. Historic earthquakes are sparsely distributed along the Tintina fault from

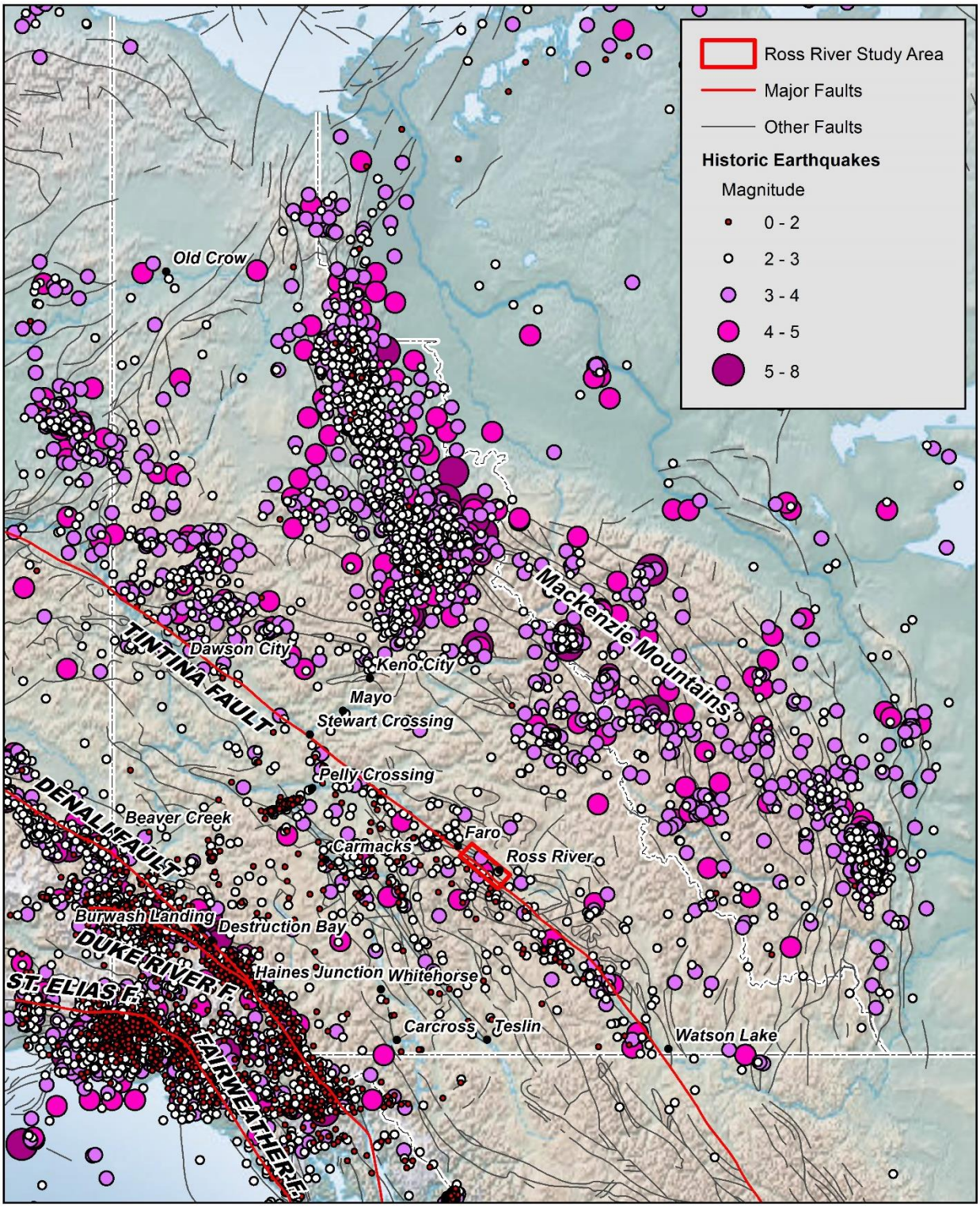

Figure 2. Historic earthquake seismicity for part of northwest Canada and eastern Alaska from the Yukon Geological Survey (2009) with faults from Garrity and Soller (2009).

Steward Crossing to Watson Lake and encompass much of the Pelly Mountains, with a magnitude 4.5 earthquake being the largest recorded event in the region. Based on various seismic data derivatives Leonard et al. (2008) estimated a potential slip rate of about 0.5 mm/yr along this part of the Tintina fault. For reference, the relative motion between the Pacific and North American plates is about 55 mm/yr.

Geodesy provides direction measurements of relative motion of the Earth's crust, typically using high resolution GPS instruments. Available GPS geodetic data for the Yukon region indicates that about 90% of the relative 55 mm/yr motion between the Pacific and North American Plates is accommodated along Denali, St. Elias, Duke River, and Fairweather faults in southwest Yukon and southeast Alaska (Fig. 2; Hyndman et al., 2005). Deformation in the Richardson and Mackenzie Mountains region accommodates much of the remaining 10% of the relative motion. The GPS data shows very little contemporary deformation between the Denali fault (southwest of Whitehorse) and the Mackenzie Mountains, suggesting that this region is behaving as a semi-rigid block, punctuated by a zone of weakness and low level seismicity associated with the Tintina fault. However, the geodetic studies covering the Yukon interior have used campaign style networks which are deployed over a couple weeks at a time and have relatively high error margins, versus higher accuracy year round continuous networks used elsewhere in the world. So if the Tintina fault is active at 0.5 mm/yr as modeled by Leonard et al. (2008), the current GPS geodetic data may not distinguish this rate of deformation.

Stress inversion calculations from earthquake focal mechanisms in northwest Canada and eastern Alaska indicate that the Tintina fault currently resides in a region with the principle horizontal stress oriented northeast-southwest to north-northeast-south-southwest (Fig. 3; Hyndman et al., 2005; Ristau et al., 2007; Heidbach et al., 2008). The northwest-striking Tintina fault is oriented nearly perpendicular to the regional maximum horizontal stress-orientation. This configuration is consistent with modern-day dextral transpression and/or compressional strain along the Tintina fault.

Heat Flow

Much of the Yukon is associated with anomalously high heat flow, averaging >100 mW/m^2 (Lewis et al., 2003). This has been attributed to above average radiogenic heat production in the upper crust and to a thin and weak lithosphere that may allow for hot asthenosphere to come in contact with the lower crust. Contrasting the high heat flow, the central Yukon is not known for abundant geothermal resources. This pattern generally fits with the relatively rigid behavior of the crust between the Denali fault and the Mackenzie Mountains which does not allow for much internal deformation, particularly extensional strain. However, the Tintina fault is a major structure that penetrates the entire thickness of the crust, is associated with historic seismicity of up to about magnitude 4.5, and considering the minimal geothermal exploration across this area, it is possible that this region hosts undiscovered blind resources.

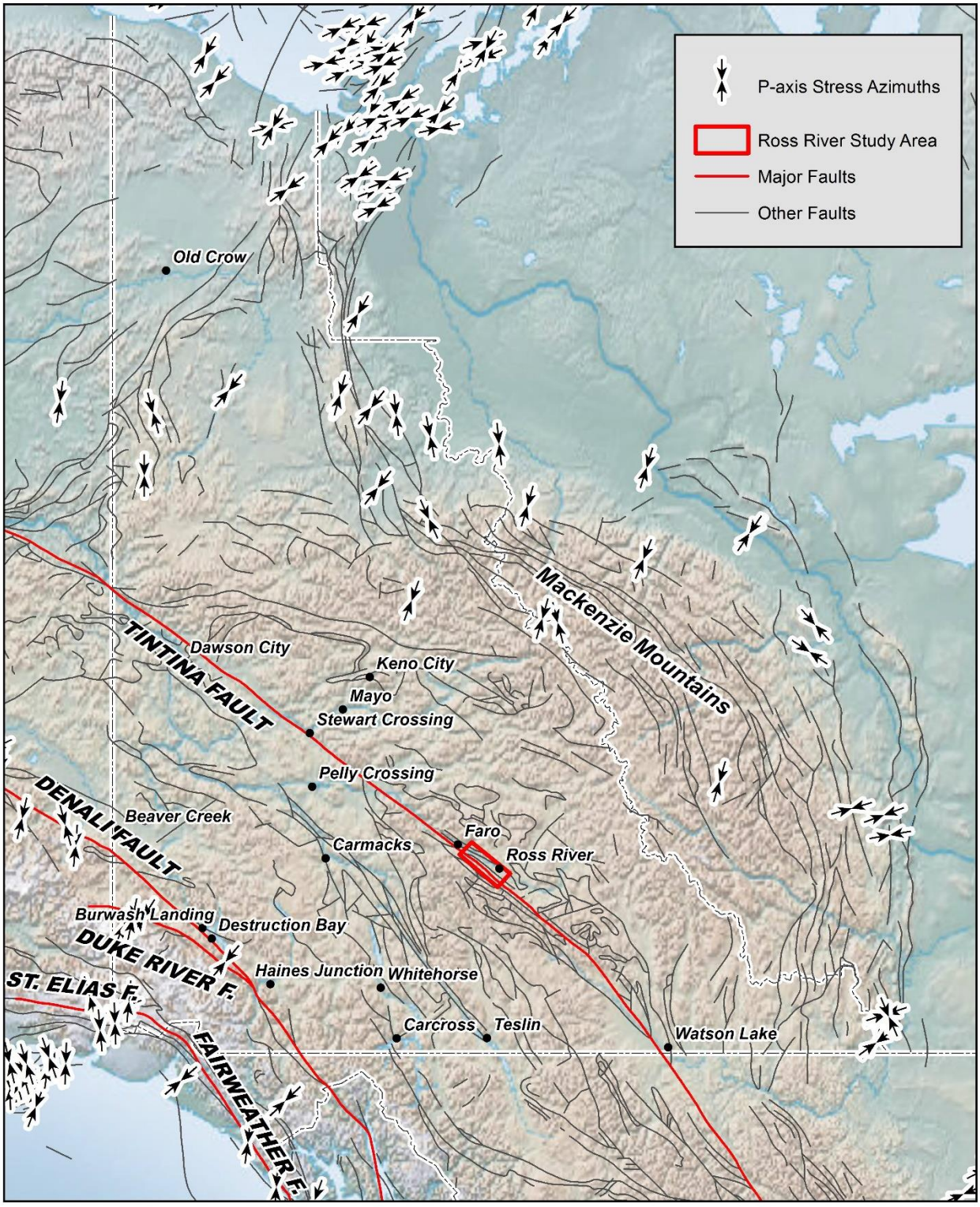

Figure 3. Principle horizontal stress orientations for part of northwest Canada and eastern Alaska from the World Stress Map (Heidbach et al., 2008) with faults from Garrity and Soller (2009).

GEOLOGIC MAPPING

Reconnaissance geologic field mapping was conducted over a one week period in October, 2014 and targeted bedrock exposures along the Campbell Highway, Canol Road, multiple unnamed dirt roads, Lapie River, Danger Creek, Grew Creek, and the Pelly River. Outcrops east of the Pelly River were not visited in this study due to limited accessibility to that side of the river and also to focus on collecting data to directly compliment the geophysical data sets (MT and aeromagnetic) which were positioned west of the Pelly River. The new field data was integrated with aeromagnetic-based interpretations provided by Mira Geosciences and from existing publically available geologic maps from the Yukon Geological Survey (Yukon Geological Survey, 2014) and the Canadian Geological Survey (Templeman-Kluit, 1971, 2012) to produce a digital 1:50,000 scale geologic map of the Ross River project area (Plate 1). The next two sections of this report discuss the bedrock structure and stratigraphy of the map area, including a quantitative analyses of structural field data.

Structure and Stratigraphy of the Ross River Area

The Ross River map area is dominated by the northwest-striking Tintina fault zone, which locally forms an approximately 10 km wide zone that is made up of nearly a dozen major sub-parallel, steeply dipping fault strands and numerous minor synthetic faults (Plate 1). The six most prominent fault strands that locally make up the Tintina fault zone were named by Templeman-Kluit (1971, 2012) and modified slightly in this study to include from west to east: 1) Tintina fault, 2) Grew Creek fault, 3) Danger Creek fault, 4) Ross River fault, 5) Lapie River fault 1, and 6) Lapie River fault 2. These faults have steep sub-vertical dips, and bracket distinct stratigraphic and structural blocks (Fig. 4). From west to east these blocks include:

- **Block A:** West of Tintina Fault: The region between the Tintina fault and the southwest edge of the map area ranges from 5-7 km-wide and comprises about 30% of the map area (Fig. 4, Plate 1). This area is composed of Cambrian through Devonian shale, siltstone, graphitic slate and shale, limestone and silty limestone (Plate 1 map units CDS1, 2, 3, 4; COK1), and is locally intruded by Cretaceous granitic rocks (mKgC) in the northern half of the map area. The Paleozoic strata have northwest- to west-strikes with moderate to vertical dips. This area is also cut by relatively minor northwest-striking synthetic splays of the Tintina fault zone.
- **Block B:** Tintina Fault to Grew Creek Fault: The Tintina and Grew Creek faults bound a 1-3 km-wide block of Carboniferous shale (Fig. 4, Plate 1 map unit CK3). The shale beds strikes consistently west to northwest with moderate to vertical dips. This block is cut by numerous north-striking high-angle faults observed in the field, on aerial imagery, and interpreted from the aeromagnetic data. An additional area of structural complexity is located along the Grew Creek fault, immediately southeast of the Canol road. There are no bedrock exposures in this area, but an approximate 2 km-wide magnetic high suggests a stratigraphic and/or structural discontinuity. One possible interpretation of this magnetic anomaly is a small intrusion along the Grew Creek fault and possibly faulted post emplacement.

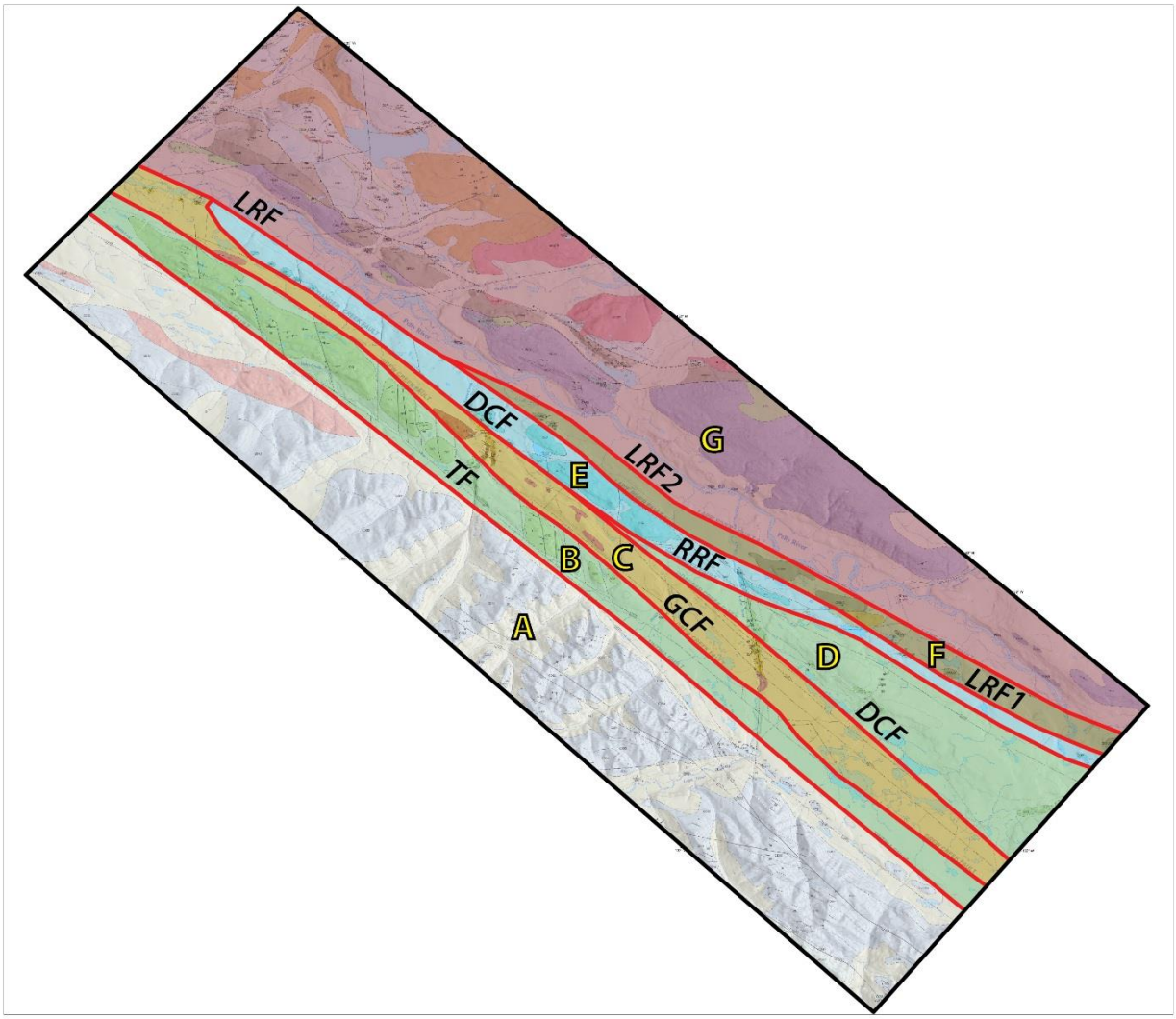

Figure 4. Major structural/stratigraphic domains of the Ross River area overlain on the Ross River Geologic Map (Plate 1). A, B, C, D, E, F, G refer to structural/stratigraphic domains described in the text. Fault labels in black font placed along east (top side in map view) of each red fault line and include: TF, Tintina fault; GCF, Grew Creek fault; DCF, Danger Creek fault; RRF, Ross River fault; LRF, Lapie River fault; Lapie River fault splay 1; LRF2, Lapie River fault splay 2.

- **Block C:** Grew Creek Fault to Danger Creek Fault: The Grew Creek and Danger Creek faults bound multiple Tertiary volcanic and sedimentary rock units (Fig. 4, Plate 1 map units Ts, Tb, Tvs, Tfv) that fill a compound 1-2.5 km wide series of transtensional pull-apart basins that extends beyond the Ross River map area. The Tertiary units generally strike northwest with steep to gentle dips and are folded along west-northwest to northwest-trending fold axes. This fault block is cut by multiple synthetic dextral northwest- striking strike-slip faults and several north to north-east striking high-angle faults.
- **Block D:** Danger Creek Fault to Ross River Fault: The Ross River Fault is a major northeast-eastern splay of the Danger Creek Fault. These two faults bound a block of Carboniferous shale (Fig. 4, Plate 1 map unit CK3) up to over 5 km wide at the sound end of the map area.

The shale strikes west to northwest with moderate dips and may correspond to fault block A between the Tintina and Grew Creek faults.

- **Block E:** Ross River and Danger Creek Faults to Lapie River and Lapie River 1 Faults: The Danger Creek/Ross River fault and Lapie River 1 faults bound a block 0.5 to 2 km-wide composed predominantly of Carboniferous limestone (Fig. 4, Plate 1 map unit CK2). The limestone is locally highly brecciated along high-angle faults that are synthetic and antithetic to the bounding northwest-striking dextral faults. This block also includes one outcrop of Carboniferous mafic volcanic rocks (CK1) and possible outcrops of Jurassic conglomerate (JFP1), however the JFP1 unit was not confirmed in the field. A single Tertiary pre-volcanic sedimentary outcrop (Ts) resides in the southern half of this fault block.
- **Block F:** Lapie River 1 Fault to Lapie River 2 Fault: The Lapie River fault splays southeast into two strands, the Lapie River 1 fault and the Lapie River 2 fault (Fig. 4). This 1 km-wide fault block consists of Carboniferous to Permian basalt (Plate 1 map unit CPSM2) and a Tertiary pre-volcanic sedimentary outcrop (Ts) that spans this fault block and fault block E.
- **Block G:** East of Tintina Fault: The region between the Lapie River fault and the northeast edge of the map area is 2-12 km-wide and comprises about 30% of the map area (Fig. 4, Plate 1). This area is composed of Proterozoic to Paleozoic metamorphic rocks (Plate 1 map units PDS2, 3, 5), Paleozoic sedimentary and volcanic rocks (CPSM1, 2, 4; ODR1, COR1, CSM1, 8; ICG1, 3), Mesozoic sedimentary rocks (JFP1, 2, 3), and Mesozoic plutons (mKgTR). This region was not covered by the October 2014 field reconnaissance.

Eocene transtension, volcanism, and geothermal activity

The Tertiary strata provide an important temporal record of tectonic, sedimentary, volcanic, and geothermal activity along the Tintina fault zone. The oldest Tertiary unit, Ts consists of sandstone and conglomerate composed of pre-Tertiary volcanic clasts and intercalated with numerous coal beds, is probably early Eocene based on plant fossils (Hughes and Long, 1980). All the other units are dominated by Tertiary volcanic rocks and include Tfv (felsic lavas, tuffs, and intrusions), Tb (basalt and basalt-clast dominated sandstone, and Tvs (sandstone and breccia composed predominantly of Tertiary mafic and felsic volcanic clasts). Basalt dikes, possibly related to the Tb unit locally intrude the Ts and Tvs units. No direct age dates have been acquired for the Tfv, Tb, or Tvs units. The similar magnitude of deformation of all four Tertiary units along the Tintina fault zone support that the volcanic units may also be Eocene. The Tertiary volcanic units probably represent a period of bimodal volcanism related to a period of local(?) transtension within the Tintina fault zone.

In the Grew Creek area, the Tertiary strata locally host epithermal mineral deposits (Stroshein, 2008). Hughes and Long (1980) also noted that many of the coal beds in Ts were anomalously high grade and were probably related to a period of relatively high geothermal gradient at some time in the past. Together the epithermal gold deposits and the anomalously high grade coal indicate a past history of anomalous heat flow. The geothermal activity may have been related

to felsic magmatism associated with the Tfv unit and/or with deep circulation of fluids along normal faults and fractures associated with the opening of pull-apart basins along the Tintina fault. Any potential modern geothermal resources would post-date the geothermal activity in the early Tertiary.

Structural Analyses

Folds, fractures, and faults were analyzed to help characterize structures associated with the Tintina fault zone and derive stress field orientations from measured strain (deformation) of the bedrock. Stress field determination is important for exploration of structurally controlled systems because the orientation of the principal and minimum horizontal stress orientations relative to fault orientations can be used to predict slip and dilation potential of faults and fractures. Critically stressed fault strands are the most likely fault segments to act as fluid flow conduits (Barton et al., 1995; Sibson, 1994; Townend and Zoback, 2000). The tendency of a fault segment to slip or to dilate provides an indication of which sections of a fault zone within a geothermal system are most likely to transmit geothermal fluids (Morris et al., 1996; Ferrill, et al., 1999). Determining the stress field is one important metric for predicting relative potential of a fault or fracture to be permeable based on its orientation relative to the current stress field. Stress field orientations can be used solitarily or combined with other geologic and geophysical-based metrics for geothermal favorability.

Fold axes form parallel to the least principle stress direction. Evaluation of folds in the Tertiary strata provide a record of stresses and resultant deformation concurrent with and/or post-deposition of these strata in the early to middle Tertiary. Whereas, evaluation of folding of Paleozoic strata could reflect folding associated with one or more tectonic events over a longer time period including events in the Paleozoic prior to the evolution of the Tintina fault zone. Twenty bedding attitudes were measured in the Tertiary strata within the Ross River map area. Poles to bedding of the Tertiary strata plotted on a stereonet have a girdle distribution with bimodal north-northeast and south-southwest dips (Fig. 5A). This distribution fits folding about an axis trending approximately 297°. This fold orientation results in a S_{Hmax} (maximum horizontal stress) oriented north- northeast and S_{Hmin} (minimum horizontal stress) oriented west-northwest, parallel to the fold axis.

Tensional fractures propagate perpendicular to the least principle stress and parallel to the principle and intermediate stress directions. Seven fracture measurements were obtained in the Paleozoic and Tertiary strata within the Ross River map area. These fractures strike north-northwest to north-northeast with steep, bimodal east and west dips (Fig. 5B). The average fracture orientation strikes 009° with 88° west dip. Although the collected data population is relatively small (n=7), the consistent distribution of fracture orientations implies development under stress orientations similar to the folds, with a S_{Hmin} oriented west-northwest.

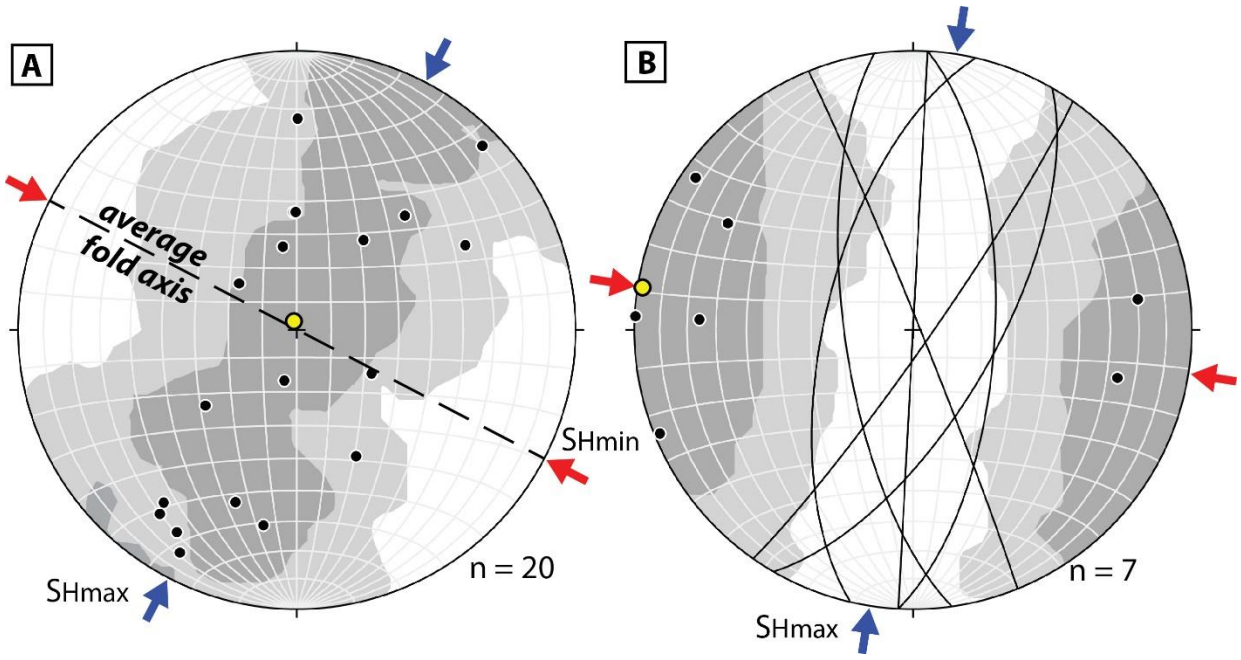

Figure 5. A) Stereographic projection of poles to bedding of Tertiary volcanic and sedimentary units from within the Ross River study area; including 14 attitudes obtained in this study and 6 attitudes from Templeman-Kluit (1971, 2012). Yellow circle is the average pole to bedding, trend and plunge = 341°, 87°. Average fold axis trend 297°. **B)** Stereographic projection of tensional fractures and poles to fracture planes from the Ross River study area; all data from this study. Yellow circle is the average pole to fracture plane, trend and plunge = 099°, 2°. **Both (A) and (B)**: Kamb contours of poles to planes in both figures at 2 sigma; blue and red arrows correspond to S_{Hmax} and S_{Hmin}, respectively.

Fault surfaces exposed in the Ross River map area were analyzed to interpret the kinematics of the fault systems and determine the orientations of principal strain and stress axes. The stress field can be derived from fault slip data assuming a linear and direct relationship between strain and the stress (e.g. PTB method in Sippel et al., 2009). The method used here is a simple kinematic analysis that calculates the three perpendicular principal strain axes for each individual fault-slip datum, i.e. maximum compressive stress (σ^1), intermediate compressive stress (σ^2 which lies in the fault plane), and the minimum compressive stress (σ^3). Employing the Mohr-Coulomb failure criterion, the method incorporates a defined fracture angle between σ^1 and the slip surface. Simple fault mechanics predict that the maximum compressive stress is oriented 30° to 45° oblique to the fault surface, parallel to the slip direction. For this study, a fracture angle of 30° was applied as that is most representative of faulting conditions around the world. The application of this process to the entire fault population of a particular location results in a comprehensive pattern of kinematic axes. This cumulative plot permits detection of kinematic consistencies as clusters of σ^1, σ^2, and σ^3 axes in a heterogeneous data set.

Thirty fault surfaces were measured within the Ross River map area (e.g., Figs. 6A, B, C). These faults include three primary populations including: northwest- to west-northwest-striking dextral faults; N-S-striking normal faults, sinistral faults, and dextral faults; and northeast- to east-

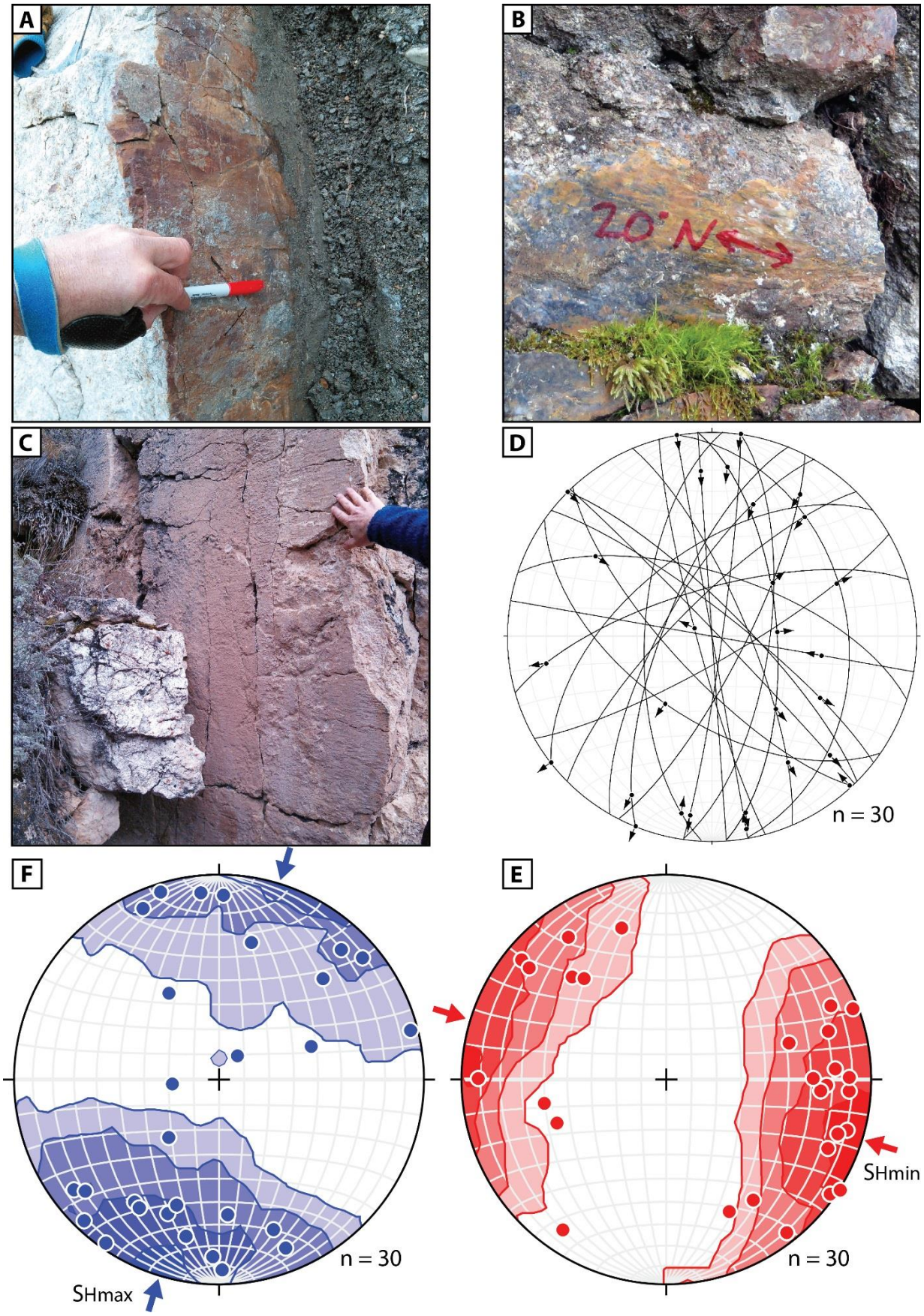
A
B
20° N
C
D
n = 30
F
E
n = 30
SHmax
n = 30
SHmin

Figure 6. (Previous page) Fault kinematics from fault surfaces exposed in the Ross River area; all data collected in this study. *Examples of fault surfaces:* **A)** WNW-ESE-striking fault surface in Tertiary volcaniclastic sedimentary rock (Tvs) with two sets of striae; one sub-horizontal and one raking 30° from north; **B)** North-striking fault with striae raking 20° from north in pre-volcanic Tertiary sediments (Ts); **C)** Northwest-striking dextral fault with sub-horizontal striae in Carboniferous limestone (CK2). *Fault kinematic data and stress inversion:* **D)** Lower hemisphere stereographic projection of fault planes and trend and plunge of slip directions of fault surfaces exposed in the Ross River map area; **E)** Lower hemisphere stereographic projection of trend and plunge of calculated σ^1 for each kinematic datum in (D), contours equal 2 sigma, average S_{Hmax} azimuth is 017°; **F)** Lower hemisphere stereographic projection of trend and plunge of calculated σ^3 for each kinematic datum in (D), contours equal 2 sigma, average S_{Hmin} azimuth is 287°.

northeast-striking sinistral faults (Fig. 6D). Stress inversion of the fault slip data indicates a relatively consistent stress pattern with S_{Hmax} oriented north-northeast/south-southwest and S_{Hmin} oriented west-northwest/east-southeast (Figs. 6E, F), consistent with the analysis of fold axes and tensional fractures.

GEOTHERMAL POTENTIAL

The Ross River area has a complex structural and stratigraphic framework. The bedrock stratigraphy is principally composed of Proterozoic metamorphic strata; Paleozoic volcanic strata, siliciclastic and carbonate sedimentary strata; and Mesozoic granitic plutons. Early Tertiary sedimentary strata fill distinct pull-apart basins along the Tintina fault zone. In the Ross River area the Tintina fault zone is about 10 km wide and composed of up to a dozen steeply dipping synthetic fault splays. The intervening fault blocks are locally cut by numerous north-striking faults. Analyses of folds, fractures, and faults primarily collected in the Tertiary strata collectively indicate S_{Hmax} oriented north-northeast/south-southwest and S_{Hmin} oriented west-northwest/east-southeast during the formation of these structures. These data (Figs. 5, 6) collectively fit with a standard strain ellipse for a northwest striking dextral fault zone (Fig. 7) and probably reflect the stress conditions during the Eocene prior to the shift from subduction to a mainly strike-slip plate boundary along the western margin of the northern Cordillera in the late Eocene. Epithermal mineral deposits and high grade coal in the Tertiary strata record a history of geothermal activity, probably coincident with transtension, volcanism, and magmatism in the Eocene. The timing of this past geothermal activity is consistent with the Tintina fault being most active in the Mesozoic and early Tertiary. Modern day motion along the Tintina fault is poorly constrained. Modeling of earthquake seismicity indicates a possible 0.5 mm/yr slip rate, however Quaternary scarps have not been documented along the Tintina fault.

One challenge for exploration in the Ross River area is that strike-slip faults are notoriously impermeable in part because large magnitude strike-slip fault zones are dominated by clay gouge which is generally less permeable than brittle fault breccia. However, some of the largest geothermal systems in the world (500 – 1000 MWe) are located along strike-slip faults such as along the San Andreas in the USA and Mexico (e.g. Salton Sea and Cerro Prieto geothermal systems) and the Great Sumatra fault in Indonesia. Smaller geothermal areas (10 to 20 MWe)

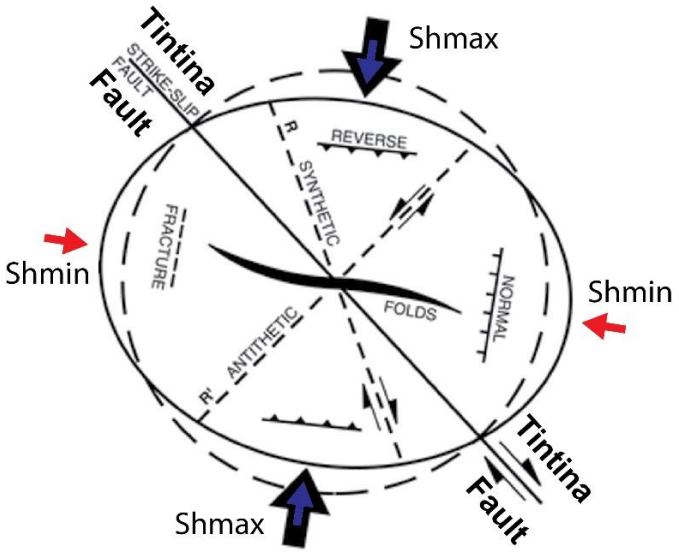

Figure 7. Strain ellipse model for a northwest-striking dextral fault with S_{Hmax} and S_{Hmin} each 45° relative to the vertical strike-slip fault plane. Correlative with strain accommodated in the Eocene (Figs. 5 and 6).

along these systems are associated with pull-aparts along strike-slip faults (e.g., Lee-Allen, Beowave) in the Great Basin region of the USA. The key to the San Andreas, Great Sumatra, or Great Basin systems is structural setting (e.g., pull-apart) and Quaternary active faults (active strain). Extensional strain drives dilation on faults and fractures, facilitating permeability for most amagmatic and magmatically heated geothermal systems around the world.

The Yukon is associated with relatively high heat-flow, comparable with the geothermal resource-rich Great Basin of the western USA (Lewis et al., 2003; SMU, 2004). The contrast in abundance of known geothermal resources in the Yukon compared with the Great Basin region is probably partly related to the contrasting tectonic setting, modern-day compression and transpression for the Yukon versus extension and transtension for the Great Basin. However, the exploration for geothermal resources in the Yukon has been minimal compared with the Great Basin, which leaves opportunity for discovering blind geothermal resources. Based on the geologic setting and absence of known surface manifestations of geothermal resources, blind, amagmatic resources are the most likely type of resource that could be found in the Ross River area. These include structurally controlled resources, radiogenically heated resources, and deep stratigraphic resources.

Potential Structural Resources

The modern-day principle tectonic stress orientations for the Ross River area is north-northeast/south-southwest to northeast-southwest for S_{Hmax}, west-northwest/east-southeast to northwest-southeast for S_{Hmin}. Faults and fractures oriented parallel or sub-parallel with S_{Hmax}, such as the N-S faults, will have the greatest potential for dilation (even without slip) and enhanced permeability. The modern day horizontal compressive stress is oriented nearly perpendicular to

the Tintina fault zone providing kinematic favorability for dextral oblique-reverse or high-angle reverse motion and minimal dilation. Areas with greater fault and fracture density locally weaken parts of the crust and may facilitate dilation relative to S_{Hmin}.

Potential Radiogenically Heated Resources

The Mesozoic granites could be considered for exploration (Plate 1 map units mKgTR and mKgC). Models of regional heat flow data imply anomalously high radiogenic heat production in the upper crust (Lewis et al., 2003). There is a large belt of anomalously radiogenic plutons across central Alaska. To date, there is no record of specific studies on the radiogenic level of granites in the Ross River area. It is possible that some plutons in the Ross River area may be anomalously radiogenic and could provide a valuable source of heat and thus targeting faults and fractures in these granites could prove fruitful.

Potential Deep Stratigraphic Resources

Primary permeability in the Paleozoic carbonates (Plate 1 map unit CK2) may facilitate greater stratigraphic-controlled convective fluid flow relative to other units. Although the local thickness of CK2 is unknown and is probably not large enough to form classic deep stratigraphic resource, this unit could facilitate enough fluid circulation to accommodate lower temperature reservoirs suitable for direct use applications.

REFERENCES CITED

Allis, R., Blackett, B., Gwynn, M., Hardwick, C., Moore, J., Morgan, C., Schelling, D., and Sprinkel, D.A., 2012, Stratigraphic reservoirs in the Great Basin – the bridge to development of enhanced geothermal systems in the US: Geothermal Resources Council Transactions, v. 36, p. 351-357.

Barkaoui, A.E., Zarhloule, Y., Verdoya, M., Pasquale, V., and Lahrach, H., 2014, Progress in understanding the geothermal sedimentary basins in northeastern Morocco, Proceedings, 39th Workshop on Geothermal Reservoir Engineering, Stanford University, Stanford, CA, Feb. 24-24, 2014.

Barton, C. A., M. D. Zoback, and D. Moos, 1995, Fluid flow along potentially active faults in crystalline rock: Geology, v. 23, p. 683-686.

Bell, J.W., and Ramelli, A.R., 2007, Active faults and neotectonics at geothermal sites in the western Basin and Range: Preliminary results: Geothermal Resources Council Transactions, v. 31, p. 375-378.

Busby, J., 2014, Geothermal energy in sedimentary basins in the UK: Hydrogeology Journal, v. 22, no. 129-141.

Cook, F.A., 1992, Racklan Orogen: Canadian Journal of Earth Science, v. 29, p. 2490–2496.

Edwards, B.R., and Russell, J.K., 2000, Distribution, nature, and origin of Neogene-Quaternary magmatism in the northern Cordilleran volcanic province, Canada: Geological Society of America Bulletin, v. 112, no 8, p. 1280-1295.

Engebretson, D.C., Cox, A., and Gordon, R.G., 1995, Relative motions between oceanic and continental plates in the Pacific Basin: Geological Society of America Special Paper 206.

Faulds, J.E., Hinz, N.H., and Kreemer, C.W., 2012, Regional patterns of geothermal activity in the Great Basin Region, western USA: Correlation with strain rates: Geothermal Resources Council Transactions, v. 36, p. 897-902.

Faulds, J.E., Hinz, N.H., Coolbaugh, M.F., Cashman, P.H., Kratt, C., Dering, G., Edwards, J., Mayhew, B., McLachlan, H., 2011, Assessment of favorable structural settings of geothermal systems in the Great Basin, Western USA: Geothermal Resources Council Transactions, v. 35, p. 777-784.

Faulds, N.H., and Hinz, N.H., 2015, Favorable tectonic and structural settings of geothermal settings in the Great Basin Region, western USA: Proxies for discovering blind geothermal systems: Proceedings, World Geothermal Congress 2015, Melbourne, Australia.

Ferrill, D.A., Winterle, J., Wittmeyer, G., Sims, D., Colton, S. and Armstrong, A., 1999, Stressed rock strains groundwater at Yucca Mountain, Nevada: Geological Society of America Today, v. 9, no. 5, p. 1-8.

Garrity, C.P., and Soller, D.R., 2009, Database of the geologic map of North America—Adapted from the map by J.C. Reed, Jr. and others (2005): United States Geological Survey Data Series 424, http://pubs.usgs.gov/ds/424/.

Heidbach, O., Tingay, M., Barth, A., Reinecker, J., Kurfe, D. and Müller, B., 2008, The World Stress Map database release 2008 doi:10.1594/GFZ.WSM.Rel2008.

Hinz, N.H., Coolbaugh, M.F., and Faulds, J.E., *in press 2015,* White Pine County Renewable Energy Feasibility Study and Resource Assessment: Nevada Bureau of Mines and Geology Open-File Report 15-X, 24 p.

Hughes, J.D., and Long, D.G.F., 1980, Geology and coal resource potential of Early Tertiary strata along Tintina Trench, Yukon Territory: Geological Survey of Canada Paper 79-32, 21 p.

Hurter, S. and Schellschmidt, R. 2003, Atlas of geothermal resources in Europe: Geothermics, v. 32, p. 779-787.

Hyndman, R.D., Fluck, P., Mazzotti, S., Lewis, T.J., Ristau, J., and Leonard, L., 2005, Current tectonics of the northern Canadian Cordillera: Canadian Journal of Earth Science, v. 42, p. 1117-1136.

Kirby, S.M., 2012, Summary of compiled permeability with depth measurements for basin fill, igneous, carbonate, and siliciclastic rocks in the Great Basin and adjoining regions: Utah Geological Survey Open-File Report 602, 9 p.

Kolker, A., 2008, Geologic Setting of the Central Alaskan Hot Springs Belt: Implications for Geothermal Resource Capacity and Sustainable Energy Production: Ph.D. Dissertation, University of Alaska Fairbanks, 203 p.

Leonard, L.J., Mazzotti, S., and Hyndman, R.D., 2008, Deformation rates estimated from earthquakes in the northern Cordillera of Canada and eastern Alaska: Journal of Geophysical Research, v. 113, B08406, doi:10.1029/2007JB005456.

Lewis, T.J., Hyndman, R.D., and Fluck, P., 2003, Heat flow, heat generation, and crustal temperatures in the northern Canadian Cordillera: thermal control of tectonics: Journal of Geophysical Research, v. 108: doi:10.1029/2002JB002090.

Morris, A., Ferrill, D.A. and Henderson, D.B., 1996, Slip-tendency analysis and fault reactivation: Geology, v. 24, no. 3, p. 275-278.

Murphy, D.C., and Mortensen, J.K., 2003, Late Paleozoic and Mesozoic features constrain displacement on Tintina Fault and limit large-scale orogen-parallel displacement in the Northern Cordillera. Geological Association of Canada – Mineralogical Association of Canada, Annual Meeting, Vol. 28, p.151.

Porro, C., Esposito, A., Augustine, C., and Roberts, B., 2012, An estimate of the geothermal energy potential in major sedimentary basins in the United States. Geothermal Resources Council Transactions, v. 36, p. 1359-1369.

Ratchkovski, N.A., and Hansen, R.A., 2002, New constraints on tectonics of interior Alaska: Earthquake locations, source mechanisms, and stress regime: Bulletin of the Seismological Society of America, v. 92, no. 3, p. 998 – 1014, doi:10.1785/0120010182.

Ristau, J., Rogers, G.C., and Cassidy, J.F., 2007, Stress in western Canada from regional moment tensor analysis: Canadian Journal of Earth Science, v. 44, no. 2, p. 127–148, doi:10.1139/E06-057.

Sibson, R.H., 1994, Crustal stress, faulting and fluid flow: Geological Society, London Special Publication, v. 78, p. 69-84.

Sippel, J., Scheck-Wenderoth, M., Reicherter, K., and Mazur, S., 2009, Paleostress states at the south-western margin of the Central European Basin System — Application of fault-slip analysis to unravel a polyphase deformation pattern: Tectonophysics, v. 470, p. 129-146.

Stroshein, R.W., 2008, Summary geologic report on the Grew Creek property, Yukon Territory, Canada: Technical report using British Columbia Securities Commission National Instrument 43-101 Guidelines prepared for Emerick Resources Corp., 54 p.

Templeman-Kluit, D.J., 1971, Geologic map of the Anvil Range zinc lead district, Yukon Territory: Geological Survey of Canada Map 1261 A, 1 sheet, 1:125,000 scale

Templeman-Kluit, D.J., 2012, Geology of Quiet Lake and Finlayson Lake map areas, south-central Yukon - An early interpretation of bedrock stratigraphy and structure: Geological Survey of Canada Open-File 5487, 13 sheets, 1:50,000 scale, 1:100,000 scale, 1:250,000 scale, 103 p.

Till, A.B., Roeske, S.M., Bradley, D.C., Friedman, R., and Layer, P.W., 2007, Early Tertiary transtension-related deformation and magmatism along the Tintina fault system, Alaska: Geological Society of America Special Paper 434, p. 233-264.

Townend, J., and Zoback, M.D., 2000, How faulting keeps the crust strong: Geology, v. 28, no. 5, p. 399-402.

Yukon Geological Survey, 2014, Update of the Yukon Bedrock Geology Map: Yukon Geological Survey digital data, 1:250,000 scale.

Mira Geoscience
...modelling the earth

Appendix 5: Magnetotelluric Data Analysis and Interpretation Report by University of Alberta

Electrical resistivity structure of the Tintina Trench at Ross River, Yukon Territory, from 3-D inversion of magnetotelluric data

Prof. Martyn Unsworth, University of Alberta, Edmonton

February 26, 2015

1. Introduction

This report summarizes the analysis of magnetotelluric (MT) data collected at Ross River by Phoenix Geophysics in 2013 and 2014. The survey crossed the Tintina Trench and was commissioned for preliminary exploration for geothermal resources. In a previous report Unsworth (2014) described the analysis of MT data collected at 24 stations on a single transect along Canol Road. These data were analysed using a 2-D inversion approach, which has the limitation that along strike variations in resistivity structure cannot be determined. With the additional MT data collected by Phoenix Geophysics at 24 stations in 2014, a grid with 48 stations was obtained and this permitted a 3-D approach to the analysis of the MT data.

2. Data quality and characteristics

In the 2014 campaign, Phoenix Geophysics collected magnetotelluric data at 25 stations on a grid located in the Tintina Trench. Most stations were located northwest of the 2013 transect on Canol Road. The processed magnetotelluric (MT) data were of high quality over the frequency range 300 - 0.001 Hz. At one station, RR1417, the data were contaminated by noise from a nearby cell phone tower and this station was excluded from subsequent analysis. The lowest quality points, as always with MT data, are observed at low frequency. This is because the number of estimates of these frequencies is less than the number of estimates of high frequency signals. Low data quality is also observed when the apparent resistivity is below 10 Ωm. This occurs because the corresponding electric field is weak, and will be more strongly influenced by noise than when the electric field is strong.

The vertical magnetic field (tipper) data were also found to be of high quality in the frequency band 300 - 0.1 Hz. The data are of acceptable quality in the frequency band 0.1 - 0.01 Hz, and it is common to see noise at these low frequencies owing to the overnight recording window used. These tipper data provide an independent estimate of subsurface resistivity structure

from the impedances, and are thus very useful in interpretation. When combined with the 24 stations collected in 2013 on Canol Road, this gave a grid of 48 MT stations as shown in Figure 1. The data were edited to eliminate noisy data points, and the distribution of usable data is shown in Figure 2.

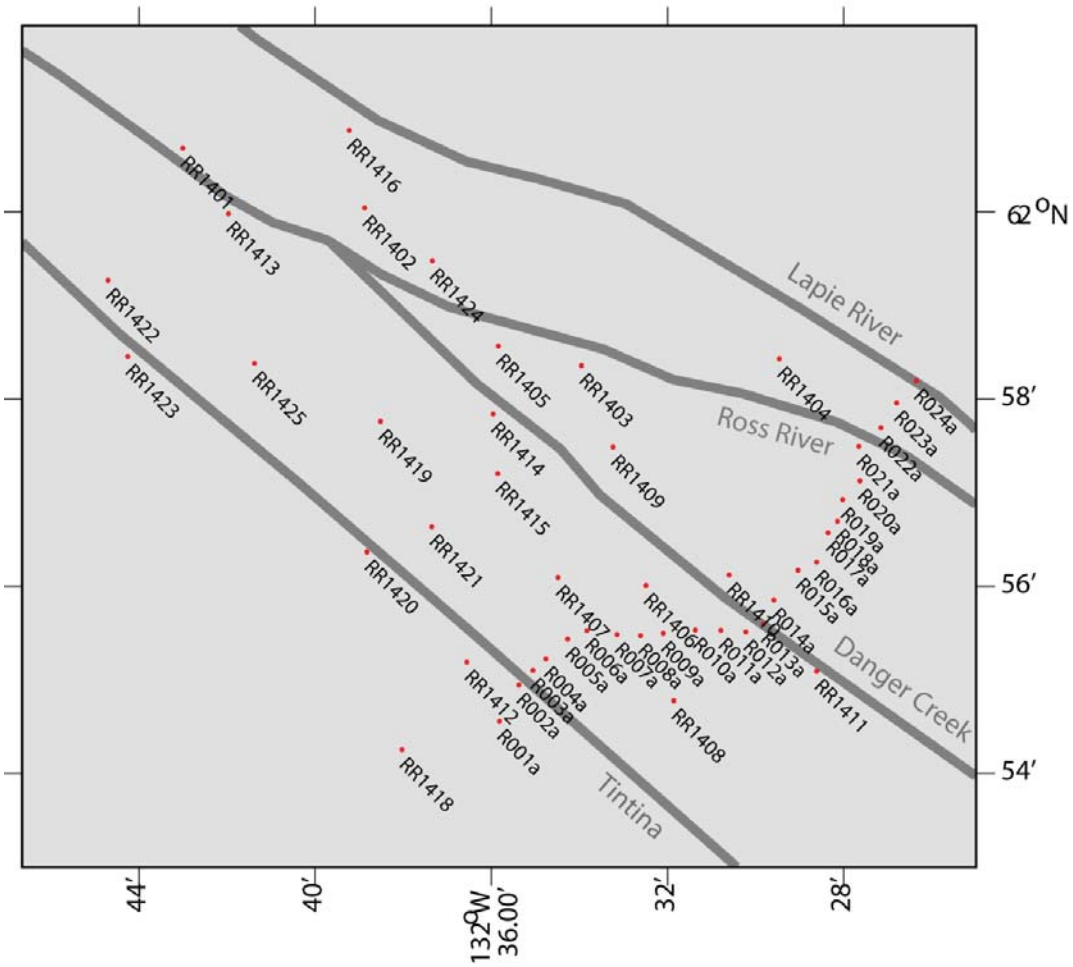

Figure 1 : Location of MT stations in the Ross River MT survey collected in 2013-2014. Major faults are shown for reference and locations are from Tempelman-Kluit (2013) and compiled by Cathie Hickson.

The data are displayed in map form in Figure 3 at two representative frequencies. This figure show the Berdichevsky average of the apparent resistivity measured in two orthogonal directions. The depth of signal penetration in MT is inversely proportional to the frequency. Thus the higher frequency (left panel) gives an image of shallow resistivity, while the lower frequency (right panel) gives an image of resistivity at depths 5-10 km. It can be seen from these data that the apparent resistivity is correlated with the location and strike of the major faults in the study area.

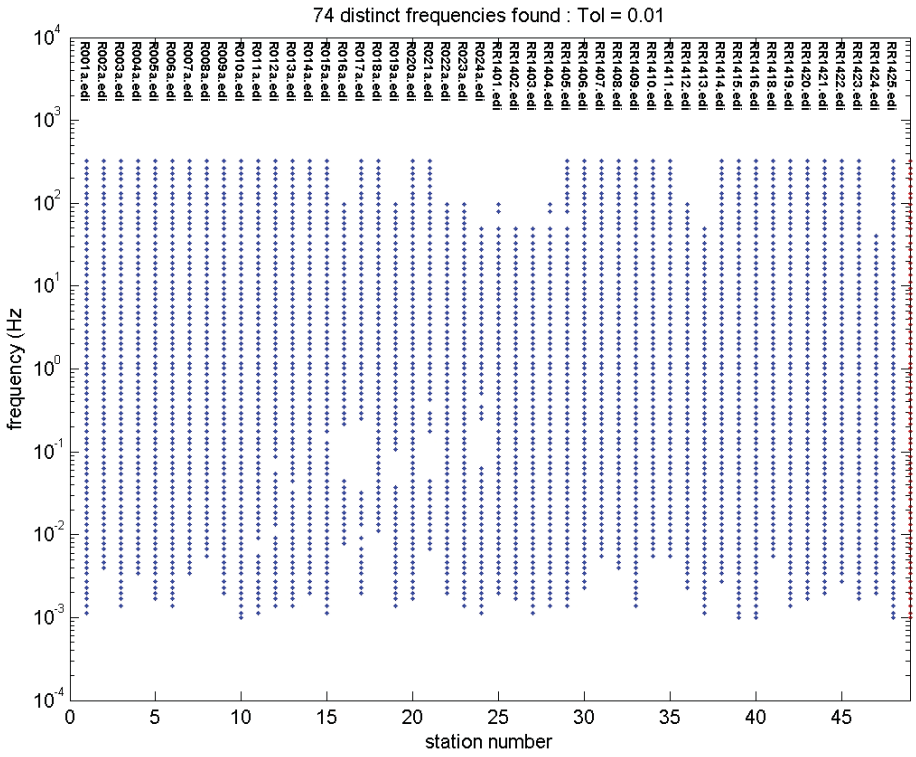

Figure 2 : Data points used in the analysis after removal of noisy points. There is good coverage at all stations from 100 - 0.001 Hz.

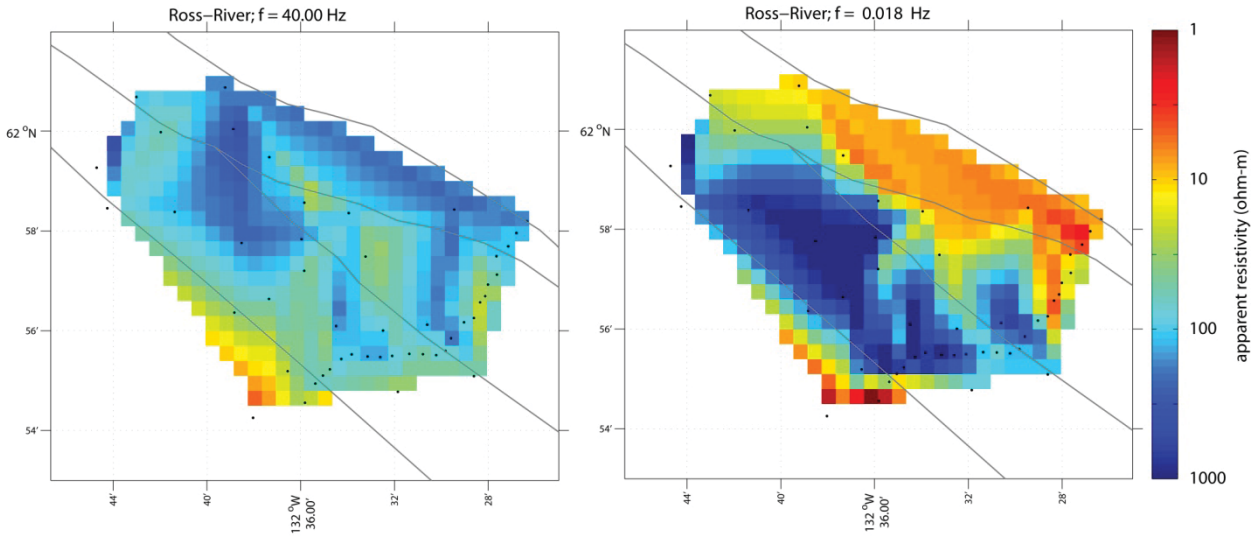

Figure 3 : Map of average apparent resistivity at 40 Hz and 0.018 Hz. The high frequency data (left) samples the near surface structure and the low frequency data (right) samples to depths of 5-10 km. Note that variations in apparent resistivity are correlated with the pattern of regional faults. MT station locations are shown by the black dots.

3. Dimensionality and directionality

A single magnetotelluric station can provide information about the azimuth of resistivity structures at depth. In MT exploration, the depth of investigation increases as the frequency decreases. Thus a study of the azimuth (geoelectric strike) as a function of frequency can give information about how the subsurface resistivity structure varies with depth.

The Phoenix report on the 2013 data on Canol Road uses a strike direction of N40°W which was derived from the polar diagrams on pages 53-59 of that report. Phase tensor analysis provides an alternative way to investigate the dimensionality of the MT data (Caldwell et al., 2004) and was used in this report. The phase tensor method has the advantage over polar diagrams in that near surface distortion can be removed from the magnetotelluric data. The following characteristics are observed:

1-D resistivity structure : With a layered Earth, there is no change in resistivity with azimuth and the phase tensor plots as a circle. The skew angle will be exactly zero.

2-D resistivity structure : This structure has a variation of resistivity with depth and in one horizontal direction. The invariant horizontal direction is called the strike direction. In this case the phase tensor plots as an ellipse, with either the major or minor axis parallel to strike. The skew angle will be zero.

3-D resistivity structure : In this case there is no strike direction and the orientation of the ellipse will reflect the local structure. The skew angle will be non-zero, and values above 5-10° are generally taken to indicate the presence of a significantly 3-D resistivity structure.

Application of the phase tensor to the Ross River data is illustrated in Figure 4 for a signal period of 2.4 s (frequency of 0.42 Hz) which samples to a depth of 3-5 km. In this figure the phase ellipses are plotted at each station, and then shown together with directions of the major axes plotted as a rose diagram. The strike direction could be either N40°E or N50°W. Magnetotelluric impedance data cannot determine which these values is correct and external information must be used. Given the well defined geological strike direction of the Tintina trench, the value of N50°W was chosen.

The orientation of the phase tensors changes when a boundary between regions of differing resistivity is crossed. Note that the major axes of the ellipses southwest of the Danger Creek fault are oriented N40°E, and they change to N50°W at stations northeast of this fault. It was shown by Caldwell et al., (2004) that this corresponds to the change from a high resistivity to a low resistivity. This confirms the trends observed in the average apparent resistivity data shown in Figure 3.

The colour of the ellipse show the skew angle, and most of the values plotted above are below 5° showing a relatively 2-D resistivity structure, but a significant number indicate 3-D structure, especially adjacent to the Tintina Fault.

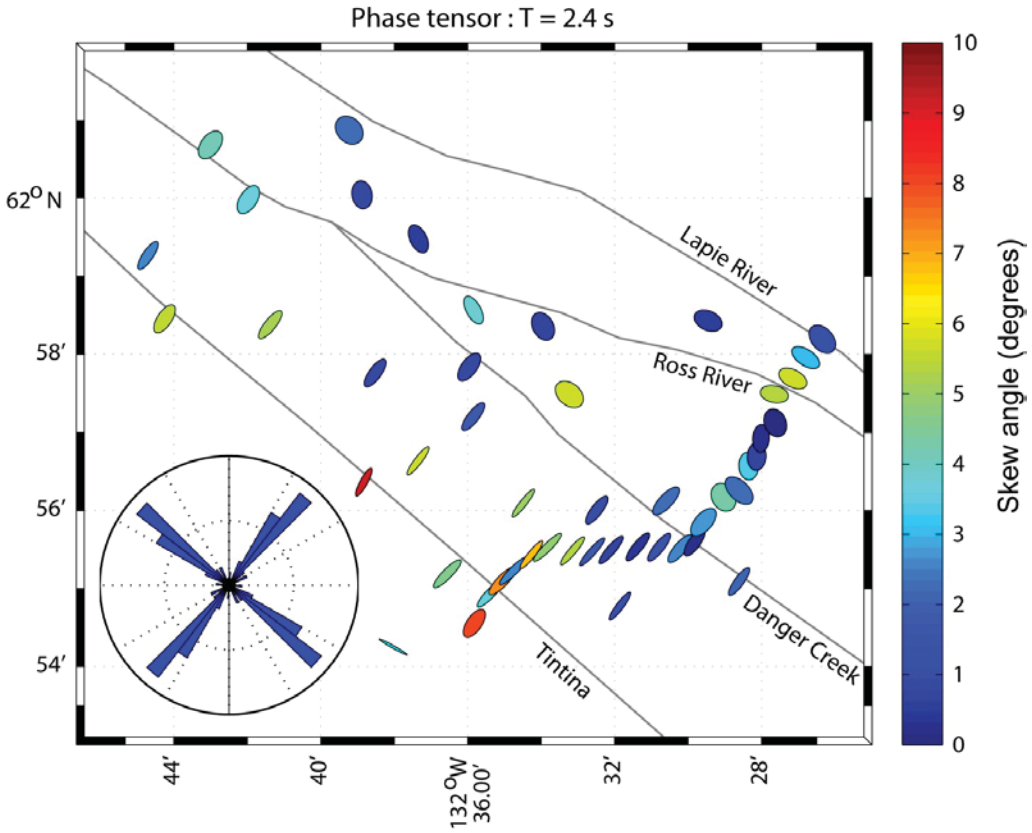

Figure 4 : The map shows the phase tensor ellipses at a period of 2.4 s, with the colour fill defining the skew angle which is a measure of the 3-D nature of the data. The rose diagram summarizes the statistical distribution of the strike directions (orientation of major axes of the ellipses). The strike direction is well defined at N50°W and essentially parallel to the Tintina Fault. Fault locations taken from Tempelman-Kluit (2013).

4. Three dimensional inversion of the Ross River MT data

The MT impedance data were inverted to produce a 3-D model of the resistivity beneath the study area. One advantage of the 3-D inversion over 2-D inversion is that no choice needs to be made about the strike direction. The inversion used the 3-D MT inversion algorithm of Siripunvaraporn et al., (2005). A number of inversions were performed in order to determine the appropriate choices of control parameters. The preferred inversion is described below and used the following options:

Resistivity model : The central part of the model had a uniform spacing of 400 m x 400 m in the horizontal directions. This region of the model was surrounded by padding with the cells increasing geometrically in size by a factor of 1.3. In the vertical direction the surface layer had a thickness of 20 m and this thickness increased geometrically with depth. The total mesh in the x, y and z directions had 64 x 72 x 45 cells. In addition, 7 rows of cells were used to model the electric and magnetic fields in the resistive air layer. The topography was not included in the inversion, since elevation differences in the study area are very limited. Thus in Figures 5 and 6, a depth of zero metres corresponds to the average elevation of the survey area.

MT impedance data : After elimination of obviously noisy points, magnetotelluric data from 48 stations were selected at 17 frequencies over the bandwith 100 - 0.001 Hz. The inversion used all four elements of the impedance tensor (Z_{xx}, Z_{xy}, Z_{yx}, Z_{yy}) with an error floor of 10% on each. A statistically ideal fit would yield an r.m.s. misfit value in the range 1-1.5 and adjustment of the error floor is often needed to avoid under-fitting or over-fitting the data. Many prior inversions of MT data have only used Z_{xy} and Z_{yx} to increase the speed of the inversion. However, this shortcut can compromise the ability of the MT data to image subsurface resistivity structure, especially if major structures are not aligned with the co-ordinate system used in the inversions (Kiyan et al., 2013).

Inversion control parameters : The default values were used for the Lagrange multipliers and regularization and found to give a stable model.

The inversion was then implemented in two stages:

(1) An initial inversion (*run5a*) was started from a uniform 100 Ωm halfspace with the grid described above. This inversion reduced the r.m.s. misfit from 12.2 to 3.83 on iteration 4.

(2) A second inversion (*run5b*), was started from iteration number 4 in *run5a*. This gave an r.m.s. misfit in the range 2-2.5. The resistivity model at each iteration was inspected, and while there was variation from iteration to iteration, the basic features of the model remained unchanged. From *run5b*, iteration 3 was selected as the preferred model.

Corresponding depth slices of *run5a-itn4* and *run5b-itn3* are shown in Figure 5. Note that at the surface and 1 km depth, the models exhibit many regions of localized high and low resistivity. This is because the station spacing is larger than the depth and is a common feature of MT inversion models. It occurs because there is limited sensitivity to structure where there are no MT stations. Note that both resistivity models show a distinct zone of high resistivity between the Tintina Fault and Danger Creek Fault, with low resistivity outside of this region to the southwest and northeast. This is as expected based on the measured apparent resistivity data

(Figure 3) and phase tensors (Figure 4). This agreement is an important test of the inversion procedure.

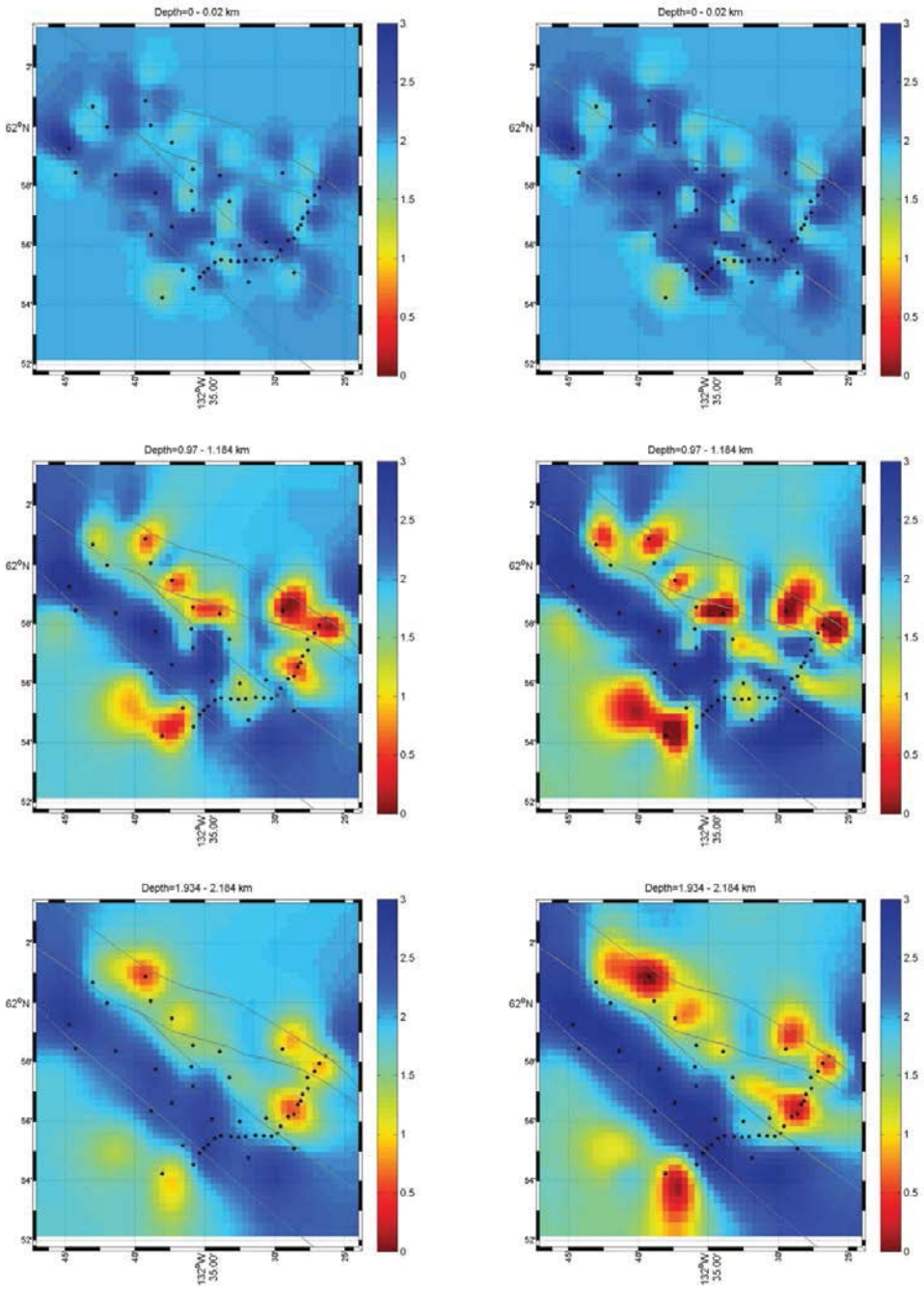

Figure 5 : Slices through the 3-D resistivity model at the surface (slice 1), at 1 km depth (slice 14) and at 2 km depth (slice 18). Left column is for model *run5a,* iteration 4 with an r.m.s. misfit of 3.83, and the right column is for model *run5b*, iteration 3 with an r.m.s. misfit of 2.39. MT stations are marked with black dots and the lines show the major faults that were labelled in Figure 1. Note that the color bar shows log10 (resistivity).

Vertical slices through the 3-D resistivity model are shown in Figure 6, and are along the profile from RR1418-R001-R024 along Canol Road. It is preferred to uses a profile slice to a straight line, because this will sample the resistivity model directly beneath the MT stations where the model is well constrained.

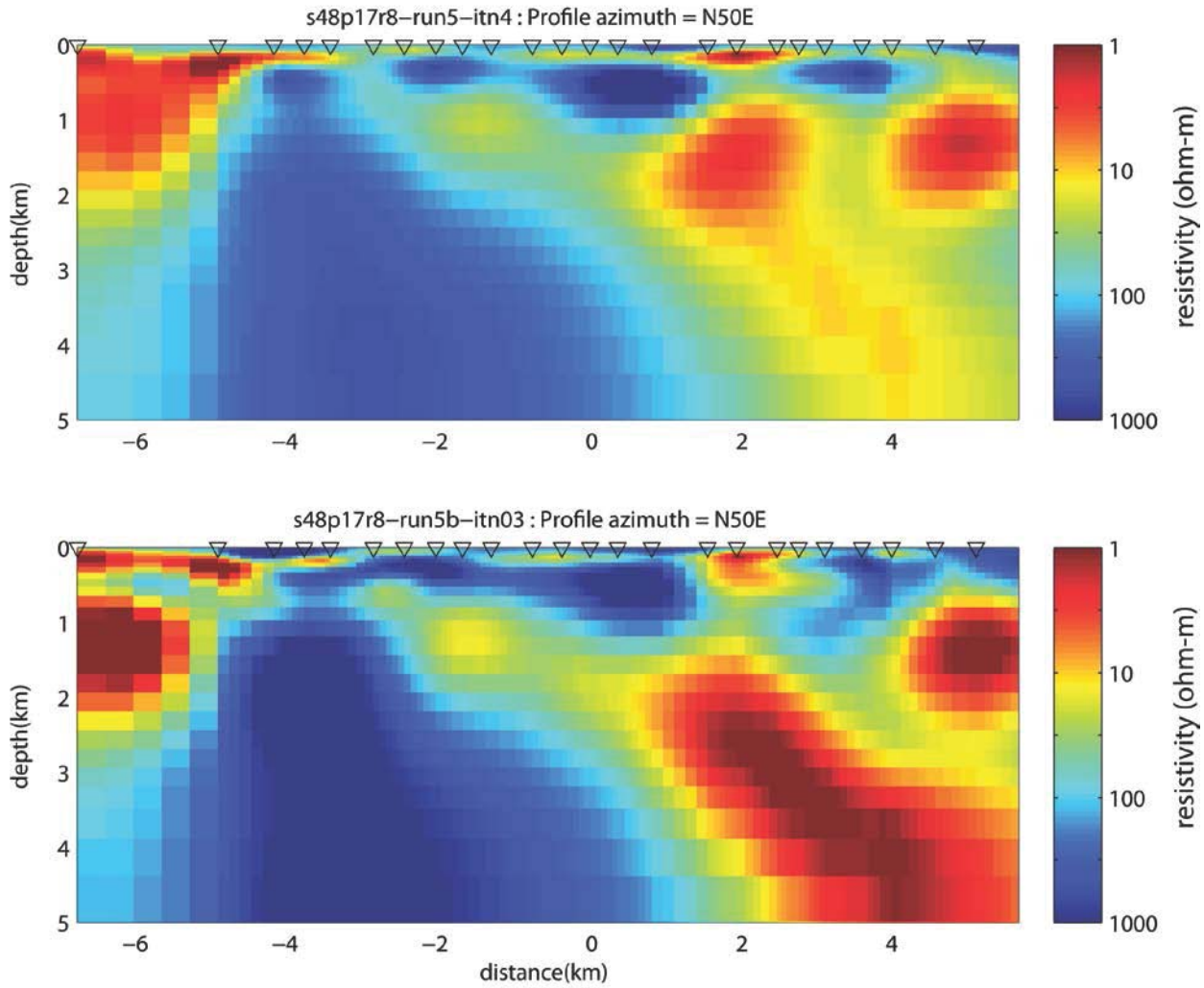

Figure 6 : Vertical slice through the 3-D resistivity models, along the transect of MT stations on Canol Road and using stations RR1418 and RR01 to R024. The slice is projected onto an azimuth of N50°E. Note that topography was not included in the inversion, so a depth of 0 km corresponds to the average surface elevation in the Tintina Trench. The inverted triangles show MT station locations. The left most station is RR1418 and the right most station is R024.

Figure 7 shows a comparison of the 3-D resistivity model developed in this report with the 2-D inversion from Phoenix Geophysics (2013). It should be noted that the two resistivity models are quite similar, which is as expected given the fact that the 3-D resistivity model appears to vary slowly along strike in Figure 5. i.e. the assumptions made in the 2-D inversion are valid. The

agreement between the 2-D and 3-D models is also consistent with the phase tensor analysis in Figure 4 that also gave evidence for a relatively 2-D resistivity structure with a strike direction of N50°W.

One difference to note is that some resistivity features appear at shallower depths in the 3-D inversion model than the 2-D inversion model. This phenomena has been observed in other inversion studies and is likely due to incorrect imaging in the 2-D inversion, since Earth structure is never exactly 2-D *i.e.* subsurface bodies are not infinite in extent along strike.

Inversion of geophysical data is an inherently non-unique process and it is important to investigate the range of models consistent with a particular data set. With the Ross River MT data set, additional inversions were undertaken to investigate the resistivity model shown in Figures 5 and 6. This included :

(a) Variation of the smoothing parameters used to regularize the resistivity model.

(b) Inversions using both the full impedance tensor and the vertical magnetic field transfer functions (the tipper).

(c) Starting models with a range of resistivity values.

These inversions all produced resistivity models that were broadly similar to those in Figures 5 and 6, indicating that these models are not dependent on a specific choice of inversion parameters.

5. Geological units present in the field area and expected resistivities

The following units are described in Tempelman-Kluit (2013) and the descriptions are repeated from Unsworth (2014). The lithological descriptions can be used to estimate the possible ranges of electrical resistivity expected, based on prior studies. These will be very broad and listed as high, intermediate and low resistivity.

CDS : Upper Harvey group : Age = Devonian and Mississippian**.** DMss: Siliceous Slate Formation: moderately resistant, black, graphitic, siliceous and pyritic slate; weathers black with rusty streaks; included Odd-s undifferentiated; gradational DMas; southwest of the Tintina Trench. Presence of graphitic slate units could give a **low resistivity.**

Ɛoc: Lower Harvey Group: Canyon Formation: Age = Upper Cambrian and Ordovician. Resistant, brown weathering, thinly interbedded shale, calcareous siltstone and argillaceous limestone; metamorphosed to biotite phyllite, termoite-calcite quartzite and impure marble; southwest of Tintina Trench. Presence of shale, with other clastics, would likely give an **intermediate resistivity.**

Cpav : Anvil Allochthonous Assemblage: Age = Carboniferous and Permian. Resistant, dark grey weathering, massive, dark green, basaltic greenstone and amphibolite; minor augite porphyry; includes Cpaub undifferentiated. Presence of igneous rocks would likely give an **intermediate to high resistivity.**

PMnu (DMN) : Nisultin Allochthonous Assemblage: Age = Paleozoic or Mesozoic. Black, siliceous phyllonite and medium green amphibole-chlorite phyllite: locally includes much interbedded gritty and pebbly greywacke containing clasts of blue quartz, white potassic feldspar and slate chips; locally included thin, black marble lenses: most rocks are strongly sheared. Presence of phyllite likely to give **an intermediate resistivity.** Presence or absence of graphite would likely dominate the resistivity.

Ts(ITR) : Ross River Conglomerate: Tertiary : White weathering, poorly indurated sandstone, conglomerate and shale; shale is brown and thin bedded with abundant coaly partings and plant debris: sandstone is coarse grained, poorly sorted arkose with beds to a meter thick; conglomerate, in beds to 20 meters thick, includes pebbles and cobbles of quartz, quartz schist, green basalt, and red cherty tuff in a sandy matrix of quartz, feldspar and muscovite; in Tintina trench SW of Ross River. Expect an intermediate resistivity.

6. Interpretation of the 3-D resistivity model

The 3-D inversion has yielded a model that is generally quite similar to the 2-D model that was presented by Phoenix Geophysics (2013). The additional MT stations collected in 2014 have shown that, despite the large inter-station spacing, the structures observed on the profile R001-R024 extend along strike.

It should be noted that MT inversion is inherently non-unique, and that other models can be found that also fit the MT data. A spectrum of resistivity models can be found that cover the range from :

(a) spatially rough resistivity models that fit the measured MT data very well. These models likely contain features (artifacts) that are due to noise in the MT data

and

(b) spatially smooth resistivity models that have a higher data misfit. These models will likely not contain the artifacts present in (a), but often do not extract all the information present in the measured MT data.

The inversion algorithm used for the 3-D inversion allows the user to control the smoothness and produce a range of resistivity models. This is controlled by the parameters defined as tau and delta in the WSINV3DMT algorithm of Siripunvaraporn et al., (2005). These inversions are currently in progress.

From southwest to northeast, the following resistivity features are interpreted. This interpretation is based on the conclusions of Unsworth (2014) and modified where the 3-D inversion model is distinctly different from the 2-D inversion.

A1 : Southwest of the Tintina Fault, the low resistivity of unit A1 is clearly consistent with the lithology of CDS that includes graphitic slate units. This feature extends southwest of the Tintina Fault and was well defined in the SNORCLE magnetotelluric data (Ledo et al., 2002). The base of A1 is poorly resolved, as is always the case of the base of a conductor imaged with magnetotelluric data. The addition of an extra station, RR1418, to the southwest of R001 has improved resolution of this feature compared to the 2-D model in Phoenix Geophysics (2013).

Tintina Fault : Geometry at depth not well defined. Could be associated with A1-A4 contact, or could be a vertical fault and located completely within A4 with minimal expression in resistivity if it was a narrow fault zone.

A2-A3 : Surface layer of folded rocks, that can be correlated with Cpav with intermediate to high resistivity. Located between the Tintina Fault and the Danger Creek Fault.

A4 : Located beneath A2-A3. The boundary between A4 and A2-A3 could be a contact, or a fault that is part of a flower structure. A4 is a high resistivity unit that probably corresponds to a crystalline rock unit bounded by the Tinitina Fault and Danger Creek Fault.

A5-A6-A7 : Folded layer of surface rocks with intermediate to high resistivity, corresponding to units PMnu(DMN) and Ts(ITR). The low resistivity unit A6 is coincident with the low ridge located between the Danger Creek Fault and the Ross River Fault.

A8 : Low resistivity unit at depth east of the Danger Creek Fault. The geometry of this feature is different in the 3-D and 2-D inversions. The upper edge appears to be uplifted between the Ross River Fault and Lapie River Fault. Based on the inferred geology, the low resistivity of A8 could be due to the presence of graphitic schist units. It could also be partly due to the presence of aqueous fluids, if the porosity of the rocks was high enough.

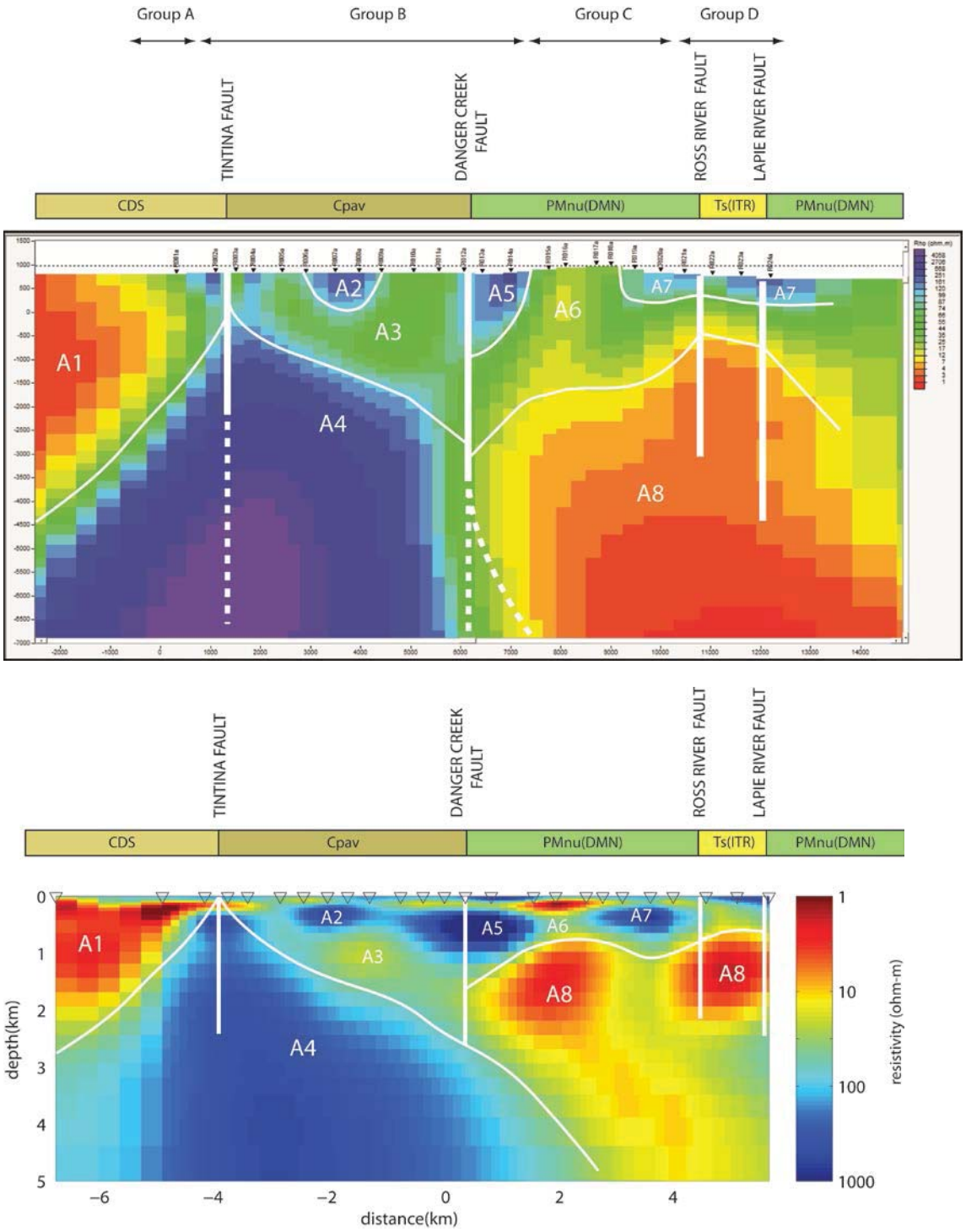

Figure 7 : Upper panel shows interpretation of the 2-D resistivity model from Unsworth (2014). Surface geology and fault locations are taken from Tempelman-Kluit (2013). Features A1 to A8 are discussed in Section 6. Thick white lines show subsurface locations of major strike-slip faults, and where dashed indicates uncertainty in location. The thin white lines are contacts or faults. Lower panel shows the interpretation of the 3-D model derived from 48 stations. Note that this is a preliminary interpretation.

Danger Creek Fault : Since the base of a low resistivity zone (conductor) is poorly resolved with MT, it is possible that the Danger Creek Fault is not vertical. but dips east at depth greater than 3 km below sea-level.

There are several possible patterns for the overall fault geometry of the Tintina Fault System. The major faults could all be sub-vertical with the system dominated by strike-slip motion. Alternatively the contacts between the various surfical rock units and basement units could be characterized by a set of northeast dipping faults e.g. the A3-A4 contact could continue to dip to the northeast, with similar features defined beneath the Lapie River Fault.

In the context of geothermal exploration, the key task is to locate regions with elevated porosity at depths with temperatures high enough to be used for heat or electricity production.

7. Conclusions

(a) The Phoenix Geophysics MT data collected in 2013 and 2014 have been inverted to produce a 3-D resistivity model. The resistivity structure is well correlated with surface geology and relatively 2-D i.e. there are limited variations along strike, subject to the broader MT station spacing northwest of Canol Road.

(b) The next stage of data analysis will be to compare the resistivity model with inversions of other types of geophysical data e.g. gravity and aeromagnetic. To facilitate this comparison, text files of the resistivity models are also supplied.

run5a Iteration 4	*s48p17r8-run5a-itn04-wsinv3dmt_all_layers.dat*
run5b Iteration 3	*s48p17r8-run5b-itn03-wsinv3dmt_all_layers.dat*

In these files, the format of each line is : longitude (°), latitude (°), depth (m), resistivity (Ωm)

(c) High resistivity zones such as A4 can be uniquely identified as dry, probably crystalline, rocks with low porosity and containing no conducting phase. Possible conducting materials include interconnected aqueous fluids, clay minerals, graphite films and sulphide minerals. These regions would not be suitable for extraction of heat through conventional hydrothermal geothermal production, although they would be potential targets for engineered geothermal systems if temperatures were high enough.

(d) In contrast, there are multiple explanations for low resistivity features such as A1 and A8. They could be high porosity rocks saturated with water i.e. an ideal geothermal reservoir. However, they could also be rocks containing interconnected graphite films or sulphide

minerals, which would be much less favourable for geothermal development. The importance of discriminating between these structures is discussed by Cumming (2009).

(e) If it can be established that viable temperatures for geothermal energy production are present in the subsurface, then additional magnetotelluric exploration could be useful to define of geometry of drilling targets in more detail.

(f) Prospective zones with elevated porosities would include the major fault zones and model resistivity features A6 and A8. Analysis of other geological and geophysical data are needed to refine the selection of drilling locations.

9. References

Caldwell TG, HM Bibby and C Brown, 2004, The magnetotelluric phase tensor, Geophysical Journal International, 158, 457-469.

Cumming W, 2009, Geothermal Resource conceptual models using surface exploration data, 34th Workshop on Geothermal Reservoir Engineering, Stanford University, Stanford, California, February 9-11, 2009.

Kiyan D, AG Jones, J Vozar, 2013, The inability of magnetotelluric off-diagonal impedance tensor elements to sense oblique conductors in three-dimensional inversions, Geophys. J. Int., doi:10.1093/gji/ggt470.

Ledo, J, AG Jones, I Ferguson, 2002, Electromagnetic images of a strike-slip fault: The Tintina Fault – Northern Canada, Geophysical Research Letters, 29, GL013408.

Phoenix Geophysics, 2013, MT survey of the Tintina Fault, Ross River, Yukon Territories, report on the acquisition and processing of MT data, October 2013.

Siripunvaraporn W, GD Egbert, Y Lenbury, M Uyeshima, 2005, Three dimensional magnetotelluric inversion : data subspace method, Physics of the Earth and Planetary Interiors, 150, 3-14.

Tempelman-Kluit, 2013, DJ Geology of Quiet Lake and Finlayson Lake map areas, south-central Yukon – An early interpretation of bedrock stratigraphy and structure, Geological Survey of Canada Open File 5487.

Unsworth MJ, 2014, Resistivity structure of the Tintina Trench at Ross River, Yukon Territory, from magnetotelluric data : implications for geothermal exploration, report submitted to Dena Nezziddi Development Corporation, March 2014.

PRELIMINARY GEOLOGIC MAP OF THE ROSS RIVER AREA, YUKON, CANADA

Nicholas Hinz, Seth Dee, and Jeff Witter

2015

Geologic map compiled from existing public data sets (1:250,000 scale Yukon Geological Survey digital data, 2014; Templeman-Kluit, 1971, 2012) and new field mapping and interpretations made from aeromagnetic data in Fall, 2014. See accompanying report by Hinz and Dee for additional information.

References Cited

Templeman-Kluit, D.J., 1971, Geologic map of the Anvil Range zinc lead district, Yukon Territory: Geological Survey of Canada Map 1261 A, 1 sheet, 1:125,000 scale

Templeman-Kluit, D.J., 2012, Geology of Quiet Lake and Finlayson Lake map areas, south-central Yukon - An early interpretation of bedrock stratigraphy and structure: Geological Survey of Canada Open-File 5487, 13 sheets, 1:50,000 scale, 1:100,000 scale, 1:250,000 scale, 103 p.

Yukon Geological Survey, 2014, Update of the Yukon Bedrock Geology Map: Yukon Geologogical Survey digital data, 1:250,000 scale, http://www.geology.gov.yk.ca/update_yukon_bedrock_geology_map.html

Symbology

Contact Solid where certain and location accurate, dashed where approximate, dotted where concealed.

Normal and Strike-Slip faults Solid where certain and location accurate, dashed where approximate, dotted where concealed; queried if identity or existence uncertain. Ball on downthrown side.

Thrust fault Solid where certain and location accurate, long-dashed where approximate, dotted where concealed.

Anticline Long-dashed where approximate; dotted where concealed. Arrow shows direction of dip.

Syncline Long-dashed where approximate, dotted where concealed. Arrow shows direction of dip.

Dike

Strike and dip of bedding

Inclined Vertical

Strike and dip of metamorphic foliation

Inclined Vertical

Aeromagnetic Data Boundary

Legend

QUATERNARY

- Q: QUATERNARY: unconsolidated glacial, glaciofluvial and glaciolacustrine deposits; fluviatile silt, sand, and gravel, and local volcanic ash, in part with cover of soil and organic deposits

EARLY TERTIARY

- Ts: ITR3: ROSS: brown, thin bedded, claystone, siltstone, shale and coal; arkosic or chert rich, thick bedded micaceous sandstone; thick bedded to massive pebble to boulder, chert-quartz conglomerate
- Tb: ITR1: ROSS: dark grey-green olivine basalt flows; volcaniclastic rocks
- Tvs: TR: ROSS: mixed bimodal volcanics (basalt (1), rhyolite (2)) and terrestrial clastics (3), dominantly along or near Tintina Fault; farther removed, scattered occurrences of rhyolitic lava and dykes (4) are also included
- Trv: ITR2: ROSS: rhyolite flows, tuffs, ash-flow tuffs and breccias

MID-CRETACEOUS

- mKgTR: TAY RIVER: granodiorite
- mKgC: CASSIAR SUITE: granodiorite, biotite-muscovite granodiorite, quartz diorite, biotite quartz monzonite, granite (Cassiar Suite)

LOWER AND MIDDLE JURASSIC, HETTANGIAN TO BAJOCIAN

- JFP1: FARO PEAK: conglomerate
- JFP2: FARO PEAK: argillite, sadnstone
- JFP3: FARO PEAK: shale, limestone

DEVONIAN, MISSISSIPPIAN AND(?) OLDER

- DMF1:Finlayson volcanic

LATE PROTEROZOIC AND PALEOZOIC

- PDS5: SNOWCAP: psammite, quartzite and amphibolite metamorphosed to eclogite facies
- PDS3: Snowcap amphibolite
- PDS2: Snowcap marble

CARBONIFEROUS

- CK1: KLINKIT: medium to dark green to purple-grey, locally amygdaloidal or vesicular intermediate to mafic volcanic flows, flow breccias, volcanic fragmentals and tuffs; blocks of calc-silicate common in the breccias and fragmentals
- CK2: CH2: HART RIVER: brown weathering limestone; equivalent to upper part of Hart River (Hart River)
- CK3: black to gray-brown slate and shale

CARBONIFEROUS TO PERMIAN

- CPSM4: SLIDE MOUNTAIN: ultramafic
- CPSM2: SLIDE MOUNTAIN (CAMPBELL RANGE): basalt
- CPSM1: SLIDE MOUNTAIN (FORTIN CREEK): chert, argillite

ORDOVICIAN TO LOWER DEVONIAN

- ODR1: ROAD RIVER - SELWYN: black, gun-blue, or silvery white weathering black graptolitic shale and black chert; resistant grey weathering, thin to medium bedded, light grey to black, greenish grey or turquoise chert; minor argillaceous limestone (Road River Gp., Duo Lake and Elmer Creek)

CAMBRIAN TO DEVONIAN OR YOUNGER

- CDS1: ST. CYR: orange to brown weathering, recessive, medium grey interlaminated calcareous shale and silty limestone or calcareous siltstone; proportion of carbonate to clastic material varies widely; includes slaty and phyllitic equivalents (Cambro-Ordovician?)
- CDS3: ST. CYR: black, recessive weathering, calcareous graphitic "sooty" slate and silty shale; includes thin beds of dark grey graphitic, very fine grained quartzite and black "sooty" crinoidal limestone (Ordovician and Silurian?)
- CDS4: ST. CYR: orange buff weathering, medium grey, thin to medium bedded, finely laminated and cross-laminated calcareous quartz siltstone and very fine grained orthoquartzite, with slaty phyllite partings; minor massive, light grey orthoquartzite (Siluro-Devonian?)
- CDS5: ST. CYR: orange to dark blue-grey phyllite and thinly laminated phyllitic limestone; minor laminated siltstone, green slate, and rare chert; platy, fetid limestone, locally crinoidal; minor shale, basalt, tuff and breccia (Upper Devonian or younger?)

CAMBRIAN TO SILURIAN

- CSM8: MENZIE CREEK: basalt
- CSM1: MARMOT: resistant, dark grey weathering, massive, locally pillowed, dark grey-green basalt, tuff and breccia (Menzie)

UPPER CAMBRIAN AND ORDOVICIAN

- COK1: KECHIKA: thin bedded, lustrous, calcareous, grey slate, phyllite, limestone, minor grey dolostone and dolomitic limestone; quartz-carbonate veins; minor sills and flows of basalt and basaltic tuff ; may include Ordovician black slate at top of succession (Kechika)
- COR1: RABBITKETTLE: thin bedded, wavy banded, silty limestone and grey lustrous calcareous phyllite; limestone intraclast breccia and conglomerate; massive to laminated, grey quartzose siltstone and chert and rare black slate; local mafic flows, breccia, and tuff (Rabbitkettle)

LOWER CAMBRIAN

- ICG1: GULL LAKE: shale, siltstone and mudstone, locally bioturbated, with minor quartz sandstone; rare green-grey chert; local basal limestone and limestone conglomerate; phyllite to quartz-muscovite-biotite schist (garnet sillimanite staurolite andalusite) (Gull Lake)
- ICG3: GULL LAKE: marble

Scale 1:50,000

100 Meter Contours

0 2.5 5 7.5 10 km

N

YGS MR-18